

AD-A042 404

DOUGLAS AIRCRAFT CO LONG BEACH CALIF
A FULLY AUTOMATIC COMBINED POTENTIAL-FLOW BOUNDARY-LAYER PROCED--ETC(U)
JUN 77 J L HESS
MDC-J7491

F/G 20/4

N00014-73-C-0059

NL

UNCLASSIFIED

OF
AD
A042404



END
DATE
FILMED
8-77
DDC

ADA 042404

Approved for Public Release: Distribution Unlimited

Reproduction in whole or in part is permitted
for any purpose of the United States Government.

12

AD 110. FILE COPY
DDC

DDC
RECEIVED
NOV 1 1977
C

DOUGLAS AIRCRAFT COMPANY

MCDONNELL DOUGLAS

CORPORATION

61153N

A FULLY AUTOMATIC COMBINED POTENTIAL-FLOW BOUNDARY-LAYER PROCEDURE
FOR CALCULATING VISCOUS EFFECTS ON THE LIFTS AND PRESSURE
DISTRIBUTIONS OF ARBITRARY THREE-DIMENSIONAL CONFIGURATIONS

by

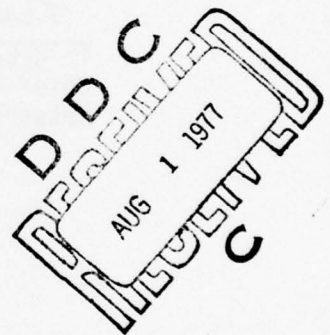
John L. Hess

Report No. MDC J7491

June 1, 1977

This research was carried out under the
Naval Ship Systems Command General Hydro-
mechanics Research Program Subproject
SR 023 01 01, administered by the Naval
Ship Research and Development Center.

Contract N00014-74-C-0059



APPROVED FOR PUBLIC RELEASE: DISTRIBUTION UNLIMITED

Reproduction in whole or in part is permitted for any purpose of the
United States Government.

Copy number

Report number

MDC J7491

A FULLY AUTOMATIC COMBINED POTENTIAL-FLOW BOUNDARY-LAYER
PROCEDURE FOR CALCULATING VISCOUS EFFECTS ON THE LIFTS AND
PRESSURE DISTRIBUTIONS OF ARBITRARY THREE-DIMENSIONAL
CONFIGURATIONS

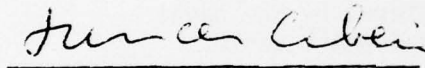
Revision date

Revision letter

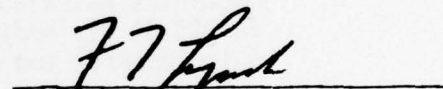
Issue date June 1, 1977 Contract number N00014-74-C-0059

Prepared by : John L. Hess


Approved by :



T. Cebeci
Chief Aerodynamics Engineer
Research



F. T. Lynch
R&D Program Development
Aerodynamics Subdivision



O. R. Dunn
Director - Aerodynamics

DOUGLAS AIRCRAFT COMPANY

MCDONNELL DOUGLAS



1.0 ABSTRACT

This report describes a method for calculating viscous effects on the lifts and pressure distributions of arbitrary three-dimensional configurations. The approach consists of combining a panel method, which calculates potential flow about arbitrary three-dimensional lifting configurations, with a boundary-layer method. Combined procedures have been constructed using a two-dimensional boundary-layer method in a strip-theory sense and using a three-dimensional small cross-flow boundary-layer method. Various fundamental and procedural aspects of the general calculation scheme are investigated and discussed. Final emphasis is on a completely automatic procedure that performs its calculations in a single computer run without intermediate human intervention. For this purpose the method based on a strip-theory boundary layer has proved very satisfactory. Calculated inviscid and viscous lift and pressure distributions are compared with experimental data for a variety of wings and wing-fuselages having both conventional and supercritical airfoil sections. The agreement of the calculations with experiment appears to be quite good.

ADDITIONAL FOR	
WIS	Write Section <input checked="" type="checkbox"/>
DDO	Dist Section <input type="checkbox"/>
UNANNOUNCED	
JUSTIFICATION	
DISTRIBUTION/AVAILABILITY CODES	
Dist.	AVAIL. and/or SPECIAL
<i>A</i>	

2.0 TABLE OF CONTENTS

	Page
1.0 Abstract	1
2.0 Table of Contents	2
3.0 Index of Figures	5
4.0 Principal Notation	8
5.0 Introduction	9
6.0 General Aspects of Procedures for Approximating Viscous Flows by Means of Combined Inviscid-Flow Boundary-Layer Methods	12
6.1 Two-Dimensional and Three-Dimensional Flows. Boundary- Layer Methods	12
6.2 Methods of Boundary-Layer Simulation	13
6.3 The Wake	14
6.4 Sequential Use of the Potential-Flow and Boundary-Layer Methods	14
6.5 Comparison of Computational Aspects of the Two Boundary- Layer Simulation Methods	16
6.6 Application of the Kutta Condition	18
6.7 Form of the Surface Vorticity	19
7.0 Two-Dimensional Studies	21
7.1 General Remarks	21
7.2 Point-Number Requirements for the Boundary-Layer Program . .	21
7.3 Effect of the Wake	22
7.4 Results for Selected Airfoils	23
7.4.1 RAE 101.	23
7.4.2 64A010	24
7.4.3 Symmetric Joukowski	24
7.5 Conclusions	25

	Page
8.0 A Three-Dimensional Procedure Based on a Strip-Theory Boundary-Layer Method	27
8.1 General Remarks	27
8.2 Some Aspects of the Three-Dimensional Potential-Flow Panel Method	28
8.3 General Description of the Combined Potential-Flow Boundary-Layer Method	29
8.3.1 The Initial Potential-Flow and Boundary-Layer Calculation	29
8.3.2 Surface Displacement Simulation	32
8.3.3 Surface Blowing Simulation	33
8.4 Comparison of Calculated Results for Isolated Wings with Experimental Data	34
8.4.1 Symmetric Swept Wing	35
8.4.2 Cambered-Twisted Swept Wing	36
8.5 Comparison of Calculated Results for Wing-Fuselages with Experimental Data	36
8.5.1 A Straight Wing on a Round Fuselage	37
8.5.2 Conventional Swept Wing Mounted Low on a Fuselage	38
8.5.3 Supercritical Swept Wing Mounted High on a Fuselage	39
8.5.4 A Supercritical Transport Configuration	40
8.6 Conclusions	41
9.0 A Three-Dimensional Procedure Based on a Small-Cross-Flow Boundary-Layer Method	43
9.1 General Remarks	43
9.2 Surface Coordinates	43
9.3 Surface Velocity Components	46
9.4 Streamline Computation	47
9.5 Curvature Calculation	48

	Page
9.6 Boundary-Layer Calculation and Simulation	48
9.7 Calculated Results	49
10.0 References	51

3.0 INDEX OF FIGURES

<u>No.</u>		<u>Page</u>
1	Representation of a three-dimensional lifting configuration. . . .	53
2	Two methods of boundary-layer simulation	54
3	Application of the Kutta condition	54
4	Calculated upper-surface displacement-thickness distributions on an airfoil obtained using various point numbers	55
5	Effect of the wake displacement thickness on calculated lift coefficients for a 11.8%-thick Joukowski airfoil at 6° angle of attack.	56
6	Comparison of calculated inviscid pressure distributions and lifts with exact values for an RAE 101 airfoil at 8.2° angle of attack. 52 surface panels	57
7	Comparison of calculated and experimental pressure distributions and lifts for an RAE 101 airfoil at 8.2° angle of attack. Constant surface vorticity distribution	58
8	Comparison of calculated and experimental pressure distributions and lifts for an RAE 101 airfoil at 8.2° angle of attack. Parabolic surface vorticity distribution	59
9	Comparison of calculated inviscid pressure distributions and lifts with exact values for a 64A010 airfoil at 8° angle of attack. 40 surface panels	60
10	Comparison of calculated and experimental pressure distributions and lifts for a 64A010 airfoil at 8° angle of attack. Constant surface vorticity distribution	61
11	Comparison of calculated inviscid pressure distributions and lifts with exact values for a Joukowski airfoil at 6° angle of attack. 54 surface panels.	62
12	Comparison of calculated and experimental pressure distributions and lifts for a Joukowski airfoil at 6° angle of attack. Constant surface vorticity distribution	63
13	Comparison of calculated and experimental pressure distributions and lifts for a Joukowski airfoil at 6° angle of attack. Parabolic surface vorticity distribution	64
14	Addition of displacement thickness to a body	65
15	Two isolated swept wings	66

<u>No.</u>	<u>Page</u>
16	Comparison of calculated and experimental spanwise distributions of section lift coefficient for a swept wing with symmetric airfoil section at 8.2° angle of attack 67
17	Comparison of calculated and experimental chordwise pressure distributions at 55.5% semi-span for a swept wing with symmetric airfoil section at 8.2° angle of attack 68
18	Comparison of calculated and experimental spanwise distributions of section lift coefficient for a cambered twisted swept wing at 8.2° angle of attack 69
19	Comparison of calculated and experimental chordwise pressure distributions at 55.5% semi-span for a cambered twisted swept wing at 8.2° angle of attack 70
20	A straight wing on a round fuselage 71
21	Comparison of calculated and experimental spanwise distributions of section lift coefficient for a straight wing on a round fuselage at 6° angle of attack 72
22	Comparison of calculated and experimental chordwise pressure distributions at 60% semi-span on a straight wing mounted on a round fuselage at 6° angle of attack 73
23	A conventional swept wing mounted as a low wing on a fuselage . . . 74
24	Comparison of calculated and experimental spanwise distributions of section lift coefficient for a conventional swept wing mounted low on a fuselage at 6.9° angle of attack 75
25	Comparison of calculated and experimental chordwise pressure distributions at 60% semi-span on a conventional swept wing mounted low on a fuselage at 6.9° angle of attack 76
26	A supercritical swept wing mounted as a high wing on a fuselage . . 77
27	Comparison of calculated inviscid pressure distributions and lifts with exact values for a two-dimensional supercritical airfoil at 7.02° angle of attack 78
28	Comparison of calculated and experimental spanwise distributions of section lift coefficient for a supercritical swept wing mounted high on a fuselage at 7.02° angle of attack 79
29	Comparison of calculated and experimental chordwise pressure distributions at 60% semi-span on a supercritical swept wing mounted low on a fuselage at 7.02° angle of attack 80
30	A supercritical transport configuration 81

<u>No.</u>		<u>Page</u>
31	Comparison of calculated inviscid pressure distributions and lifts with exact values for a three-dimensional transport-type supercritical airfoil at 2.06° angle of attack	82
32	Comparison of calculated and experimental spanwise distributions of section lift coefficient on the wing for a supercritical transport configuration at 2.06° angle of attack	83
33	Comparison of calculated and experimental chordwise pressure distributions at the 50% semi-span location on the wing for a supercritical transport configuration at 2.06° angle of attack	84
34	Definition of surface coordinates for a wing	85
35	A wing in its coordinate space	85
36	An individual surface panel	86
37	Block diagram of the combined potential-flow small-cross-flow-boundary-layer program	86
38	Calculated streamlines on a swept wing with symmetrical airfoil section at 8.2° angle of attack	87
39	Calculated spanwise distributions of displacement thickness along the upper-surface trailing edge of a swept wing with symmetrical airfoil section at 8.2° angle of attack	88
40	Comparison of calculated and experimental spanwise distributions of section lift coefficient for a swept wing with symmetric airfoil section at 8.2° angle of attack	89

4.0 PRINCIPAL NOTATION

C_L	total lift coefficient: equals total integrated pressure force on a body in a direction perpendicular to the freestream divided by the product of a reference area and freestream dynamic pressure
C_p	pressure coefficient: equals difference of local static pressure from freestream static pressure divided by freestream dynamic pressure
C_{ℓ}	section lift coefficient: equals the component perpendicular to the freestream of the integrated pressure force on a strip of elements on a wing divided by the product of freestream dynamic pressure and the projection of the area of the strip into the plane containing the chord line of the wing
L	total arc-length of an N-line
N-line	a curve on the surface of a body defined by input points (figure 1)
\hat{n}	unit normal vector to the body surface
Re	Reynolds number
t	integration variable for calculating surface streamlines
U	freestream velocity
u, v	nonorthogonal coordinates in a body surface
u_o, v_o	values of u and v pertaining to the midpoint of a panel
V	surface velocity
w	width of a lifting strip of elements (figures 34 and 36)
x/c	distance along an airfoil as a fraction of its chord
x, y, z	Cartesian coordinates
δ^*	boundary-layer displacement thickness
ξ, η	orthogonal coordinates in the plane of a panel (figure 36)

5.0 INTRODUCTION

At the present time powerful and accurate computer methods exist for calculating inviscid flow about two- and three-dimensional configurations. One class of methods is approximate in the sense that some small-perturbation assumptions have been incorporated, and such methods are applicable only to a limited class of geometric configurations. A second class of methods is "exact" in the sense that no restrictive assumptions are employed, and such methods are applicable to all configurations. Especially powerful are the so-called "panel methods" for low-speed flow [1]. This last class of methods takes advantage of the fact that only in the low-speed regime is the governing flow equation linear, and it employs the principle of superposition of elementary solutions. The result is that panel methods need consider only the surface of the body about which flow is to be computed, as opposed to exact methods in other speed regimes, which must consider the entire flow field even if flow on the body is the only interest. Thus, low-speed panel methods are very efficient. They can calculate flow about a given configuration in far less time than other exact methods, or, alternatively, for reasonable computing times a panel method can calculate flow about a much more complicated configuration than other exact methods can.

Despite the neglect of viscosity, surface pressure distributions calculated by low-speed panel methods agree with experiment remarkably well in a wide variety of cases [1]. There are only two important exceptions: (1) lifting flows, and (2) flows with large regions of separated flow. An example of the first class is the flow about a lifting wing at a moderate angle of attack, for which the flow is essentially unseparated. Examples of the second class are flow about a sphere and flow about a lifting wing near maximum lift. Surface pressures on a nonlifting body with essentially unseparated flow agree very closely with inviscid surface pressures. The calculation of fully separated flows is currently an unsolved problem, despite much effort by various investigators. The subject of this report is the calculation of "essentially-unseparated" flow about a body for which the boundary layer either is unseparated or else separates so near the downstream end of the body that extrapolation of the displacement thickness to the end of the body is justified. In view of the above discussion, only a lifting body experiences significant

viscous effects, and the method to be presented concentrates on this case. The requirement also has been imposed that the method be fully automatic. The user simply specifies the geometry of the body and the flow conditions, and the method calculates all the required viscous and inviscid flow properties without further action on the part of the user.

Because of considerations of computing time, an "exact" numerical solution of the Navier-Stokes equations is not practical at this time. Such a solution would require far more computing time than any inviscid method, even one that considers the entire flow field, let alone a relatively fast panel method. Accordingly, many investigators have concentrated on methods that take advantage of the fact that for essentially unseparated flow about a body at a practical Reynolds number, the effects of viscosity are appreciable only in a very thin boundary layer adjacent to the body's surface and in a thin wake downstream of the body. Such methods attempt to "patch together" an inviscid solution and a boundary-layer solution to represent a real flow. This is the approach adopted in the present investigation. Previous papers [2], [3] have presented methods of this type applicable to two-dimensional lifting flow. The present work is an attempt to construct a similar method for three-dimensional lifting flow. Various procedures are possible, each having a different degree of approximation, and several have been tried.

Many of the ideas to be applied to the three-dimensional case have direct two-dimensional analogies. Accordingly, series of two-dimensional studies have been conducted to determine the effectiveness of various procedures without incurring the high three-dimensional computing costs. The general conclusion to be drawn is that in view of all the approximations being applied to the calculation, in particular those associated with the inviscid-flow boundary-layer "patching," the simpler procedures for representing viscous three-dimensional flows are likely to be as accurate as more elaborate methods.

Two combined potential-flow boundary-layer programs have been constructed. The first combines a three-dimensional low-speed panel method with a two-dimensional boundary-layer method applied in a "strip-theory" sense. The second combines the same panel method with a three-dimensional boundary-layer

method based on a small cross-flow assumption. The various sections of this report describe these methods, the various assumptions employed, and the evidence supporting the validity of the assumptions. Also presented are calculated results for a variety of configurations and comparison of these results with experimental data. The most fully developed method is that based on the two-dimensional boundary-layer calculation. This combined program is fully automatic and essentially without "bugs." Moreover, its predictions agree with experiment very well. It may be considered an operational design tool. The more elaborate program based on the small cross-flow boundary-layer technique is somewhat more difficult to run and may be said to require an expert user. Moreover, for most geometries, no substantial gain in accuracy over that of the simpler program can be achieved. Nevertheless, the second program has been fully documented and it does produce answers, including both boundary-layer information and new potential-flow information such as surface streamlines. Presumably the second program will prove useful in cases where the three-dimensional nature of the boundary layer is essential.

6.0 GENERAL ASPECTS OF PROCEDURES FOR APPROXIMATING VISCOUS FLOWS BY MEANS OF COMBINED INVISCID-FLOW BOUNDARY-LAYER METHODS

6.1 Two-Dimensional and Three-Dimensional Flows. Boundary-Layer Methods.

The basic procedure for combining an inviscid-flow method and a boundary-layer method is the same for two-dimensional and three-dimensional flows in all speed regimes. The dimensionality and the speed regime affect only what particular inviscid-flow method and what particular boundary-layer method are used in the combined procedure. There are, of course, several choices of both types of method available even after the dimensionality and the speed regime are fixed.

In the present work attention is restricted to the low-speed regime, where either the flow is incompressible or compressibility effects are small enough to be accounted for by simple corrections to an incompressible flow method. The inviscid-flow method considered is the well-known "exact" surface-panel method for incompressible potential flow [1]. Several versions of this method exist, but all represent the surface of the body about which flow is to be computed by some combination of source and vortex singularities distributed on surface "panels" that represent the body surface. A three-dimensional lifting body represented by surface panels is shown in Figure 1. Two- and three-dimensional versions of this method exist. They are direct analogies of each other, so that very fast two-dimensional computer calculations may be used to discover important properties of the very time-consuming three-dimensional procedure. The version employed in the present work is the source-panel method of [1], [4]. In the interest of brevity, a detailed description of the potential-flow panel method is not given here. For details, reference should be made to [1], [4]. Certain properties of the method that are important for the present application are mentioned as needed without discussion.

With regard to boundary-layer methods, a two-dimensional combined program [2] is based on a finite-difference boundary-layer procedure (see Section 7.1). In the present work the same boundary-layer method has been incorporated into a combined program using a strip-theory approach. In the combined program the potential-flow calculation dominates the computing time, especially for large panel numbers. (Potential flow computing time varies as the square or the

cube of the panel number, whereas boundary-layer computing times vary as the first power.)

Of course more elaborate three-dimensional boundary-layer methods may be combined with the panel method of [4]. A first step in this direction was taken in the present work by using a boundary-layer method based on an assumption of small cross-flow normal to the potential-flow streamlines. (See Section 9.1.)

6.2 Methods of Boundary-Layer Simulation

Once the inviscid potential-flow method and the boundary-layer method have been decided upon, there still remains the question of how they are to be used to arrive at an approximation to high Reynolds number viscous flow, which is assumed to be "essentially" unseparated. What has to be done is to use the quantities calculated by the boundary-layer method to define a modified potential flow that is the desired approximation. This process may be thought of as one of simulation of the boundary layer in the potential-flow calculation.

Four methods for simulating the presence of a boundary layer in both two-dimensional and three-dimensional potential flow are contained in a fundamental paper by Lighthill [5]. Two of these are much more commonly used than the other two and appear to have a clearer physical significance. These are the two procedures that have been included in the present study. They are illustrated in Figure 2. In the first method, which will be denoted that of surface displacement (Lighthill's designation is flow reduction), the boundary-layer displacement thickness is added to the original body in the direction along the local normal to the body surface. Thus, a thicker body is produced. The potential flow about this modified body is the desired modified potential flow that approximates viscous flow. In the second method a surface blowing distribution is defined in such a way that the dividing streamline of the flow is the same as the modified body used in the first method above. (Lighthill's designation is equivalent sources.) The potential flow about the original body subject to this nonzero normal-velocity boundary condition on the body surface is the desired modified potential flow that approximates the viscous flow. In both simulation methods the displacement thickness is the only boundary-layer quantity that affects the modified potential flow, although this may require some involved calculations in the truly three-dimensional case.

6.3 The Wake

The procedures put forward by Lighthill [5] assume that the boundary-layer is simulated not only on the body surface but also in the wake, i.e., everywhere viscous effects are important. Thus, in the surface blowing method of section 6.2, a suction velocity distribution is utilized along the semi-infinite wake. In the surface displacement method the thickened modified body should be augmented by a thin semi-infinite solid extension representing the wake displacement thickness. This last procedure can lead to numerical instabilities in the source panel method and certainly yields increased computing time. It probably would be better to use the suction simulation of the wake even with the surface displacement method. In any case accounting for viscous effects in the wake would greatly complicate calculation of the modified potential flow.

The possible difficulties expressed in the previous paragraph are somewhat academic, because there is a more serious problem connected with simulating the wake. At present there are no accurate procedures available for calculating viscous wakes behind lifting airfoils, so there is no accurate means for obtaining the wake displacement thickness. Of course, an approximate wake displacement-thickness distribution could be used for all bodies, on the theory that small differences in the wake cannot greatly affect the flow on the body surface. It is customary, however, to make an even stronger assumption, namely that the wake can be neglected completely without significantly affecting the lift and pressure distribution on the body. Published two-dimensional [2], [3] methods neglect the wake. As part of the present study, calculations were performed for a two-dimensional airfoil with and without a wake, on which the displacement thickness had been determined experimentally (section 7.3). Differences in the computed lifts and pressure distributions were quite small. Accordingly, it is concluded that the wake may be safely neglected in calculating lift and pressure distribution and the present method takes advantage of this simplification.

6.4 Sequential Use of the Potential-Flow and Boundary-Layer Methods

The simulation schemes of section 6.2 define the modified potential flow that approximates viscous flow in terms of the boundary-layer displacement thickness. This last must be obtained from a boundary-layer method, which

requires as input the velocity distribution at the edge of the boundary layer. This velocity distribution is not the velocity distribution obtained by an inviscid-flow technique for flow about the body without the boundary layer. Rather it is the velocity distribution corresponding to flow about the body with the boundary layer already simulated. Thus, the key flow quantities are mutually dependent: the displacement thickness is calculated from the edge-velocity distribution, which in turn is calculated from the modified potential flow which depends on the displacement thickness.

The standard remedy for this dilemma is iteration. To fix ideas consider the surface displacement method of boundary-layer simulation. (The procedure for the surface-blowing simulation is similar.) This method can be used iteratively as follows. First calculate potential flow about the actual body shape. Second, use the resulting surface velocity distribution as input to a boundary-layer method. Third, add the resulting displacement thickness to the body to obtain a modified body. Fourth, calculate potential flow about the modified body, and iterate the entire procedure until convergence is obtained. Experience in two dimensions [2] has shown that usually several iterations are required for convergence. This can be time-consuming (see section 6.5) and adds an element of uncertainty to the calculation.

It is very tempting to terminate the above process after one iteration; i.e., obtain displacement thickness from the inviscid velocity distribution on the actual body, add this to the body to obtain the modified body, and use the inviscid velocity distribution on this first modified body as the approximation to viscous flow. How legitimate is this simplification? Or, equivalently, how closely does the displacement thickness calculated from the inviscid velocity distribution on the body approximate the actual displacement thickness? Since surface velocities are not radically changed by adding the displacement thickness to the body, it would appear that the above is a reasonable procedure. The main objection to the above is that there is one location at which addition of the displacement thickness does significantly change the surface velocity. If the aft end or "trailing edge" of the body or airfoil is not cusped, i.e., is either blunt or subtends a nonzero angle, the inviscid velocity there is theoretically zero. After the displacement thickness has been added to the body, the velocity at the trailing edge is near that of the free stream — a large change but a very local one. The preceding objection

is not valid for a body with a cusped trailing edge where the inviscid velocity is near free-stream or for any body on which the velocity distribution near the trailing edge is "faired out" to eliminate the very local stagnation region. The situation is unclear for this case. Van Dyke [6] treats this problem from a fundamental standpoint by means of matched asymptotic expansions, but unfortunately only for the case of a flat plate at zero angle of attack. For this simple case, the conclusion is that iterating the above boundary-layer simulation procedure is not justified.

When the panel method of [1], [4] is used to calculate flow about an airfoil or other body, velocity is not calculated at the trailing edge itself. The nearest point to the trailing edge where velocity is calculated is the middle of the panel whose downstream edge is the trailing edge. In three-dimensional cases, computing time restraints dictate that no more than about 60 panels be used on a wing section, so that the midpoints of the panels adjacent to the trailing edge are at least one-percent of the airfoil chord away from the trailing edge. Because of the local nature of the trailing-edge stagnation region, the velocity at these midpoints is about 90 percent of free-stream velocity. Thus because of the crudeness of the numerical representation, all airfoils, even those with finite trailing-edge angles, have velocity distributions similar to those on cusped airfoils. Therefore, as a practical matter, iteration of the boundary-layer simulation procedure is of questionable value in calculating lifts and pressure distributions.

A limited number of two-dimensional cases were run using the above iterative procedure. No consistent gain in accuracy was achieved by iteration compared to the results obtained after one iteration. Thus, none of the cases presented below continued the iterations past the first.

6.5 Comparison of Computational Aspects of the Two Boundary-Layer Simulation Methods

From the discussion of section 6.4, it is evident that the procedure for approximating a viscous flow by a potential flow with boundary-layer simulation requires at least one boundary-layer calculation and two potential-flow calculations: flow about the actual body and the modified potential flow. (If the process were iterated n times, it would require n boundary-layer and $(n + 1)$ potential-flow calculations.) This is true for either method of

boundary-layer simulation. However, the required computational effort is not the same for the two methods. A procedure based on surface blowing is faster, because the second potential-flow calculation (and all subsequent potential-flow calculations if iteration is used) can use many of the quantities computed during the first potential-flow calculation.

The basic panel-method calculation [1], [4] consists of two major parts, which together comprise over 90 percent of the required computing time. The first is the calculation of the "matrix of influences" that express the velocities induced by the panels on each other. The second is solution of a set of linear equations for the singularity strengths on the panels. Both the "matrix of influences" and the coefficient matrix of the linear equations have order equal to the total number of panels, and both matrices are "full," i.e., neither contains a large number of zeros.

The basic difference between the two methods of boundary-layer simulation is that the surface blowing method leaves the geometry of the body unchanged and changes the boundary condition (from zero to nonzero normal velocity), while the surface displacement method leaves the boundary conditions unchanged but changes the geometry. Both the "influence-matrix" and the coefficient matrix of the linear equations depend only on the geometry. Thus, when calculating the modified potential flow, the surface displacement procedure must recalculate these matrices; while the surface blowing procedure need not. Moreover, if a direct matrix solution, e.g., Gaussian elimination, is used to solve the linear equations, information equivalent to the inverse of the coefficient matrix can be saved from the first potential-flow solution and used in the modified potential flow for the surface blowing procedure where the matrices remain unchanged. The result is that the procedure based on surface blowing requires only a little more computing time than a single potential flow solution (even if iteration is used). On the contrary the procedure based on surface displacement must perform a completely new calculation for the modified potential flow, and thus the computing time is doubled compared to a single inviscid case. (If n iterations are used the factor is $n + 1$.) The above assumes all computing times, including that of the boundary-layer method, are small compared to the potential-flow computing time. This appears to be a good approximation. If an iterative matrix solution is used for the linear equations, both boundary-layer simulation procedures must solve the

linear equations for the modified potential flow from the beginning. In that case the computational advantage of the surface blowing procedure comes only from not having to form new matrices. It is evident that the surface blowing method of boundary-layer simulation is much preferable to the surface displacement method from the standpoint of computing time.

6.6 Application of the Kutta Condition

As was pointed out in the Introduction, the effect of an essentially unseparated boundary layer has an important effect on the flow field only for lifting bodies, i.e., wings. The essence of this effect is that the boundary-layer changes the circulation about the airfoil and thus its lift. That this is the most important effect has been demonstrated in two dimensions by performing inviscid calculations at the same lift coefficient as the experiments rather than the same angles of attack. The resulting calculated pressure distributions are indistinguishable from the corresponding experimental ones.

In an analytic or computational method the circulation about a wing or airfoil is determined by applying the so-called Kutta condition at the sharp trailing edge. Thus, it is fair to say that the present method is calculating the effect of the boundary layer on the Kutta condition. The fundamental basis of the Kutta condition lies in the fact that for any angle of attack of the onset flow there is a unique value of circulation that renders the inviscid velocity finite at the trailing edge. This criterion can be applied directly in an analytic method by examining the flow singularities and determining what value of circulation is necessary to make them "cancel out." However, a computational procedure cannot handle infinite quantities directly and other criteria, theoretically equivalent to the Kutta condition, must be applied. Several choices may be made for this "equivalent" criterion, as is discussed at some length in [4]. Because of the crucial role played by the Kutta condition in determining the boundary-layer effects on lift and thus on pressure distribution, it is possible that various choices of this criterion could lead to somewhat different solutions. This matter has not been studied at length. However, it is important to define precisely the way in which the Kutta condition is applied in the present work to facilitate possible future comparisons with alternate approaches.

Since a fluid cannot support a pressure discontinuity, the pressure on the lower surface of an airfoil must approach the same limit at the trailing edge as the upper-surface pressure does. It turns out that this fact may be used as an alternate criterion for the Kutta condition. In the present method the numerical implementation of this requirement is accomplished by equating the pressures at the "midpoints" of the upper and lower surface panels adjacent to the trailing edge, as shown in Figure 3. (In three-dimensional cases a "midpoint" is the centroid of the area of the panel.) This is the procedure that has been used for several years with the method of [1], [4] and has been found to have certain advantages compared to other methods of applying the Kutta condition for the case of inviscid flow [4].

6.7 Form of the Surface Vorticity

The present method is basically a surface-source technique because the source strengths on the panels are mutually adjusted to give zero normal velocity at the panel midpoints. In lifting cases, however, vorticity is required to produce circulation. Theoretically, the "chordwise" distribution (i.e., distribution along the length of the wing or airfoil in the stream direction) is immaterial. All chordwise vorticity distributions should produce the same lift and pressure distribution after the Kutta condition has been satisfied. This is the case in both two and three dimensions. In practice, of course, some vorticity distributions have more favorable numerical properties than others. The present method utilizes vorticity distributed on the body surface (as opposed to inside the body). There are two chordwise variations of vorticity available as options. In the first, the vorticity strength is simply constant all around the airfoil surface. In the second, the vorticity varies parabolically with arc length around the airfoil section in such a way that it approaches zero at the trailing edge from both the upper and the lower surface [4]. The choice of surface-vorticity option can have an effect on the calculated circulation in some cases, and this is of some importance.

A detailed study was conducted to determine the effect of the surface vorticity options (among other things) on the calculated flow about several airfoils [7]. This study was two-dimensional, but the panel numbers used to approximate the airfoils were typical of those used in three-dimensional cases. Of course, only inviscid calculations were considered, i.e., there were no

boundary-layer corrections. The basic conclusions were: (1) that the constant vorticity distribution gives a more accurate solution for all airfoils having a finite trailing-edge angle, and (2) that for airfoils with cusped trailing edges including the so-called "supercritical" airfoils, the constant vorticity distribution leads to errors near the trailing edge, and the parabolic vorticity distribution is preferable. More recent work has shown that the constant distribution gives better results even in some cusped cases if the approach to the cusp is sufficiently local. Thus, in doubtful situations the constant vorticity distribution is to be preferred.

It is important to mention that a user of the present three-dimensional method need not use general rules to decide on the form of the vorticity distribution. He may run his particular airfoil section with both vorticity options as a two-dimensional case, inviscid or with boundary layer, and see which option gives the better results. The cost of the two-dimensional cases are negligible. Examples of this procedure are shown in section 8.0.

7.0 TWO-DIMENSIONAL STUDIES

7.1 General Remarks

As part of the present work a series of two-dimensional studies were conducted to learn as much as possible about the problem of simulating viscous flow by a combined potential-flow boundary-layer method without incurring the expense of three-dimensional computing times. These two-dimensional studies were restricted to cases whose results have a direct bearing on the corresponding three-dimensional problem. In particular, the panel numbers used were those that are feasible for three-dimensional cases about 30-60 around the airfoil surface. Furthermore, the so-called "higher-order" potential flow technique [7] was not employed, because it is not yet available in three-dimensions. A large amount of two-dimensional experience previously obtained [2] was judged not appropriate for the present purpose because the panel numbers employed were in the range 100-150. Accordingly, it should be emphasized that the accuracies of the inviscid solutions presented below are by no means typical of the two-dimensional panel technique used to its full power. Even with these relatively small panel numbers the higher-order technique will yield about an order of magnitude more accuracy.

7.2 Point-Number Requirements for the Boundary-Layer Program

In three-dimensional potential flow the number of panels used for a calculation is dictated largely by considerations of economy. Typically, 30-60 panels are used around a wing section at each particular spanwise location (lifting strip in Figure 1). On the contrary, the number of points at which inviscid velocity must be input to the boundary-layer program is dictated largely by considerations of computational accuracy. To determine what kind of input should be furnished the boundary layer program a series of two-dimensional calculations were performed for a 10percent thick RAE 101 airfoil at an inviscid lift coefficient of 0.985 for a Reynolds number of 1.6 million. The standard of comparison was the distribution of displacement thickness on the upper surface of the airfoil - the crucial side for the present application. Cases were run using potential flow panel numbers of 26, 52, and 102 around the airfoil with velocities corresponding to each panel midpoint input to the boundary-layer program. Further calculations used more complicated procedures, which involved inputting velocity distributions

corresponding to one case at the locations corresponding to another case, e.g., velocity from the 102 panel case input at locations corresponding to midpoints of the 26 element case and vice-versa. Some cases were run by inputting the boundary-layer parameter $[\beta = (x/U_e)(dU_e/dx)]$ at each point instead of velocity. In all about a dozen different cases were run. The results are shown in Figure 4. All calculations except the very crude 26-panel case yield displacement thickness distributions that lie in a narrow band that appears to represent a kind of irreducible noise level. In particular this band includes a case where the potential flow velocity obtained from the 26-panel case was interpolated to 102 locations (51 on each of the upper and lower surfaces) for input into the boundary-layer program. Because this procedure appears to be as accurate as any and is much cheaper, it has been adopted for the three-dimensional strip-theory technique of Section 8.0. Specifically, the potential flow velocities are obtained from the number of panels input, which are chosen on economic grounds. Interpolation is then used to obtain velocities at 50 chordwise points on both the upper and the lower surface at each spanwise station on the wing. The distribution of the 50 points has been fixed as one that gave good results for the case of Figure 4.

7.3 Effect of the Wake

As discussed in Section 6.3 the theory underlying the simulation of boundary-layer effects in potential flow calls for simulating the displacement thickness not only on the body, but also along the wake. Since this cannot be done accurately with current methods, the hope is that the wake effect is negligible. To test this possibility, calculations were performed for a particular airfoil with the wake accounted for and with the wake ignored.

The airfoil is an 11.8-percent thick symmetric Joukowski for which experimental displacement thickness distributions are available on the body surface and in the wake [10]. Calculations were performed with 54 panels for an angle of attack of 6-degrees at a Reynolds number of 0.4 million. In addition to the inviscid solution, three viscous simulations were considered, each with a different assumption concerning the wake: (1) wake ignored, (2) wake at 0° along the extension of the trailing edge, and (3) wake at 6° inclination with respect to the trailing edge, i.e., parallel to the free

stream. In cases (2) and (3) the experimental wake displacement thickness was used to define a suction distribution on the wake. On the body the displacement thickness calculated from the inviscid velocity distribution was used in the simulation. Both surface displacement and surface blowing methods of boundary-layer simulation were used on the body, but the wake in both simulations used a suction distribution.

Results are shown in Figure 5, which shows the airfoil and wake geometries for the two cases and compares calculated and experimental displacement thicknesses. These last are seen to be in fairly good agreement. The main data of the figure are the calculated values of lift coefficient for the various procedures. It can be seen that the presence or absence of a wake has a very small effect on lift with either method of boundary-layer simulation. Accordingly, it is ignored in all subsequent calculations.

7.4 Results for Selected Airfoils

7.4.1 RAE 101

Calculations were performed for a 10-percent thick symmetric RAE 101 airfoil at 8.2 degrees angle of attack using 52 panels. Figure 6 compares calculated inviscid pressure distributions obtained using constant and parabolic vorticity distributions with an "exact" solution obtained by conformal mapping techniques. The constant-vorticity solution is clearly the more accurate, as had been found previously for airfoils with finite trailing edges [7].

Figure 7 presents viscous pressure distributions and lift coefficients obtained for both methods of boundary-layer simulation using the constant vorticity distribution and compares these with experimental results obtained at a Reynolds number of 1.6 million. Both methods of boundary-layer simulation give quite good values for the viscous lift coefficient and reasonable pressure distributions. When experimental uncertainties are taken into account it may be said that the two methods of boundary-layer simulation are about equally accurate with the displacement solution slightly preferable.

Figure 8 shows the same set of results as Figure 7 only for a parabolic vorticity distribution. Again both methods of boundary-layer simulation give solutions of approximately the same accuracy, but the results are spoiled by

the erroneously high values of inviscid lift predicted by the panel method with parabolic vorticity distribution. The predicted change in lift due to viscosity is somewhat too small by both simulation methods, but by far the bigger source of error is due to the erroneously high lift level of the inviscid solution.

7.4.2 64A010

A study similar to that of Section 7.4.1 was performed for a 64A010 airfoil at 8-degrees angle of attack using 40 surface panels. Figure 9 compares calculated inviscid solutions with an exact solution. As before the use of a constant surface vorticity distribution gives a rather accurate solution considering the low panel number, but the use of a parabolic surface vorticity distribution gives a value of lift that is significantly too high.

Figure 10 presents viscous pressure distributions and lifts obtained for both methods of boundary-layer simulation with a constant surface vorticity distribution and compares these with experimental values obtained at a Reynolds number of 4.1 million. The change in lift due to viscosity is about half as large as that found in Section 7.4.1. Again both simulation methods lead to solutions of about equal accuracy, which is fairly good.

7.4.3 Symmetric Joukowski

As an example of a cusped airfoil a symmetric 11.8-percent thick Joukowski at 6 degrees angle of attack was selected. Experimental data are available in [10]. Figure 11 compares calculated inviscid pressure distributions obtained using 54 elements with the exact conformal-mapping solution. As had been previously reported [7], the use of a constant surface vorticity distribution gives a pressure distribution that has a fictitious "crossing" in the vicinity of the trailing edge and thus a value of lift that is considerably too low. The solution obtained using a parabolic surface vorticity distribution is considerably more accurate. It avoids the "crossing" of pressure in the trailing-edge region and gives a considerably more accurate value of lift coefficient, although it is too large.

Figure 12 presents viscous pressure distributions and lifts for both methods of boundary-layer simulation obtained with a constant surface vorticity distribution and compares these with experimental results obtained at a Reynolds

number of 0.4 million. As might be expected, the fact that the calculated value of the inviscid lift coefficient is considerably too low leads to calculated viscous lift coefficients that are also considerably too low and thus renders both calculated solutions rather inaccurate. Note that the inviscid lift is less than the experimental. Although pressure distributions for both simulations agree closely over most of the chord, the blowing simulation has a larger error in the trailing edge region, which leads to a significantly lower lift coefficient.

Figure 13 compares calculated pressure distributions and lifts obtained using a parabolic surface vorticity distribution with the same experimental data that was shown in Figure 12. It can be seen that both methods of boundary-layer simulation give lift coefficients in very good agreement with experiment and pressure distributions that agree quite well with each other but that deviate somewhat from experiment on the lower surface. However, the overall accuracy of the calculations is quite good and much better than the constant-vorticity calculations.

7.5 Conclusions

Based on the results of the above two-dimensional studies, several conclusions may be made. With the exception of the statement marked with an asterisk (*) these conclusions apply to the three-dimensional case also, and their consequences have been used in the following section on three-dimensional techniques.

1. In the present application the potential-flow calculation dominates the computing time of a combined potential flow boundary-layer method.
2. For good accuracy input to the boundary-layer program should consist of potential-flow velocities at about 50 stations along each of the upper and lower surfaces of the airfoil, even if these are obtained by interpolation from fewer potential-flow stations.
3. The displacement thickness in the wake can be ignored with a negligible effect on lift and surface pressure distribution.

4. The potential-flow panel method with a constant surface vorticity distribution gives a more accurate solution than with a parabolic vorticity distribution for airfoils with finite trailing-edge angles.
5. For airfoils with cusped trailing edges the use of a parabolic vorticity distribution may give considerably better accuracy than use of a constant vorticity distribution. (As is shown in the next section, for some cusped airfoils there is little to choose between the two forms of the vorticity distribution.)
- *6. Both methods of boundary-layer simulation give about equally accurate results for the simulated viscous flow, and this accuracy is quite good.

General Conclusion: With all the approximations involved in the calculation of viscous flow by a combined potential-flow boundary method there is a certain limit on accuracy attainable. Attempts to refine a method beyond this limit are doomed because they will be in the "noise level."

8.0 A THREE-DIMENSIONAL PROCEDURE BASED ON A STRIP-THEORY BOUNDARY-LAYER METHOD

8.1 General Remarks

Perhaps the simplest way to construct a fully-automatic procedure for calculating three-dimensional viscous effects is by combining a three-dimensional potential-flow method with a two-dimensional boundary-layer method applied in a "strip-theory" fashion. This is also about as accurate a procedure as can be constructed for many applications considering the above-mentioned accuracy limitations of combined potential-flow boundary-layer methods. Certainly there are some applications, such as wing tips and wing-fuselage intersections, where three-dimensional effects dominate the problem. For such cases more elaborate boundary-layer methods are required. For many common configurations, such as wing-fuselages for transport aircraft, the procedure of this section appears to be generally satisfactory. Accordingly, this procedure has been given more attention than any other in the present study. It is anticipated that it will be the design "workhorse" method, because of its stability and simplicity. Thus Section 8.0 is the central one of this report, and the comparison Sections 8.4 and 8.5, present the most important information, namely experimental verification of the validity of this approach.

The basic reason that the strip-theory boundary-layer procedure is so simple and stable is that the two-dimensional boundary-layer method requires as input from the potential-flow method only a table of surface velocity versus arc length - information that the potential-flow program has readily available. (Additional input consists solely of a few control numbers, such as Reynolds number.) Three-dimensional boundary-layer methods require considerable additional information (Section 9.0).

Even for the simple strip-theory boundary-layer procedure there are several compatibility problems connected with "marrying" two such major programs as the three-dimensional potential flow and the two-dimensional boundary-layer methods. The philosophy was adopted that such problems would be resolved in the simplest possible way to maximize the stability of the combined program, even at the expense of some additional inaccuracy. This

policy takes advantage of the fact that many other areas of approximation are already inherent in the procedure.

8.2 Some Aspects of the Three-Dimensional Potential-Flow Panel Method

The potential flow method used in the present study is the panel method of [4]. In the interest of brevity, this method is not described here in any detail. Familiarity with the general calculational philosophy of panel methods is assumed, and [4] is available for specifics. Nevertheless it seems worthwhile to outline some features of the method of [4] that dictate some of the procedures adopted in the present study.

The principal input to the method of [4] consists of coordinates of a set of points that define the surface of the body about which flow is to be computed. The input of these points is organized so that they successively define a set of "section curves" lying in the surface. Usually but not always, each such curve is planar and lies at a constant value of one of the coordinates. For example, it is customary to define a wing by successively defining sections each at a particular spanwise location. Whether they are planar or not, curves formed by connecting successive input points are designated "N-lines" (Figure 1). Obviously, the logic of the input must determine which input points belong to each N-line so that distinct section curves are defined. This procedure is among the details of the method to be found in [4]. Surface panels are generated from groups of four input points - two consecutive points on an N-line and the two corresponding points on the next N-line. Thus each N-line is involved in the formation of two "strips" of panels (Figure 1), namely the two strips lying on either side of the N-line. Most input points are used in the formation of four panels. (The exceptions are the points around the edges of the body.) Among the geometric quantities calculated for each panel are the coordinates of the centroid of the panel area - the so-called "midpoint" where the zero normal velocity boundary condition is applied and where surface velocity and pressure are eventually calculated.

The logic of the procedure divides the total configuration into lifting and non-lifting portions (Figure 1). A lifting portion is characterized by having a sharp trailing edge where a Kutta condition is to be applied and from

which issues a trailing vortex wake. Thus, a bound vorticity distribution must be provided on a lifting portion. Non-lifting portions have no bound vorticity and no trailing wake. (They may, however, turn out to be subject to a non-zero force.) To facilitate application of the Kutta condition in the manner of Figure 3, the N-lines on the lifting portion must be input beginning at the trailing edge, proceeding around the airfoil section, and ending at the trailing edge, on the non-lifting portion the N-lines are unrestricted. For the case of a fuselage the most common form of input takes the N-lines as planar cross-section curves normal to the fuselage axis. This, however, is not what the present method requires (Section 8.3).

Once the input has been accomplished, the panel method then proceeds to the major parts of the calculation. It forms a "matrix of influences" that expresses the velocities induced by the panels at each others midpoints, solves a set of linear equations for the values of source density on the panels, and calculates velocities and pressures at the midpoints of all panels. Some consequences of this calculation logic are discussed in Section 6.5.

8.3 General Description of the Combined Potential-Flow Boundary-Layer Method

8.3.1 The Initial Potential-Flow and Boundary-Layer Calculation

The user of the method inputs the points defining the surface, the onset flow (angle of attack), Reynolds number, and a small number of control quantities. First the method calculates the ordinary inviscid lifting flow about the configuration in the manner described in [4] and outlined above in Section 8.2. From these results inputs for the two-dimensional boundary-layer program [8] are prepared.

The boundary-layer program requires a table of surface velocity versus arc length beginning with a stagnation point (which of course is always present on a two-dimensional airfoil). A three-dimensional body such as the wing-fuselage of Figure 1, has only one stagnation point, at the nose of the fuselage. However, there is no intention of calculating the boundary-layer on the wing starting at the nose of fuselage. In the strip-theory formulation of this section the velocity distribution of each lifting strip of elements is

input to the boundary-layer program as a two-dimensional distribution. The initial point of the distribution is taken as the location of the "stagnation line" on that strip. This may be defined as the location near the leading edge where the flow divides, part passing under the wing and part passing over it. Computationally, this location is found by taking the dot product of the velocity at the midpoint of each panel with the average of the unit tangent vectors of the two N-lines bordering the panel. This dot product changes sign exactly once on each lifting strip. The desired "stagnation point" is obtained by interpolation with respect to values of the dot product between the midpoints on either side of the sign change. Arc lengths are computed between successive midpoints and between the "stagnation points" and the adjacent midpoints. Then by addition two arc length tables are constructed, both of which start at the "stagnation point". One table gives arc length corresponding to successive midpoints on the upper surface of the strip back to the trailing edge. The second does the same for the lower surface midpoints. Each value of arc length in these tables is associated with the value of total inviscid surface velocity at the corresponding midpoint. The velocity at the "stagnation point", which is also the origin of arc length, is input as zero, even though the velocity there has a non-zero value, which depends mainly on the sweep angle of the leading edge. In this way two tables of velocity versus arc length are formed. By means of certain interpolation routines these tables are "enriched" up to 50 entries on each of the upper and the lower surfaces. It is these latter tables that are input into the finite difference boundary-layer program [8]. Thus two boundary-layer calculations are performed for each lifting strip.

For non-lifting strips it is assumed that the user has input the generating N-lines in such a way that the midpoint of the first element of the strip may be taken as the stagnation point. For example, in the configuration of Figure 1, this requires that the N-lines on the fuselage be input from nose to tail. The velocity at the first midpoint is set to zero regardless of its calculated value. Then a table of arc lengths and total surface velocities is input to the boundary layer program. There is only one boundary-layer calculation for each non-lifting strip.

The input order required for non-lifting strips is incompatible with the usual procedure of inputting fuselage cross-sections as mentioned in Section 8.2. This latter form of input is so convenient that a special provision has been made to simply omit boundary-layer calculation on non-lifting portions at the user's option. This is compatible with the fact mentioned in the Introduction that unseparated boundary layers on non-lifting bodies have very little effect on the flow. Indeed the wing-fuselage cases of Section 8.5 used this option.

Using the input data described above, the boundary-layer program computes two-dimensional boundary layers on all strips. The method [8] provides the user with the option of prescribing the transition location or allowing the program to calculate it by Michele's criterion. Normally, the latter option is used, but the former might be used if it was desired to compare the calculated results with experimental data obtained using transition strips.

After the boundary layers have been calculated on all strips, considerable information, such as momentum thickness and wall shear, is available at the 50 points used in the calculation. This information is output. (Velocity profiles are not saved, but this could be done with a resulting huge increase in output.) Interpolation routines are used to obtain displacement thicknesses at the panel midpoints from those of the 50 "enriched" locations.

While the present method is applicable to "essentially unseparated" flow it may be that the boundary-layer method calculates separation near the trailing edge of a strip. At such a point the boundary-layer calculation must cease, and there will be no boundary-layer output downstream of this point. The combined program continues, however, using fictitious values of displacement thickness downstream of separation all the way to the midpoint of the panel adjacent to the trailing edge. These fictitious values are obtained by linear extrapolation from the values of displacement thickness at the two midpoints just upstream of separation. The boundary-layer output informs the user of the locations of any separations, so he may judge the validity of this extrapolation.

8.3.2 Surface Displacement Simulation

In this simulation the displacement thickness is added normal to the body surface. The basic rule is that a panel is translated parallel to its normal vector by an amount equal to the value of displacement thickness calculated at its midpoint. Symbolically, if Δx , Δy , Δz are the changes of the coordinates of a point on the panel, n_x , n_y , n_z the components of its unit normal vector, and δ^* the calculated displacement thickness, then

$$\begin{aligned}\Delta x &= \delta^* n_x \\ \Delta y &= \delta^* n_y \\ \Delta z &= \delta^* n_z\end{aligned}\tag{1}$$

If x_k , y_k , z_k , $k = 1, 2, 3, 4$ are the original coordinates of the corner points of a panel and x_k^* , y_k^* , z_k^* the new coordinates, then

$$\begin{aligned}x_k^* &= x_k + \Delta x \\ y_k^* &= y_k + \Delta y \\ z_k^* &= z_k + \Delta z\end{aligned}\tag{2}$$

This modification is performed for all panels.

When the above calculation has been carried out, edges of adjacent panels that used to be coincident (or essentially coincident as explained in [4]) have been moved apart (Figure 14) or, what is the same thing, a point on an N-line that used to be a vertex (essentially) for two consecutive panels of the strip no longer has that distinction, but has been replaced by two points, each representing the displacement of the original point by a different amount (δ^* on the two elements) and in a different direction (normal vectors on the two elements). A single point on the N-line is regained by simply averaging these two points. The process is illustrated in Figure 14.

Similarly when all panels have been treated in the above manner the single N-line that used to lie between two strips of elements has been replaced by two N-lines, each of which results from displacements corresponding to one of the strips. This situation is remedied by averaging corresponding points on these N-lines to produce a single N-line.

Thus finally a complete new set of N-lines and input points is produced that describes the modified body. These are input into the panel method, and a second potential flow is calculated. This serves as an approximation to the viscous flow. Since two complete potential flows are calculated and all other portions of the calculation are fast, the computing time required for the above procedure is about twice that of an ordinary potential-flow calculation.

8.3.3 Surface Blowing Simulation

In this simulation a surface blowing distribution is defined. The prescribed normal velocity V_n at any point is

$$V_n = \frac{d}{ds} (V \delta^*) \quad (3)$$

where V is the total inviscid tangential velocity from the initial potential-flow calculation and where s is the arc length along the curve joining the midpoints of the panels on the strip. This is the two-dimensional formula [5], and is compatible with the strip-theory approach.

The calculation proceeds as described in 8.3.1 to obtain tables of arc length s , total (inviscid) surface velocity V , and displacement thickness δ^* at the midpoints of all panels of each strip beginning with the "stagnation point" and proceeding to the trailing edge (or aft end for non-lifting portions). Define the quantity q as

$$q = V \delta^* \quad (4)$$

then it is dq/ds that is desired at all midpoints. Let subscript k denote the value of a quantity associated with the k th midpoint of strip, where $k = 0$ denotes the "stagnation point" and $k = K$ denotes the midpoint of the panel adjacent to the trailing edge. The numerical differentiation formula for q is based on fitting a parabola through three successive points. Specifically

$$\left(\frac{dq}{ds}\right)_k = \frac{q_k - q_{k-1}}{s_k - s_{k-1}} \left[1 - \frac{s_k - s_{k-1}}{s_{k+1} - s_{k-1}}\right] + \frac{q_{k+1} - q_k}{s_{k+1} - s_k} \left[1 - \frac{s_{k+1} - s_k}{s_{k+1} - s_{k-1}}\right]$$

$$k = 1, 2, \dots, K-1 \quad (5)$$

$$\left(\frac{dq}{ds}\right)_K = \frac{s_K - s_{K-1}}{(s_{K-1} - s_{K-2})(s_K - s_{K-2})} q_{K-2} - \frac{s_K - s_{K-2}}{(s_{K-1} - s_{K-2})(s_K - s_{K-1})} q_{K-1} + \frac{2 s_K - s_{K-1} - s_{K-2}}{(s_K - s_{K-2})(s_K - s_{K-1})} q_K \quad (6)$$

The above equations (3), (5), and (6) define a blowing distribution, i.e., a set of non-zero normal velocities at all the panel midpoints. The potential flow corresponding to this boundary condition is calculated. All matrices from the initial potential-flow calculation have been saved: the "matrix of (velocity) influence", the coefficient matrix of the linear equations, and information equivalent to the inverse of this matrix. This last (equivalent inverse) is used with a new "right side", the above normal-velocity distribution, to obtain a new set of values of surface source density on the panels. These are simply added to the corresponding values obtained for the uniform onset flow at the given angle of attack to produce a modified source distribution. This last now replaces the uniform-flow distribution in the Kutta-condition procedure to obtain a new set of bound vorticity strengths ("spanwise circulations") and thus new lift- and pressure distributions. This additional calculation requires a negligible computing time compared to the initial potential-flow calculation. Thus computing time for the combined potential-flow boundary-layer program is not substantially greater than that for an inviscid calculation.

8.4 Comparison of Calculated Results for Isolated Wings with Experimental Data

For any new method of flow calculation the most important criterion by which it is judged is how well its predictions agree with real flow. Thus comparisons of calculated and experimental results are essential and should be made, not just for one or two cases, but for as many configurations and flow conditions as possible. This experimental verification is especially necessary for the present method, because of the several areas of approximation involved. Experience with the analogous two-dimensional method has shown that conclusions can vary depending on the number of panels employed. Thus all cases presented used panel numbers that are felt to be realistic for three-dimensional cases.

The first cases considered are two isolated swept wings, both of which have the same planform, which is shown in Figure 15a. Also indicated in this figure are the panel numbers used. Eight lifting strips have been used across the semi-span, as shown in Figure 15a, and 30 panels have been used around the airfoil sections, as shown in Figures 15b and 15c. Thus a total of 240 panels are used on the right half of each wing with the left accounted for by symmetry. Both these airfoil sections have finite trailing-edge angles. Thus, as discussed in Section 6.7 and [7] and illustrated in Figures 6 and 9, the use of a constant surface vorticity distribution is to be preferred. This could have been verified explicitly by running the airfoils of Figures 15b and 15c as two-dimensional cases, but it was felt that the evidence previously obtained was sufficient.

8.4.1 Symmetric Swept Wing

The swept wing with symmetric airfoil section that is defined by Figures 15a and 15b is the geometry that has been most thoroughly investigated. Calculations have been made at 4.1° and 8.2° angles of attack, although only the 8.2° results are shown here, because that is the more extreme condition. Moreover, both surface displacement and surface blowing methods of boundary-layer simulation have been employed.

Figures 16 and 17 compare calculated and low-speed experimental [11] results for a Reynolds number of 18 million based on mean aerodynamic chord. The more important figure is Figure 16, which shows force coefficients, while Figure 17 shows pressure distributions. Not only are forces usually the quantities of main interest, but it is in the force calculation where the effect of viscosity shows up most clearly. From the lift distributions and values of total lift presented in Figure 16 it can be seen that in this case the method based on the surface displacement simulation of the boundary layer is remarkably effective in predicting viscous flow. Essentially all of the experimentally obtained 12 percent loss of lift compared to the inviscid value is accounted for by the calculation, and the spanwise distribution is given correctly as well. By contrast the method based on the surface blowing simulation of the boundary layer grossly underpredicts the effect of viscosity. The calculated loss of lift is only a small fraction of the

experimental one. Figure 17 shows pressure distributions at approximately mid semi-span. The pressures there are typical of all span locations. The above observations generally apply to the pressure distributions as well as the lifts. It is simply a fact that viscous effects are less conspicuous in pressure distributions.

8.4.2 Cambered Twisted Wing

Calculations have been performed for the cambered twisted swept wing illustrated by Figures 15a and 15c. The total amount of twist from the symmetry plane to the wing tip is 5 degrees. In view of the above results only the surface displacement method of boundary-layer simulation has been employed for this case.

Figures 18 and 19 compare calculated and low-speed experimental results [12] for a Reynolds number of 12 million based on mean aerodynamic chord. Figure 18 again shows that the calculations are quite accurate in predicting the effect of viscosity on lift distribution and total lift. The calculated viscous pressure distribution of Figure 19 is somewhat less accurate, but is still a considerable improvement over the inviscid pressure distribution. The results are essentially the same at all spanwise locations.

8.5 Comparison of Calculated Results for Wing-Fuselages with Experimental Data

Wing-fuselages have been given the main emphasis in the present study. Such configurations are complicated enough to illustrate the generality of the method, yet are simple enough to avoid taxing the limits on panel number and/or computing time. Moreover, wing-fuselages are interesting cases for the designer. Four wing fuselages are considered below. Two have wings with finite trailing-edge angles, and two have so-called "supercritical" wing sections, which have cusped trailing edges. For these latter, two-dimensional investigations were conducted to determine whether the constant vorticity distribution or the parabolic vorticity distribution yields the more accurate solution. These investigations illustrate the procedure that may be followed by a user. It is interesting that of the two cases considered the parabolic distribution was more accurate for one and the constant distribution for the other.

In the comparisons discussed below the quantities of most importance are the lift distributions across the wing and the total lifts of the configuration. In all cases the total lift includes the lift on the fuselage. As mentioned in Section 8.3.1 it is often more convenient to ignore displacement-thickness on the fuselage, and account for it only on the wing. This procedure has been followed in all four cases shown below. All panel numbers in the following subsections refer to the right half of the configuration only. Symmetry is used to account for the left half [1,4].

In three of the four cases, those in subsections 8.5.2, 8.5.3, and 8.5.4, the experimental results were obtained at a Mach number of 0.5. At this rather low Mach number compressibility effects are not too important. Nevertheless an approximate compressibility correction based on a Goethert transformation has been applied to the calculated results.

8.5.1 A Straight Wing on a Round Fuselage

The first wing-fuselage to be considered is that shown in Figure 20. The wing has a rectangular planform and a symmetric 9 percent thick RAE 101 airfoil section. It is mounted as a midwing on the fuselage. This case was selected because it has previously been considered by several other investigators, e.g., [13], and it thus provides a means for comparing different methods. While the geometry of the configuration is relatively simple, it has all the essential features of any wing fuselage. Moreover the test data, to which the calculated results are compared, were obtained at the very low Reynolds number of 0.31 million based on wing chord. Thus viscous effects are rather large, and the comparison represents a severe test of the present method. Since the airfoil section of the wing is virtually the same as that of Figure 6 (9 percent thick versus 10 percent thick), a constant vorticity distribution around the wing sections has been used in the calculations. Geometric representation for this case consists of: 8 strips of panels on each wing, 28 panels around the wing section on each strip, and 270 panels on the fuselage - a total of 494 panels.

Figures 21 and 22 compare calculated results for both methods of boundary-layer simulation with low-speed experimental data [14] for an angle of attack of 6 degrees. The large viscous effect in this case is evident in

Figure 21, which shows the experimental lift value to be approximately 20 percent lower than the inviscid lift. This loss of lift is predicted rather well by the present method using the surface displacement method of boundary-layer simulation. The spanwise lift distribution is also predicted quite well. The surface blowing method of boundary-layer simulation accounts for about half of the lift loss. This is considerably better than the results for the swept wing (Figure 16), but is still not good enough. Comparing the results of Figures 16 and 21 with the two-dimensional results of Section 7.4, where the two simulation methods yield approximately equal accuracy, suggests the speculation that in some manner wing sweep and aspect ratio contribute to the very small lift losses predicted by the surface blowing simulation.

Figure 22 compares calculated and experimental pressure distributions at a typical spanwise location (60 percent semispan). The pressure distribution obtained by the surface displacement method agrees very well with experiment, except for the downstream half of the lower surface where it agrees more nearly with the inviscid pressure distribution. The pressure distribution obtained by the surface blowing simulation method generally "splits the difference" between the inviscid and viscous pressure distributions.

8.5.2 Conventional Swept Wing Mounted Low on a Fuselage

The second wing-fuselage is a low-wing configuration, as shown in Figure 23. Also shown in Figure 23 is the wing airfoil section, which is seen to be a conventional one with a finite trailing edge angle. Thus in view of the two-dimensional results of Section 7.4, the calculated results use a constant vorticity distribution around the wing sections. Wind tunnel tests were conducted by Douglas personnel for this configuration at 6 degrees angle of attack, a Mach number of 0.5 and a Reynolds number of 6.25 million based on mean aerodynamic chord. Calculations have been performed for this case using the surface displacement method of boundary-layer simulation. Panel distributions are: 8 lifting strips on the wing, 32 panels per strip around the wing section, and 135 fuselage panels - a total of 391 panels.

Figures 24 and 25 compare calculated and experimental results for spanwise lift distributions and for pressure distributions at a typical spanwise station (60 percent semispan), respectively. It appears from Figure 24 that the loss

of lift due to viscosity has been overestimated in the calculations by a factor of about two. However, closer examination indicates that the inviscid and the experimental results are too close together, i.e., based on experience the loss of the lift represented by the difference between the inviscid and the experimental lift distributions appears to be too small. The fault could lie either in the data or in the inviscid calculations. One possible source of error in the calculations is the compressibility correction. It was noticed that the inclusion of compressibility increased the lifts from their incompressible values far less than, for example, the increases noted for the wing-fuselages discussed in the next two subsections. While explanations can be postulated, it must be stated that at present the discrepancies between calculation and experiment for the wing-fuselage of this subsection are unexplained.

8.5.3 Supercritical Swept Wing Mounted High on a Fuselage

The third wing-fuselage is a high wing configuration as shown in Figure 26. Also shown is the wing airfoil section, which is of the so-called "supercritical" type that has been shown to possess favorable transonic characteristics. Such airfoils have cusped trailing edges, and thus the proper surface vorticity distribution to use must be determined by investigation. Calculations have been performed in which the airfoil section of Figure 26 is considered to be a two-dimensional airfoil represented by 40 surface panels at 7.02 degrees angle of attack (the condition used in the test described below). Figure 27 compares the two-dimensional pressure distributions and lifts obtained using both surface vorticity variations with the exact values obtained by conformal mapping. While the calculated total lifts and pressure distributions are about equally accurate, the form of the two calculated pressure distributions are quite different. The constant vorticity distribution gives better results in the midchord region, but the parabolic vorticity distribution gives better results in the neighborhood of the trailing edge. In the trailing-edge region the pressure distribution for the constant vorticity distribution almost "crosses" in the manner of Figure 11 and as a result lies considerably "inside" the exact curve. The trailing edge region is crucial for the present application where the principal result is a change of lift due to an altered Kutta condition. On this basis the parabolic vorticity variation was selected

for this case. To further verify this selection a simplified three-dimensional case was calculated, which even more strongly indicated the superiority of the parabolic-vorticity approach in the trailing edge region.

Wind tunnel tests were conducted by Douglas personnel for the configuration of Figure 26 at 7.02 degrees angle of attack, a Mach number of 0.5 and a Reynolds number of 6.25 million based on the mean aerodynamic chord of the wing. Calculations for this configuration have been performed using the surface displacement method of boundary-layer simulation and a geometric specification consisting of: 11 lifting strips of panels on the wing, 40 panels around the airfoil section on each strip, and 278 panels on the fuselage - a total of 718 panels.

Figure 28 compares calculated and experimental spanwise lift distributions and total lifts. The agreement of the calculated viscous solution with the data is quite remarkable except for a small region near the wing-fuselage intersection. Discrepancies in this region could be due to use of a strip-theory boundary-layer procedure or to neglect of the fuselage boundary layer. The loss of lift due to viscosity seems suspiciously large in this case and may imply the presence of compensating errors. However, it is known that the viscous effect on lift is larger for supercritical airfoils than for conventional airfoils. Figure 29 compares calculated and experimental chordwise pressure distributions near mid-semispan, where the results are typical of those at all spanwise locations. The calculated viscous pressure distribution agrees with experiment very well.

8.5.4 A Supercritical Transport Configuration

The fourth wing-fuselage considered is a supercritical transport configuration as shown in Figure 30, which also shows the airfoil section used for the wing. This is of the "supercritical" type, but is a rather different design from the airfoil of subsection 8.5.3. A comparison of Figures 26 and 30 shows that the trailing edge cusp is considerably less pronounced for the wing of the present subsection. This difference is quite important for the numerical procedure.

To determine which surface vorticity distribution is more effective, two-dimensional calculations at 2.06 degrees angle of attack have been run for the airfoil of Figure 30 using 62 surface panels. Pressure distributions and lifts calculated for each of the surface vorticity distributions are

compared with exact conformal-mapping in Figure 31. It is seen that use of a constant vorticity distribution gives a slightly more accurate value of lift and more accurate pressures in the region of midchord. This is similar to the airfoil of subsection 8.5.3. The difference occurs in the trailing edge region. In contrast to the results of the previous subsection, Figure 30 shows that the pressure distribution near the trailing edge is only slightly less accurate using constant vorticity than using parabolic vorticity. Virtually none of the previously observed "crossing" tendency is evident in Figure 30. Certainly the small additional discrepancies associated with the constant vorticity distribution in the trailing-edge region are not expected to affect the Kutta condition to any significant degree. Thus the constant vorticity distribution is preferable in this case, because of its more accurate lift and its simpler numerical implementation. It has been used in the three-dimensional calculations.

The present method has been applied to the configuration of Figure 30 using: 8 lifting strips of panels on the wing, 62 panels around the wing section on each strip, and 172 panels on the fuselage - a total of 668 panels. Experimental data for this configuration was obtained by Douglas personnel for an angle of attack of 2.06 degrees, a Mach number of 0.5, and a Reynolds number of 4.07 million based on mean aerodynamic chord.

Figure 32 compares calculated and experimental spanwise lift distributions and total lifts. Again the rather large loss of lift (approximately 20 percent in this case) due to viscous effects that appears to be inherent in supercritical configurations is evident. The calculated lift distribution with viscous correction is barely distinguishable from the data. Pressure comparisons at mid-semi span are shown in Figure 33, and here also the agreement of calculation and experiment is most gratifying. The fact that the calculated viscous pressure distribution agrees with experiment in the trailing-edge region justifies the choice of constant vorticity a posteriori.

8.6 Conclusions

Based on the results of the three-dimensional comparisons with experiment discussed in Sections 8.4 and 8.5, some conclusions can be made concerning

the present method of calculating viscous flow by combining a three-dimensional potential-flow method [4] with a two-dimensional boundary-layer method [8] applied in a strip theory sense.

1. The constant surface vorticity distribution should be used for all wings with finite trailing-edge angles.
2. For wings with cusped trailing edges two-dimensional calculations should be performed to decide whether the constant or the parabolic vorticity distribution should be used in the three-dimensional calculations.
3. The surface displacement method of boundary-layer simulation should be used in all cases.

General Conclusion: Used with above options the method of this section appears to be accurate in calculating three-dimensional lifting viscous flow about wings and wing-fuselages.

Recommendation: Effort should be directed toward remedying the deficiencies in the surface blowing method of boundary-layer simulation, so that this faster procedure may be used in the future.

9.0 A THREE-DIMENSIONAL PROCEDURE BASED ON A SMALL-CROSS-FLOW BOUNDARY-LAYER METHOD

9.1 General Remarks

It appears, from the results of the previous section, that in many cases of design interest three-dimensional effects enter mainly through the inviscid flow, not through the boundary-layer flow. Nevertheless, it was decided to pursue methods based on three-dimensional boundary-layer techniques; both to help determine the limits of validity of the method of Section 8.0, and to provide a more general alternative in cases where that method proves inapplicable. This undertaking is complicated by the fact that use of three-dimensional boundary-layer methods is fraught with difficulty. There are fundamental problems, such as definitions and criteria for separation and transition, as well as more mundane problems, such as calculation of surface streamlines and curvatures. To minimize these difficulties, the most general three-dimensional boundary-layer methods were not considered, but rather a method based on an assumption of small cross-flow velocity normal to the inviscid streamlines was employed [15]. In the interest of brevity, this method will not be described here, but ref. [15] will be relied on. Use of such a method may be considered intermediate between the strip-theory of Section 8.0 and a fully general method. However, use of this method involves most of the complications and problems associated with fully general techniques. Thus, many of the routines developed will prove useful when general three-dimensional techniques are considered. On the other hand, the presence of these problems cause frequent complications in trying to use the program. While these can usually be overcome, it cannot be said that the combined method of this section is a fully automatic procedure in the sense that the method of Section 8.0 is. Rather, the method of this section has proved the feasibility of attempting sophisticated "patchings" of three-dimensional potential-flow and boundary-layer methods. Moreover, the method may be applied as it stands by a user who understands the inherent difficulties, although some "man-in-the-loop" interaction may be required.

9.2 Surface Coordinates

Among the requirements of the three-dimensional boundary-layer method [15] are the inviscid surface streamlines and to calculate these, the discretized panel representation of the surface must be abandoned and a smooth representation

substituted. This necessity has been ignored by some investigators, who thus obtained kinked streamlines of limited usefulness, while other investigators were driven to excessively elaborate reformulations of the problem in an attempt to obtain the requisite smoothness. The approach adopted here is somewhat different. The panel discretization defines quantities such as velocity, normal vector, or surface coordinates only at the midpoints and/or corner points of the panels. Values of quantities at other points of the surface are obtained by interpolation in such a way that all variations are smooth. Thus, the panel discretization disappears from the problem. The penalty for accomplishing this is the necessity for an interpolation routine in two independent variables. Such a routine is far from trivial and indeed represents a major program in its own right. The interpolation procedure incorporated in the present method is based on cubic splines.

In order to accomplish the required interpolation, two independent surface coordinates must be defined in such a way that values can be assigned to all panel midpoints and corner points. Moreover, all quantities of interest must be single-valued functions of these coordinates. For example, ordinary Cartesian coordinates are unsuitable. As discussed in the Introduction, a lifting wing is the case on which the present investigation has concentrated. Accordingly, surface coordinates have been defined that are well-adapted to this case, but they can be used for any body, presumably with some deterioration in accuracy.

Suppose a wing is defined by input points on several N-lines, as shown in Figure 34. The first surface coordinate u is constant along N-lines with zero value on the first N-line (wing tip). Each strip of panels is assigned an average width w_k , $k = 1, 2, \dots, K$. The constant value of u on the $(k + 1)$ th N-line is then denoted u_k and is defined by

$$\begin{aligned} u_0 &= 0 \\ u_k &= \sum_{m=1}^k w_m, \quad k = 1, 2, \dots, K \end{aligned} \tag{7}$$

In the usual case the N-lines defining a wing are planar curves, each at a constant value of spanwise location (Figure 34). Thus, each w_k can be set

equal to the actual physical width of the strip, and u is a true spanwise coordinate, which represents distance from the wing tip. However, if the N-lines converge or diverge slightly, the representation is still valid, because u is, simply, an interpolation coordinate and need not have physical significance.

The second surface coordinate v represents arc length measured around an N-line beginning at the lower-surface trailing edge and proceeding along the lower surface to the leading edge and back to the trailing edge along the upper surface. The total arc length of the $(k+1)$ th N-line is denoted L_k , and this quantity is computed by the program of [4]. Thus, the v -coordinate of the upper surface trailing edge on the $(k+1)$ th N-line is L_k . In "uv-space" the wing is as sketched in Figure 35.

The above defines uv-coordinates for points on the N-lines and thus, in particular, for the corner points of the panels. It is necessary to define a means for finding uv coordinates at any point of a panel, but it is necessary to evaluate these coordinates only for the midpoint of a panel. Consider a trapezoidal surface panel as shown in Figure 36. An orthogonal distance coordinate system $\xi\eta$ has been constructed in each panel, where η denotes distance measured normal to the parallel sides, and ξ denotes distance parallel to these sides [4]. The origin of coordinates is the panel midpoint. Each panel side lies at a constant value of the η coordinate, say η_1 for the side between points 1 and 2 and η_3 for the side between points 4 and 3. Each of these sides also lie along an N-line, and thus each has a constant value of the u -coordinate, u_k for the side between points 1 and 2 and u_{k+1} for the side between points 4 and 3. It is natural to require that every interior line parallel to the parallel sides of the panel (i.e., any $\eta = \text{constant}$ line) should have a constant value of u coordinate. This defines u for interior points as

$$u = u_0 + m_u \eta \quad (8)$$

where

$$m_u = -\frac{u_{k+1} - u_k}{w} = \frac{u_k - u_{k+1}}{\eta_1 - \eta_3} \quad (9)$$

$$u_0 = \frac{\eta_1 u_{k+1} - \eta_3 u_k}{w} \quad (10)$$

It should be pointed out that $w = \eta_1 - \eta_3$ is the physical panel width and is not equal to w_k unless the input N-lines lie in parallel planes (the usual case). Definition of the v -coordinate is somewhat more arbitrary. Since v is arc length along an N-line, it also denotes distance along each of the parallel sides measured from some origin. Thus, v varies linearly along $\eta = \eta_1$ and $\eta = \eta_3$, and it was decided to require it to vary linearly along the $\eta = \text{constant}$ line. This condition implies

$$v = v_0(\eta) + \xi \quad (11)$$

Along side 12

$$v = L_F + \xi - \xi_1 \quad \eta = \eta_1 \quad (12)$$

Along side 43

$$v = L_S + \xi - \xi_4 \quad \eta = \eta_3 \quad (13)$$

In each case the L denotes total arc along the N-line up to the initial point 1 or 4 (see [4]). Linear interpolation in η then gives the required form as

$$v = \xi + m_v \eta + v_0 \quad (14)$$

where

$$m_v = -\frac{1}{w} [L_S - \xi_4 - L_F + \xi_1] \quad (15)$$

$$v_0 = -\frac{1}{w} [(L_F - \xi_1)\eta_3 - (L_S - \xi_4)\eta_1] \quad (16)$$

The only values of u and v that are actually used in the calculation are those corresponding to the midpoint, u_0 and v_0 , equations (10) and (16).

9.3 Surface Velocity Components

The potential-flow panel method [4] yields Cartesian velocity components with respect to a reference coordinate system in which the complete body is defined. On each element these may be resolved in an elementary way, into components V_ξ and V_η parallel to the ξ and η axes, respectively (that is parallel and normal to the parallel sides of the panel). Then by differentiating equations (8) and (14) with respect to time, what amounts to u

and v velocity components may be obtained in the form

$$\frac{du}{dt} = m_u V_n = F(u_0, v_0) \quad (17)$$

$$\frac{dv}{dt} = V_\xi + m_v V_n = G(u_0, v_0)$$

These values, which are, of course, associated with the point u_0, v_0 , are used to compute streamlines.

9.4 Streamline Computation

Equations (17) apply only to panel midpoints. However, when the complete set of midpoint values have been obtained, a two-variable interpolating routine can be used to evaluate the right-side sides of (17) and any values of u and v . Thus, conceptually a first-order system of two differential equations is produced.

$$\begin{aligned} \frac{du}{dt} &= F(u, v) \\ \frac{dv}{dt} &= G(u, v) \end{aligned} \quad (18)$$

where the variable t , which has the physical significance of time, may be considered to be a dummy variable of integration.

A streamline calculation is initiated at the midpoint of every panel that lies adjacent to the wing trailing edge. Thus, there are twice as many streamlines as lifting strips of panels. A standard Runge-Kutta routine is applied to (18). Every evaluation of the functions $F(u, v)$ and $G(u, v)$ is accomplished by means of the interpolation routine. The streamline calculation is terminated when the streamline either: (1) leaves the wing, e.g., at the wing tip, or (2) reaches the "stagnation line" near the wing leading edge. This last is defined as the locus of relative minima of velocity magnitude.

Because of the various calculations that need to be performed, a total of nineteen quantities are required as functions of u and v at each point of every streamline. All these quantities are obtained by the interpolation routine from their values at the panel midpoints. In addition to du/dt

and dv/dt the other required quantities are: Cartesian coordinates of the point (for arc length calculation); Cartesian and $\xi\eta$ velocity components (for velocity magnitude, $F(u,v)$ and $G(u,v)$ calculations); and the nine Cartesian components of three mutually orthogonal unit vectors, one normal and two tangent to the surface (for projecting points into the local tangent plane).

9.5 Curvature Calculation

The small-cross-flow boundary-layer method [15] requires, as input, the velocity magnitude as a function of arc length along the streamline and also the geodesic curvature of the streamline and of the orthogonals to the streamline. For any curve lying in the surface the geodesic curvature at any point can be defined as the two-dimensional curvature of the projection of the curve into the tangent plane of the surface at that point. Thus, for each streamline point, the preceding and succeeding streamline points are projected into the tangent plane, a circle passed through the three coplanar points, and the curvature of the circle used for the geodesic curvature of the streamline at the central point.

To compute the orthogonal to the streamline at each point, a velocity is defined that is orthogonal to the surface velocity there by the relations

$$v_{\xi} = -V_{\eta} \quad , \quad v_{\eta} = V_{\xi} \quad (19)$$

These velocity components are used in (17) to obtain du/dt and dv/dt for the orthogonal curve, and a one-point Runge-Kutta calculation is performed in each direction ($\pm dt$). The two points thus obtained are projected into the tangent plane and a circle passed through them and the streamline point to obtain the geodesic curvature of the orthogonal.

9.6 Boundary-Layer Calculation and Simulation

A small-cross-flow boundary-layer calculation [15] is performed for each streamline beginning with the "stagnation line." Of the several difficulties involved in this calculation, perhaps care with the starting values and specification of transition locations are worthy of mention. If for any reason the boundary-layer calculation terminates, e.g., separation, quantities of

interest are linearly extrapolated to the trailing edge. The result of the calculation is a complete set of boundary-layer data at all streamline points. These data are output.

The simulation of boundary-layer effects is accomplished by defining a modified potential flow according to the ideas of Lighthill [5]. Either a surface displacement or a surface blowing simulation may be used, but, in view of the results of Sections 8.4 and 8.5, only the former has been incorporated into the program. It is consistent with the assumption of small-cross-flow velocity magnitude to neglect the three-dimensional integral terms of [5] and simply add the calculated displacement thickness to the surface. First, displacement thicknesses at the panel midpoints are obtained by "back interpolation" using an altered version of the interpolation routine and then new input points are obtained from these in the manner described in Section 8.3.2. Finally, another potential-flow calculation is performed starting with the new input points.

As may be inferred from the above, the final combined program is rather complicated, consisting as it does of an assemblage of several large programs. Figure 37 presents a block diagram showing the sequence of calculation. The major programs involved are shown as large boxes. All interfaces between programs require certain routines, which are omitted for simplicity. As might be expected, the computing time for the program of this section is longer than for the surface-displacement option of the method of Section 8.0. It is about 50 percent longer for small panel numbers. For larger panel numbers, the percent increase is not as great.

9.7 Calculated Results

To illustrate the use of the program of this section, calculations were performed for the swept wing with symmetric airfoil section described in Section 8.4. The panel distribution used is the same one described there.

Figure 38 shows the calculated streamlines superimposed on the wing planform. The lower surface streamlines are asymptotic to the "stagnation line" on the lower surface. Streamlines of the upper surface go around the wing leading edge, and the portions of these streamlines on the lower surface are shown dotted to reflect this fact. While the lower-surface streamlines

deviate markedly from the stream direction, the upper-surface streamlines do not. Since it is the development of the boundary layer on the upper surface that largely determines the viscous correction, the results for this case are expected to be not very different from the strip-theory results of Section 8.41.

Figure 39 compares calculated displacement thicknesses at the midpoints of the last panels on the upper surface obtained by the method of Section 8.0 and the method of this section. It can be seen that the small cross-flow boundary-layer procedure gives a somewhat thinner boundary layer but that the difference is not excessive and the spanwise distribution is the same. (The "bump" in the curve near 25 percent semi-span is undoubtedly due to numerical error.) Much of the problem is due to the fact that the surface pressure distribution (Figure 17) contains a narrow high peak. This type of variation is a very difficult one for the interpolation routine, which tends to "round down" the peak at intermediate points. Thus the pressure peak on a streamline may be considerably lower (less negative) than the peak on a streamwise strip of elements, unless by chance a point of the streamline lies very near the pressure peak on a strip. It is believed that this phenomenon is largely responsible for the low and somewhat erratic values of displacement thickness shown in Figure 39. Clearly this matter deserves further study.

Calculated values of section lift coefficient are shown in Figure 40. It can be seen that the method of this section and that of Section 8.0 give virtually identical results. Based on Figure 39 it would be expected that the lifts calculated by the method of this section would be nearer to the inviscid values than those of the strip-theory method, but this turned out not to be the case. At present no explanation is known for this result. However, it points up once again that there is a residual "noise level" in combined potential-flow boundary-layer calculations, which defeats attempts to refine the calculations past a certain degree of accuracy.

10.0 REFERENCES

1. Hess, J.L.: Review of Integral-Equation Techniques for Solving Potential-Flow Problems with Emphasis on the Surface-Source Method. *Computer Methods in Applied Mechanics and Engineering*, Vol. 5, No. 2, March 1975.
2. Callaghan, J.G. and Beatty, T.D.: A Theoretical Method for the Analysis and Design of Multi-Element Airfoils. *J. of Aircraft*, Vol. 9, No. 12, December 1972.
3. Dvorak, F.A. and Woodward, F.A.: A Viscous/Potential Flow Interaction Analysis Method for Multi-Element Infinite Swept Wings. NASA CR 2476, 1974.
4. Hess, J.L.: The Problem of Three-Dimensional Lifting Potential Flow and Its Solution by Means of Surface Singularity Distribution. *Computer Methods in Applied Mechanics and Engineering*, Vol. 4, No. 3, November 1974. (A somewhat more complete description of the method is contained in McDonnell Douglas Report MDC-J5679, October 1972.)
5. Lighthill, M.J.: On Displacement Thickness. *J. of Fluid Mech.*, Part 4, 1958.
6. Van Dyke, M.: *Perturbation Methods in Fluid Dynamics*. Academic Press, New York, 1964.
7. Hess, J.L.: The Use of Higher-Order Surface Singularity Distributions to Obtain Improved Potential-Flow Solutions for Two-Dimensional Lifting Airfoils. *Computer Methods in Applied Mechanics and Engineering*, Vol. 5, No. 1, February 1975.
8. Cebeci, T. and Smith, A.M.O.: *Analysis of Turbulent Boundary Layers*. Academic Press, New York, 1974.
9. Keller, H.B. and Cebeci, T.: Accurate Numerical Procedures for Boundary-Layers. II. Two-Dimensional Turbulent Flows. *AIAA Journal*, Vol. 10, No. 9, September 1972.
10. Piers, W.J. and Slooff, J.W.: Calculation of the Displacement Effect in Two-Dimensional Subsonic Attached Flow Around Airfoils. Examples of Calculations Using Measured Displacement Thicknesses. NLR TR 72116U, 1972.
11. Kolbe, C.D. and Boltz, F.W.: The Forces and Pressure Distributions at Subsonic Speeds on a Plane Wing Having 45° of Sweepback, an Aspect Ratio of 3, and a Taper Ratio of 0.5. NACA RM A51G31, October 1951.
12. Boltz, F.W. and Kolbe, C.D.: The Forces and Pressure Distributions at Subsonic Speeds on a Cambered and Twisted Wing Having 45° of Sweepback, an Aspect Ratio of 3, and a Taper Ratio of 0.5. NACA RM A52D22, July 1952.

13. Labrujere, Th.E., Loeve, W., and Slooff, J.W.: An Approximate Method for the Calculation of the Pressure Distribution on Wing-Body Combinations at Subcritical Speeds. AGARD Conference Proceedings No. 71, Aerodynamic Interference, September 1970.
14. Körner, H.: Untersuchungen zur Bestimmung der Druckverteilung an Flügel-Rumpf-Kombinationen. Teil I: Messergebnisse für Mitteldeckeranordnung aus dem 1, 3 m-Winkanal. Bericht 69/21 Braunschweig, 1969. (DFVLR-Bericht Nr. 0562).
15. Cebeci, T.: Calculation of Three-Dimensional Boundary Layers. I. Swept Infinite Cylinders and Small Cross Flows. AIAA J., Vol. 12, No. 6, June 1974 (Also McDonnell Douglas Report No. MDC-J5694, November 1972.)

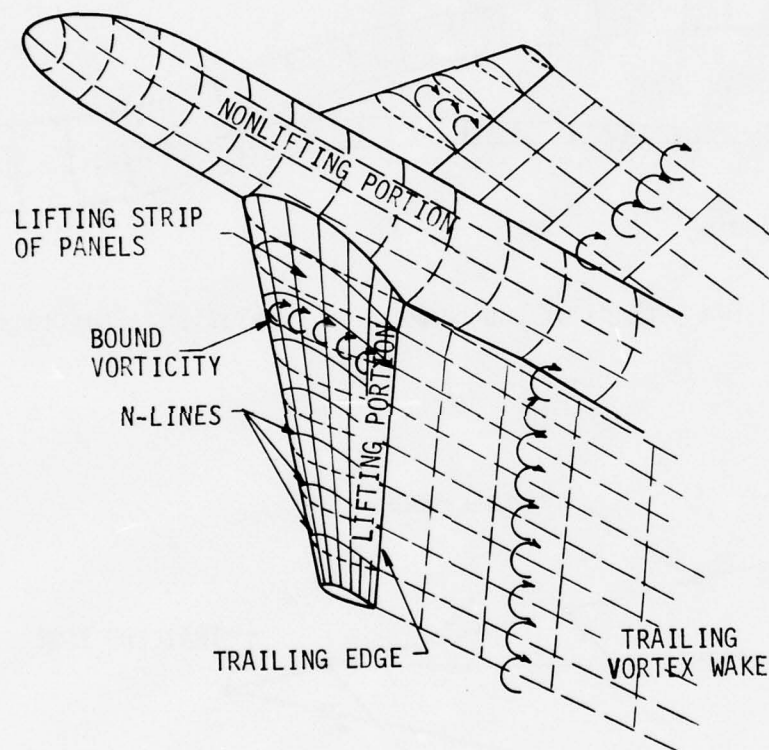


Figure 1. Representation of a three-dimensional lifting configuration.

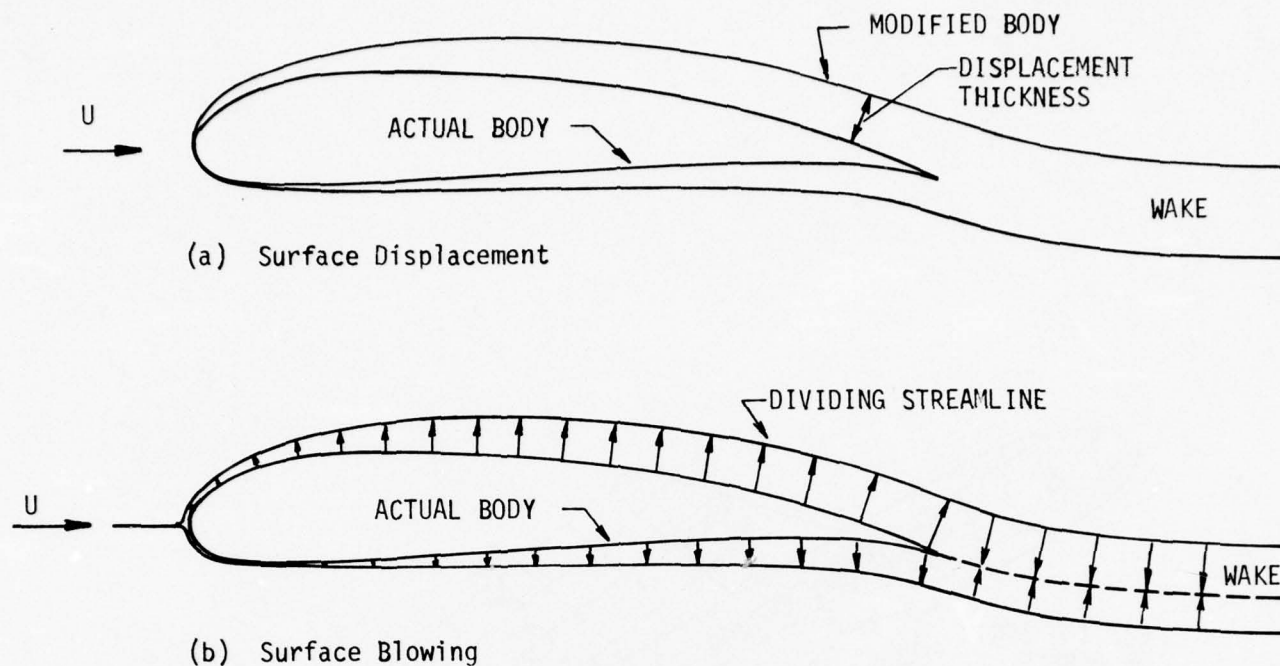


Figure 2. Two methods of boundary-layer simulation. (Not to scale.)

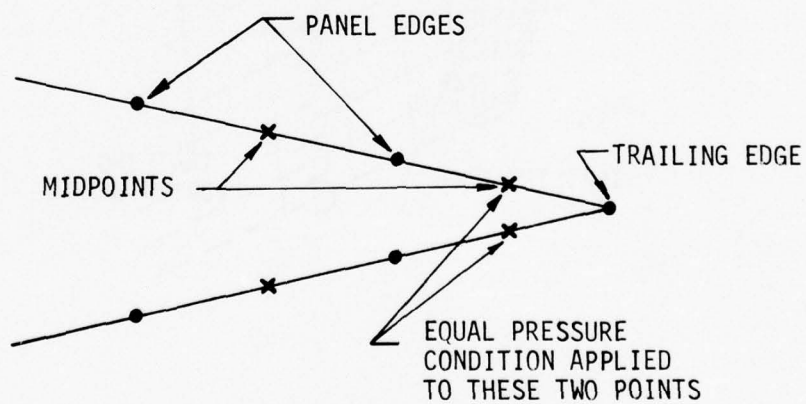


Figure 3. Application of the Kutta condition.

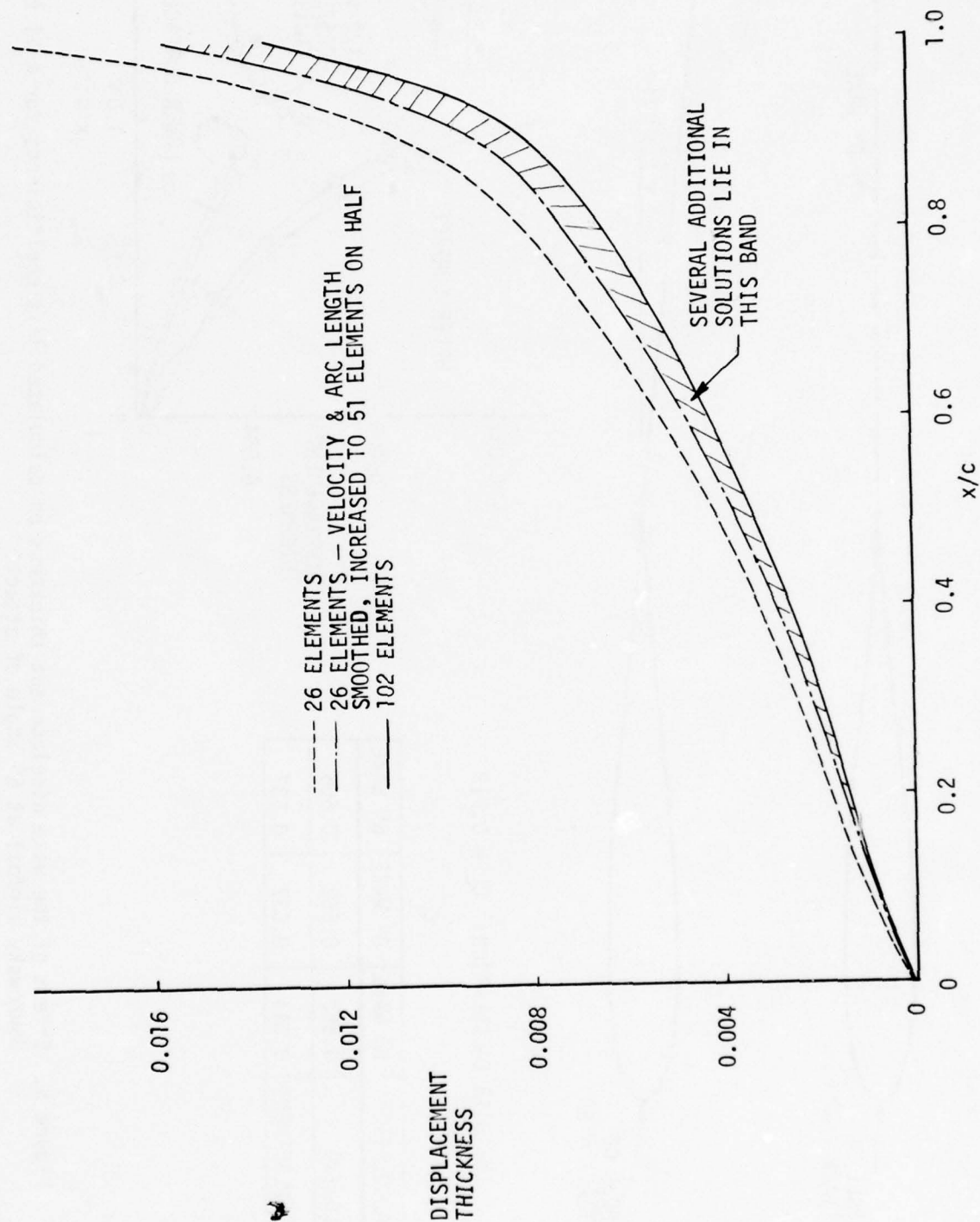
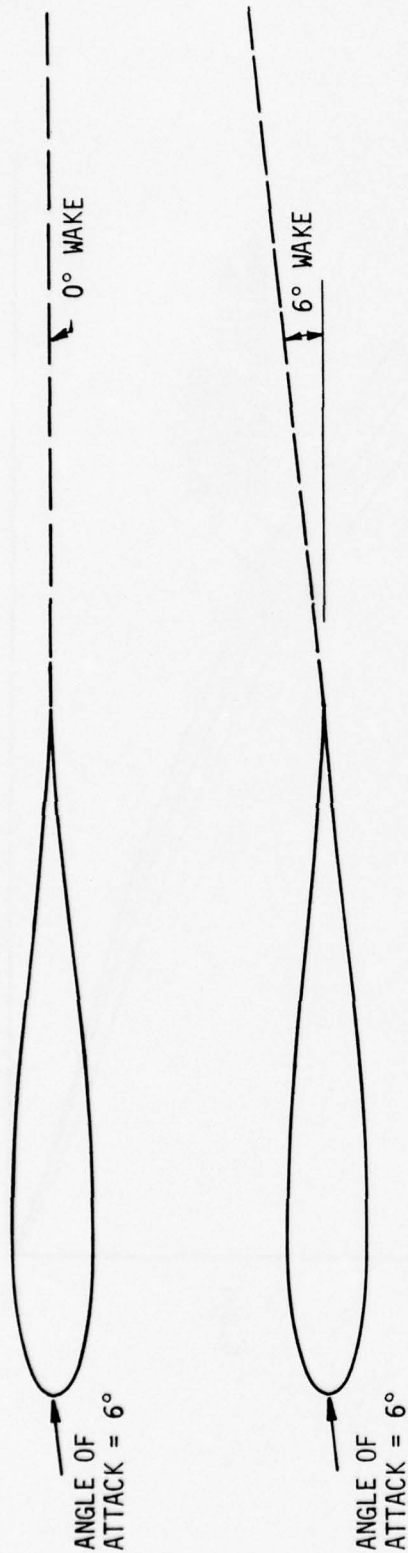


Figure 4: Calculated upper-surface displacement-thickness distributions on an airfoil obtained using various point numbers.



INVISCID CALCULATION: $C_L = 0.713$

CALCULATION	C_L		
	NO WAKE	0° WAKE	6° WAKE
BLOWING	0.662	0.662	0.666
DISPLACEMENT	0.644	0.637	0.637

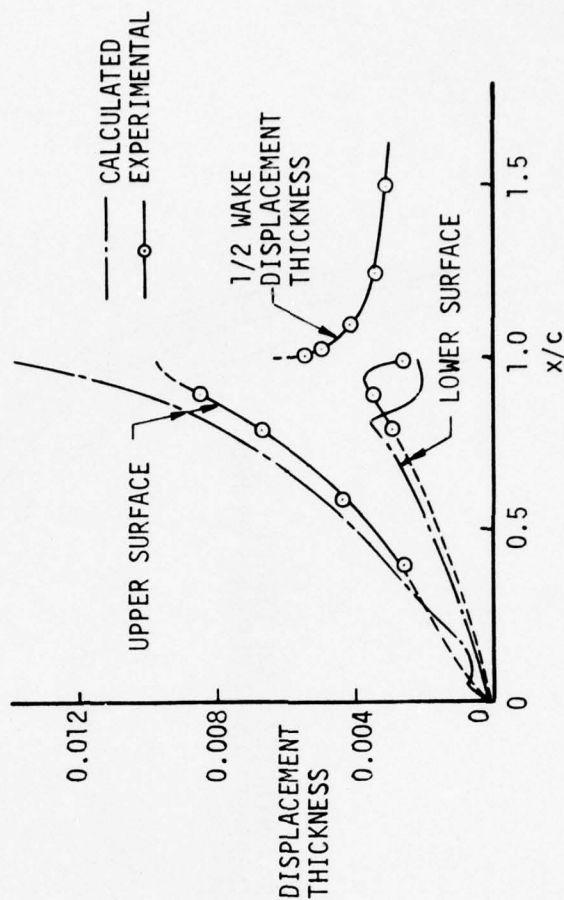


Figure 5. Effect of the wake displacement thickness on calculated lift coefficients for a 11.8%-thick Joukowski airfoil at 6° angle of attack.

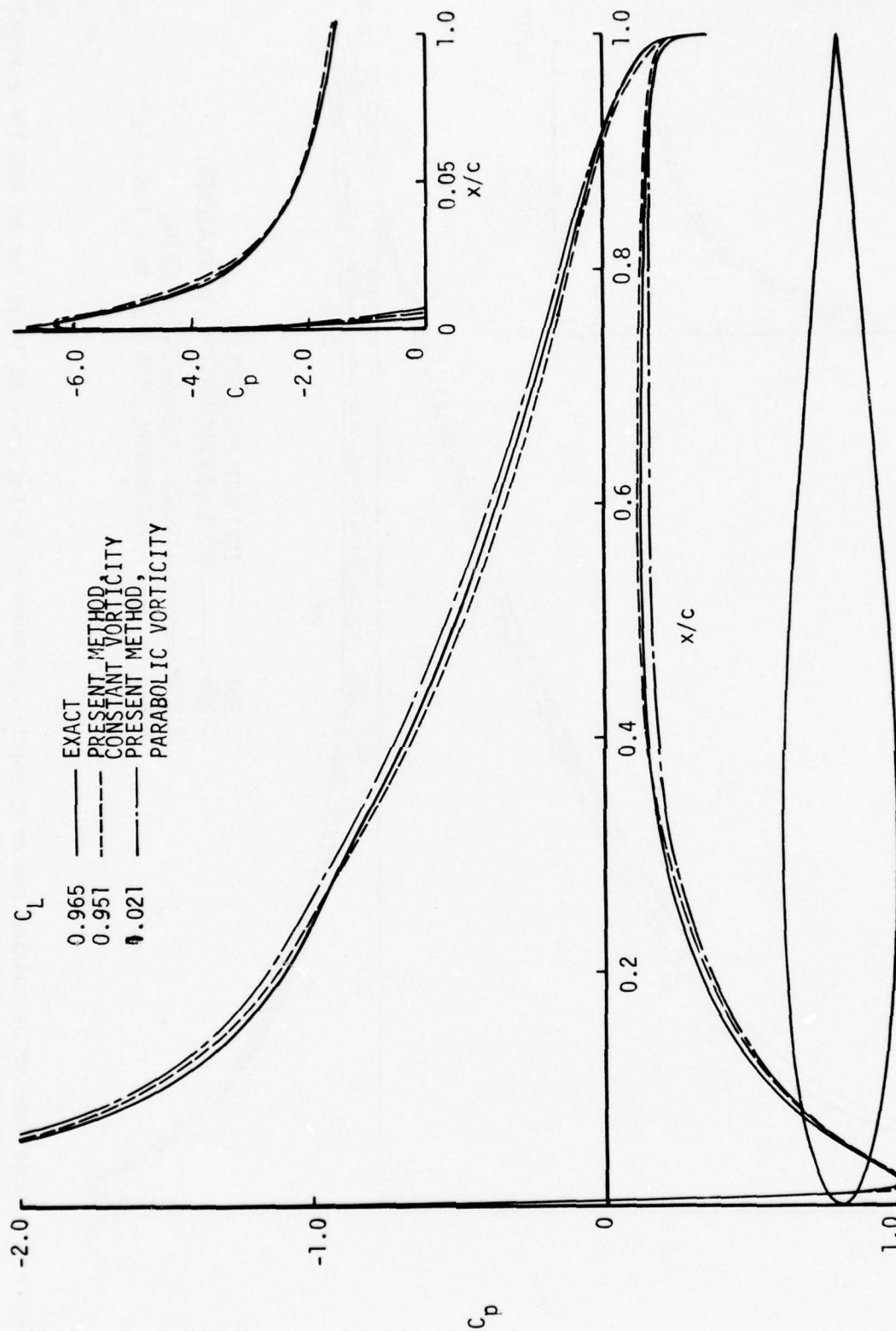


Figure 6. Comparison of calculated inviscid pressure distributions and lifts with exact values for an RAE 101 airfoil at 8.2° angle of attack. 52 surface panels.

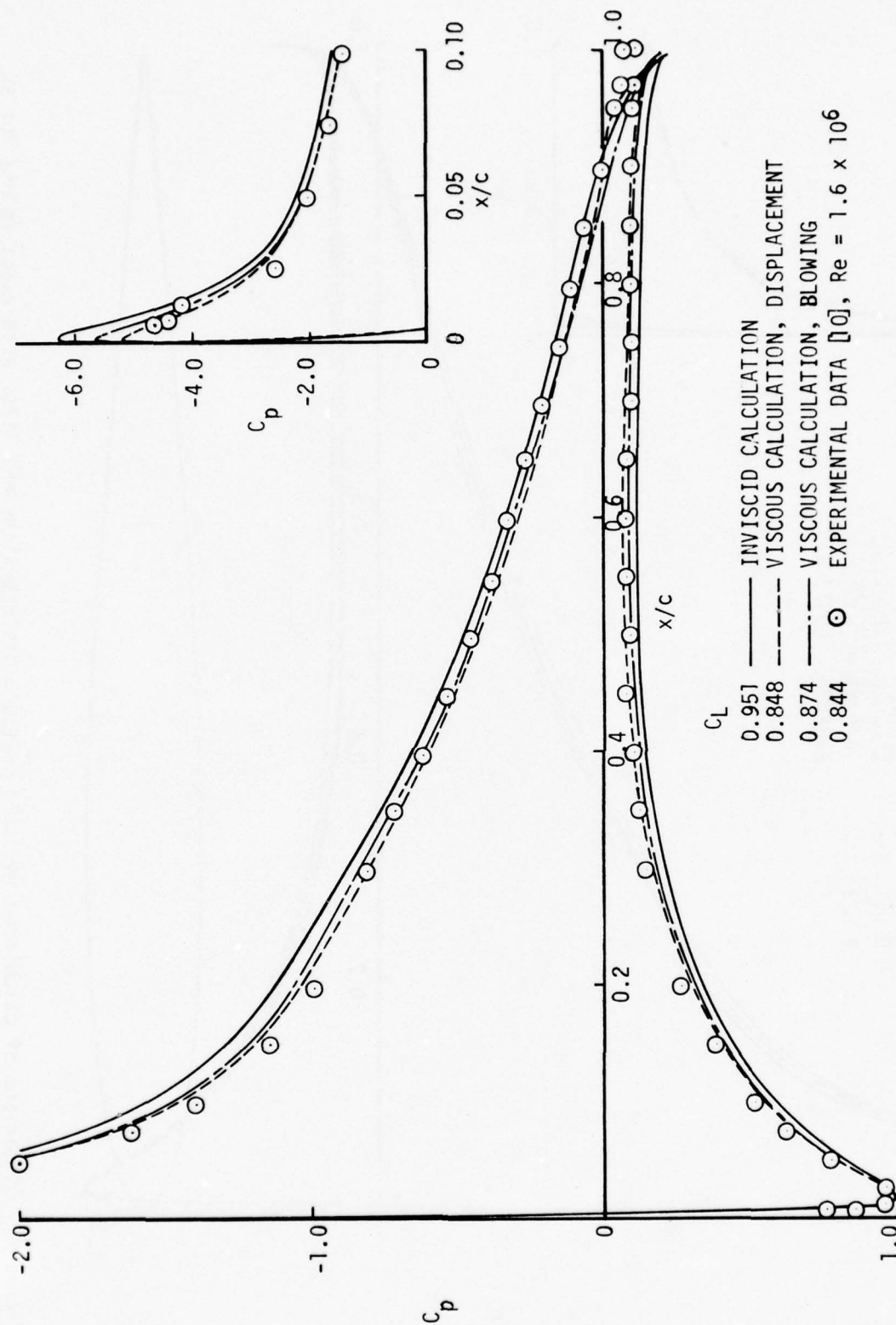


Figure 7. Comparison of calculated and experimental pressure distributions and lifts for an RAE 101 airfoil at 8.2° angle of attack. Constant surface vorticity distribution.

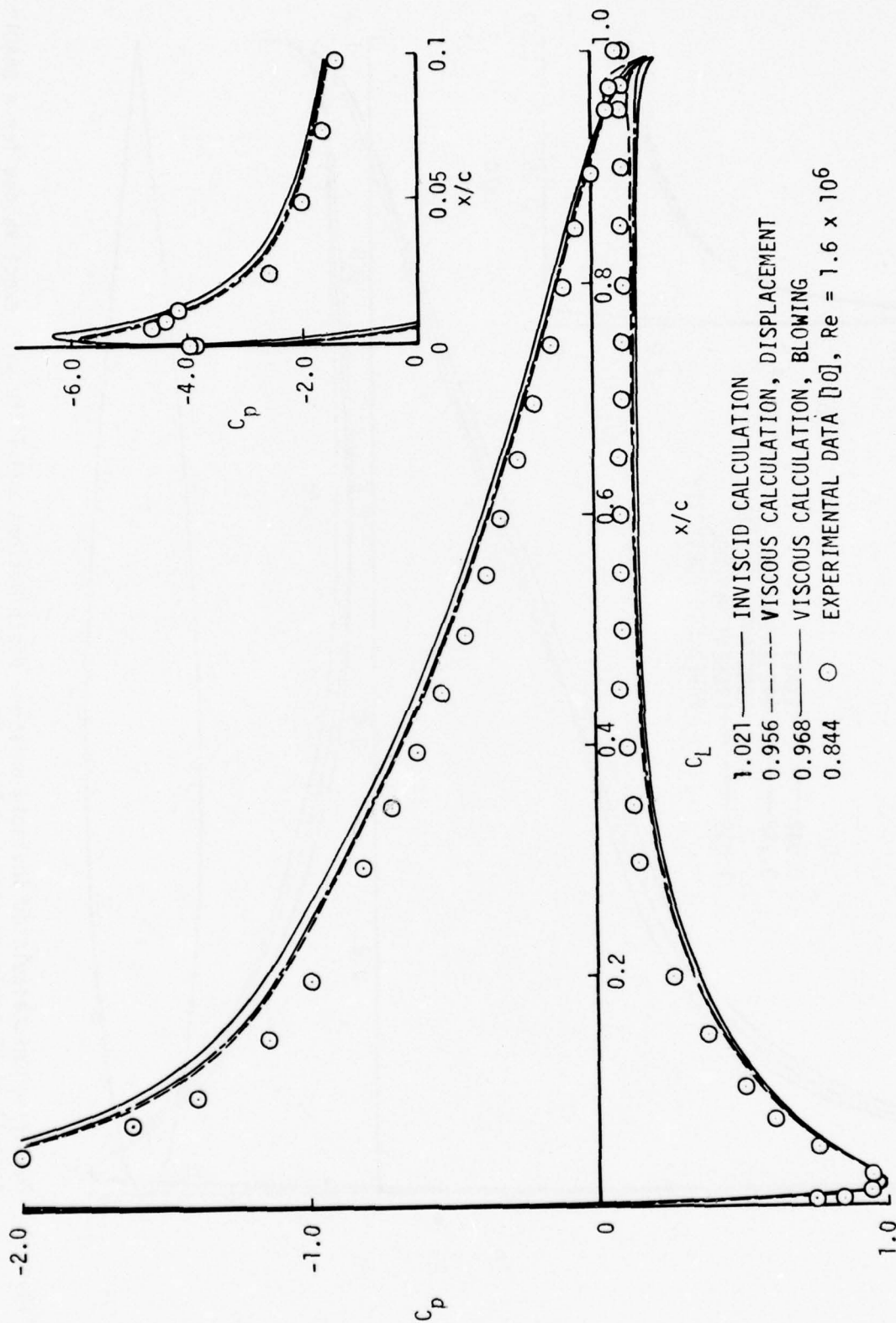


Figure 8. Comparison of calculated and experimental pressure distributions and lifts for an RAE 101 airfoil at 8.2° angle of attack. Parabolic surface vorticity distribution.

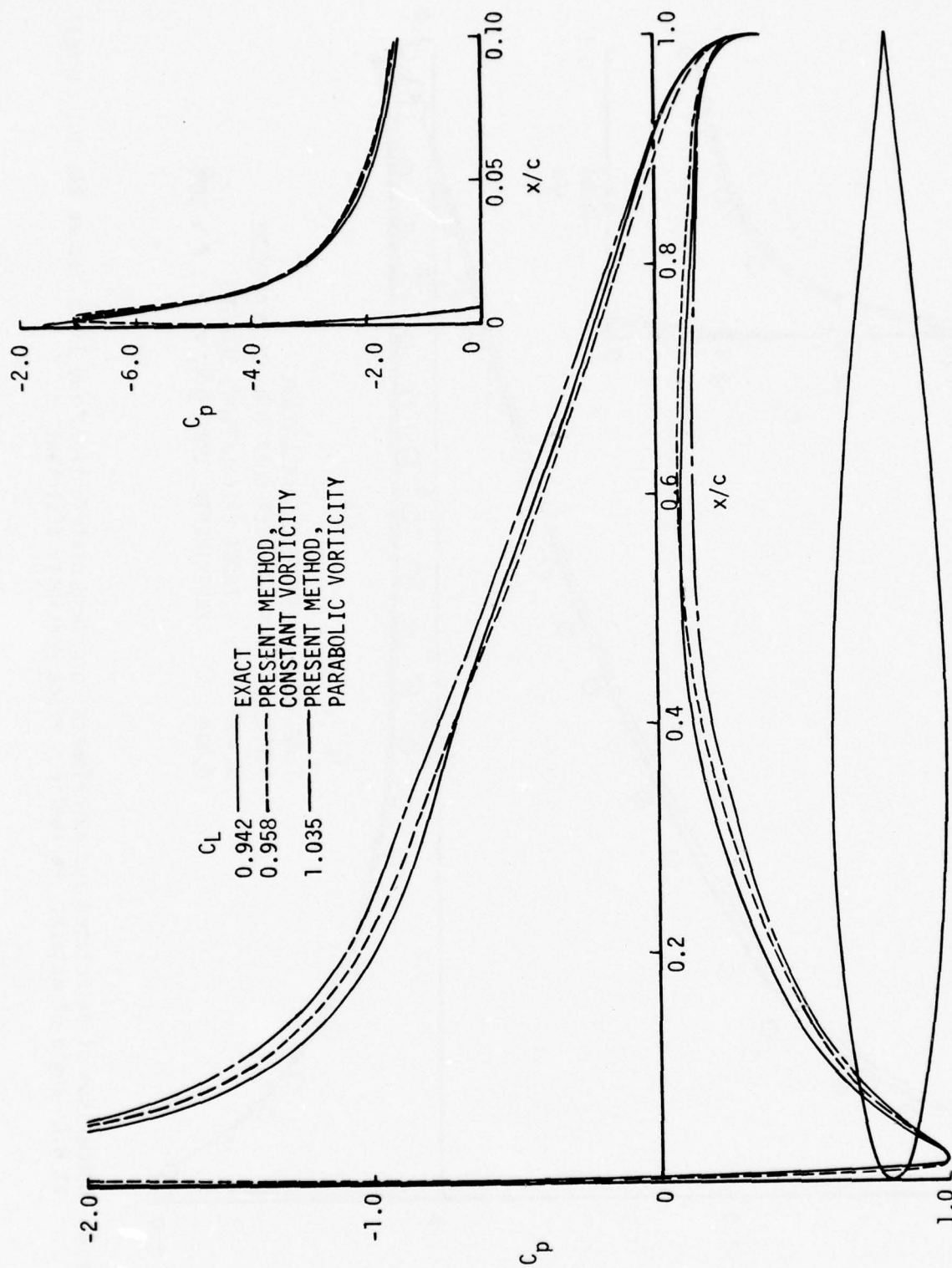


Figure 9. Comparison of calculated inviscid pressure distributions and lifts with exact values for a 64A010 airfoil at 8° angle of attack. 40 surface panels.

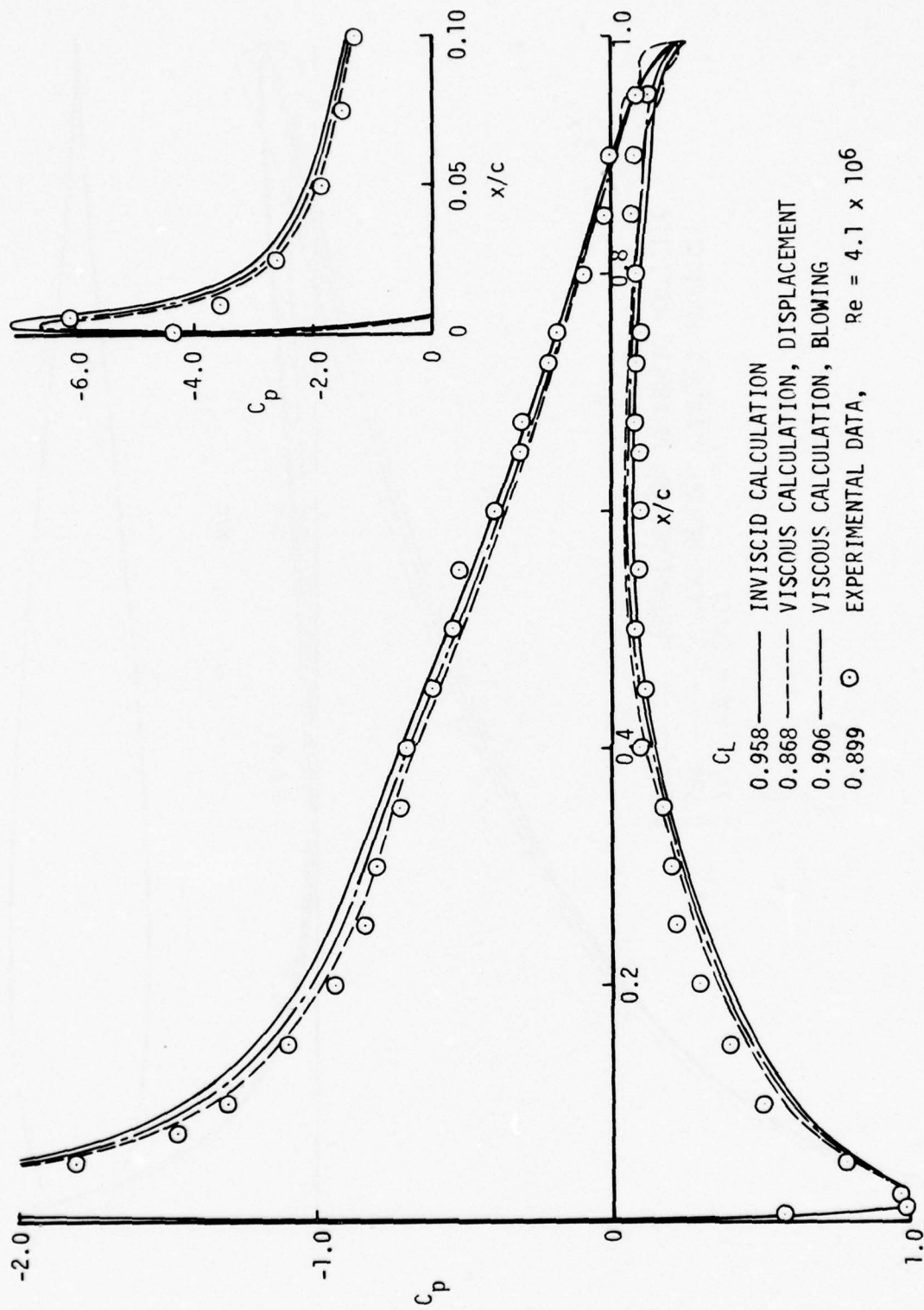


Figure 10. Comparison of calculated and experimental pressure distributions and lifts for a 64A010 airfoil at 8° angle of attack. Constant surface vorticity distribution.

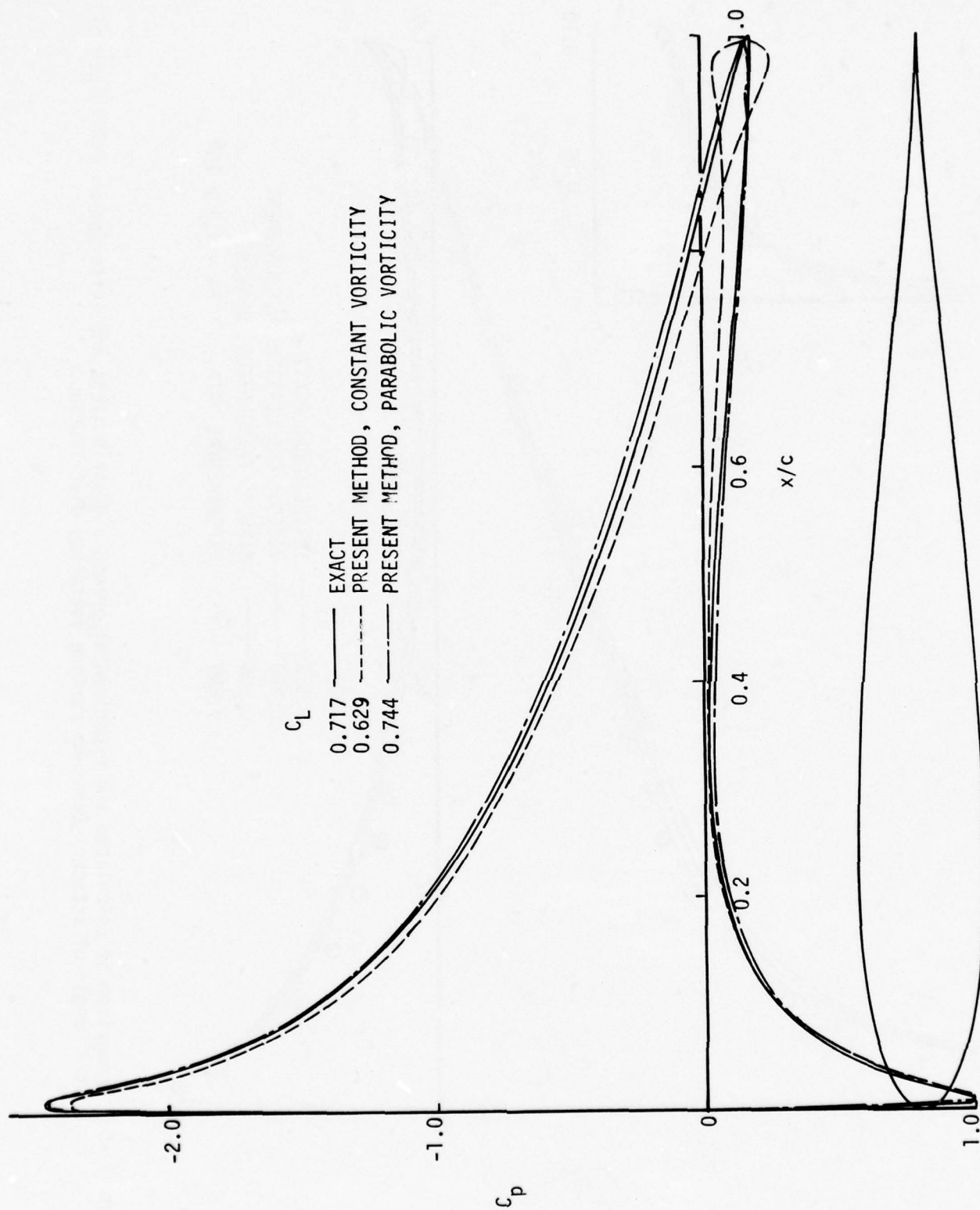


Figure 11. Comparison of calculated inviscid pressure distributions and lifts with exact values for a Joukowski airfoil at 6° angle of attack. 54 surface panels.

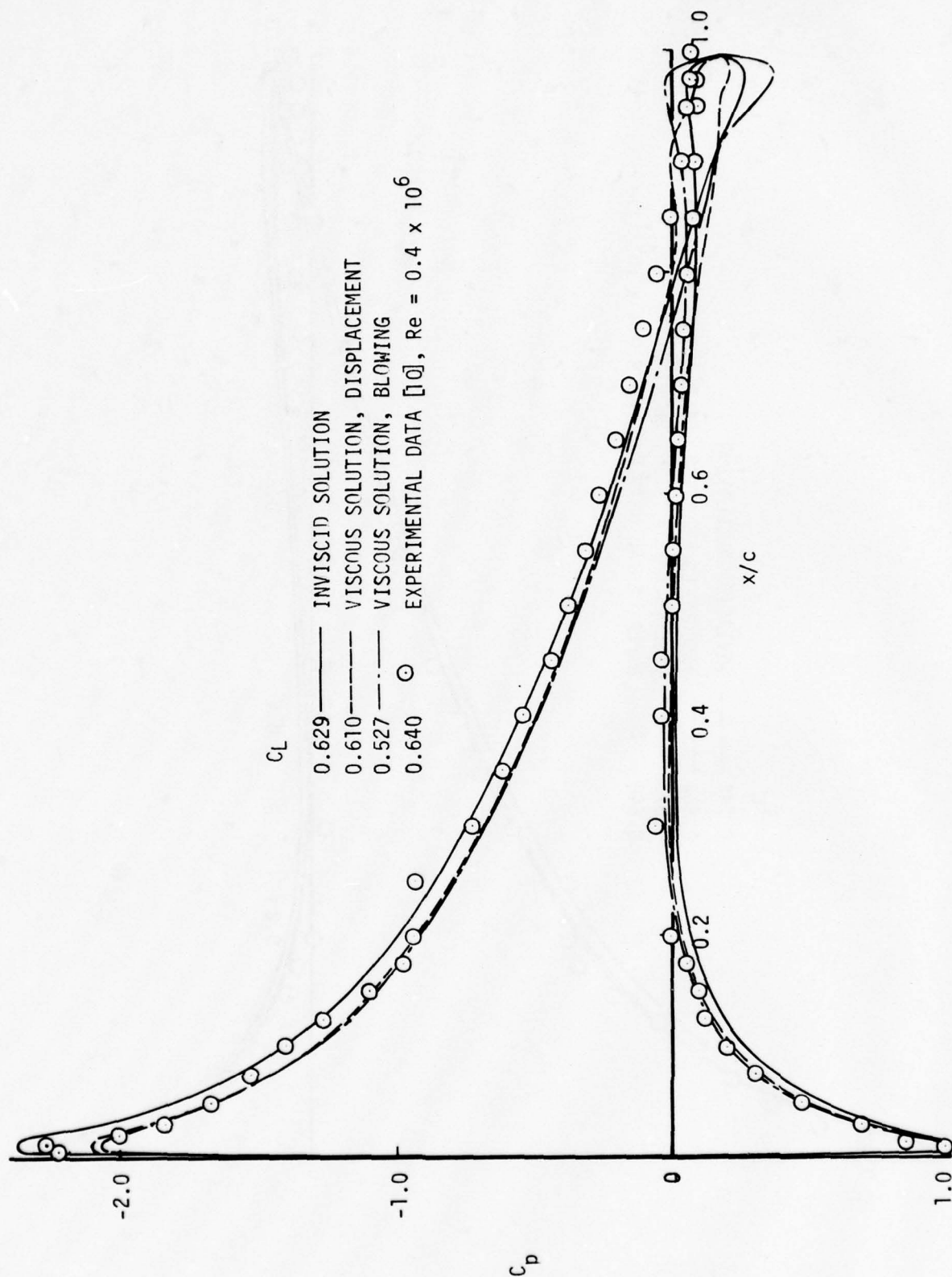


Figure 12. Comparison of calculated and experimental pressure distributions and lifts for a Joukowski airfoil at 6° angle of attack. Constant surface vorticity distribution.

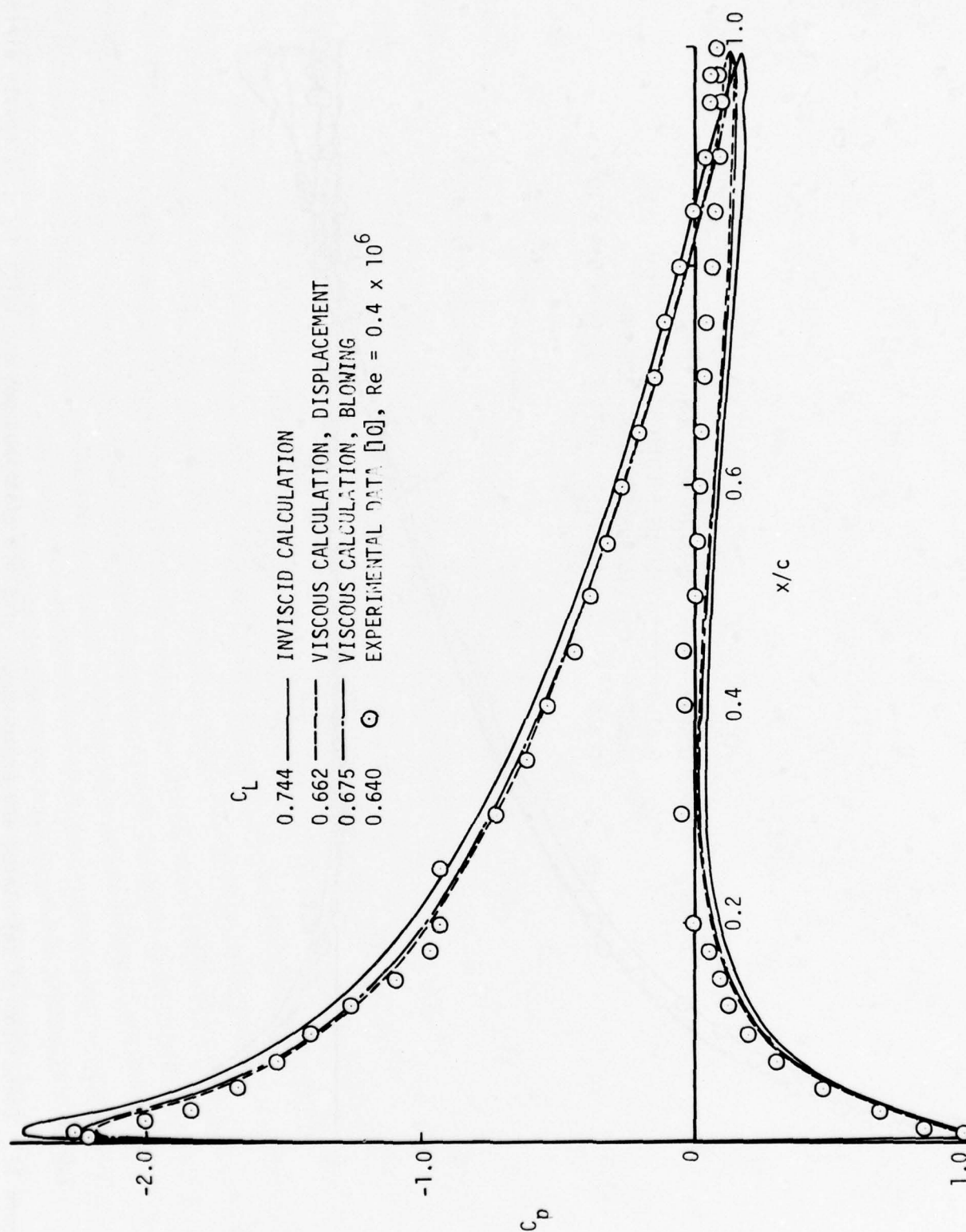


Figure 13. Comparison of calculated and experimental pressure distributions and lifts for a Joukowski airfoil at 6° angle of attack. Parabolic surface vorticity distribution.

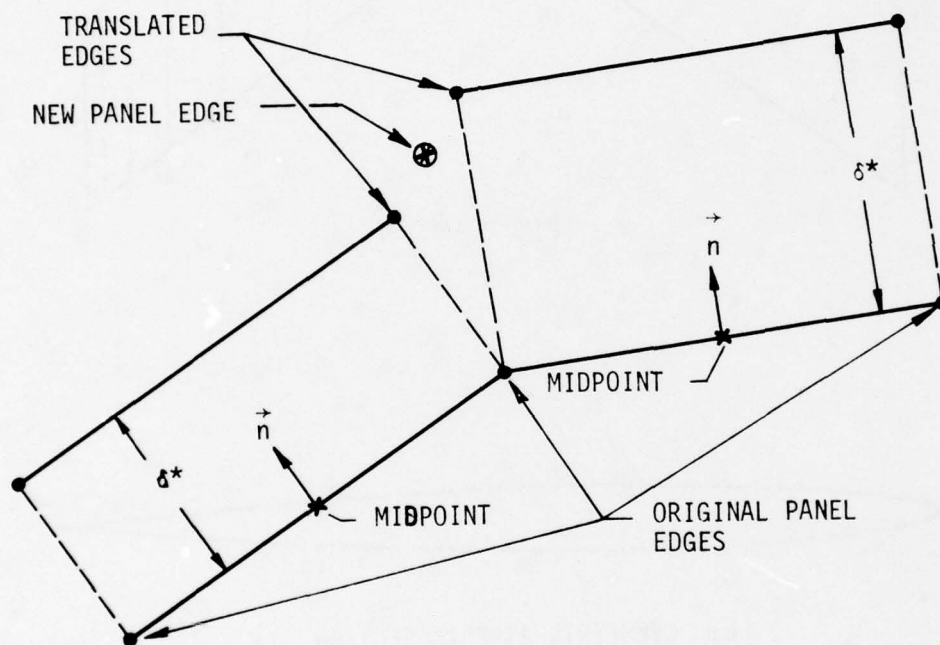
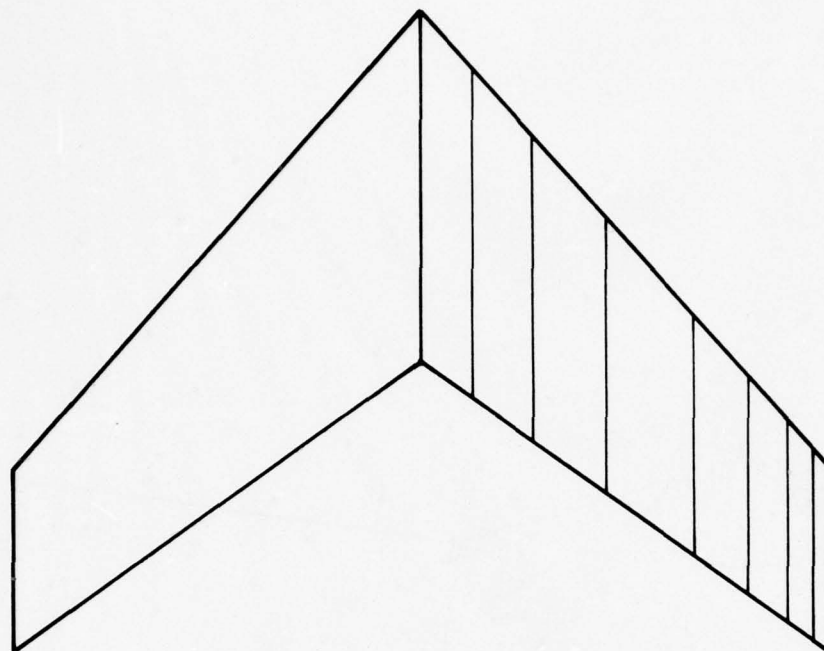
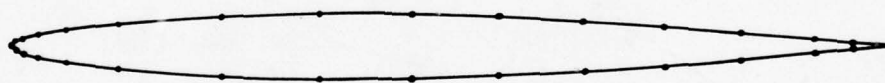


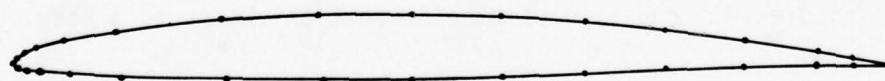
Figure 14. Addition of displacement thickness to a body.



a. WING PLANFORM



b. SYMMETRIC AIRFOIL SECTION



c. CAMBERED AIRFOIL SECTION

Figure 15. Two isolated swept wings.

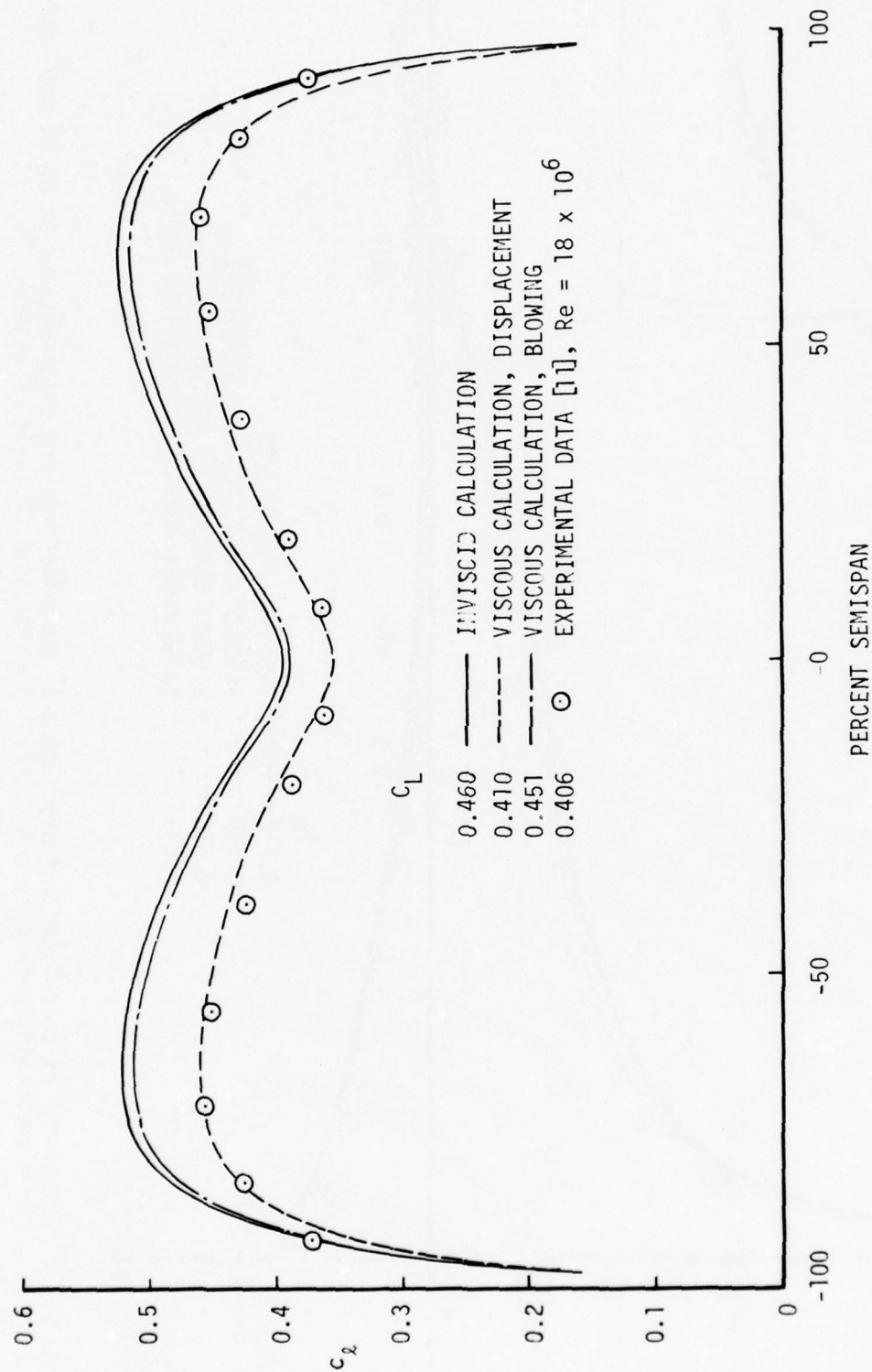


Figure 16. Comparison of calculated and experimental spanwise distributions of section lift coefficient for a swept wing with symmetrical airfoil section at 8.2° angle of attack.

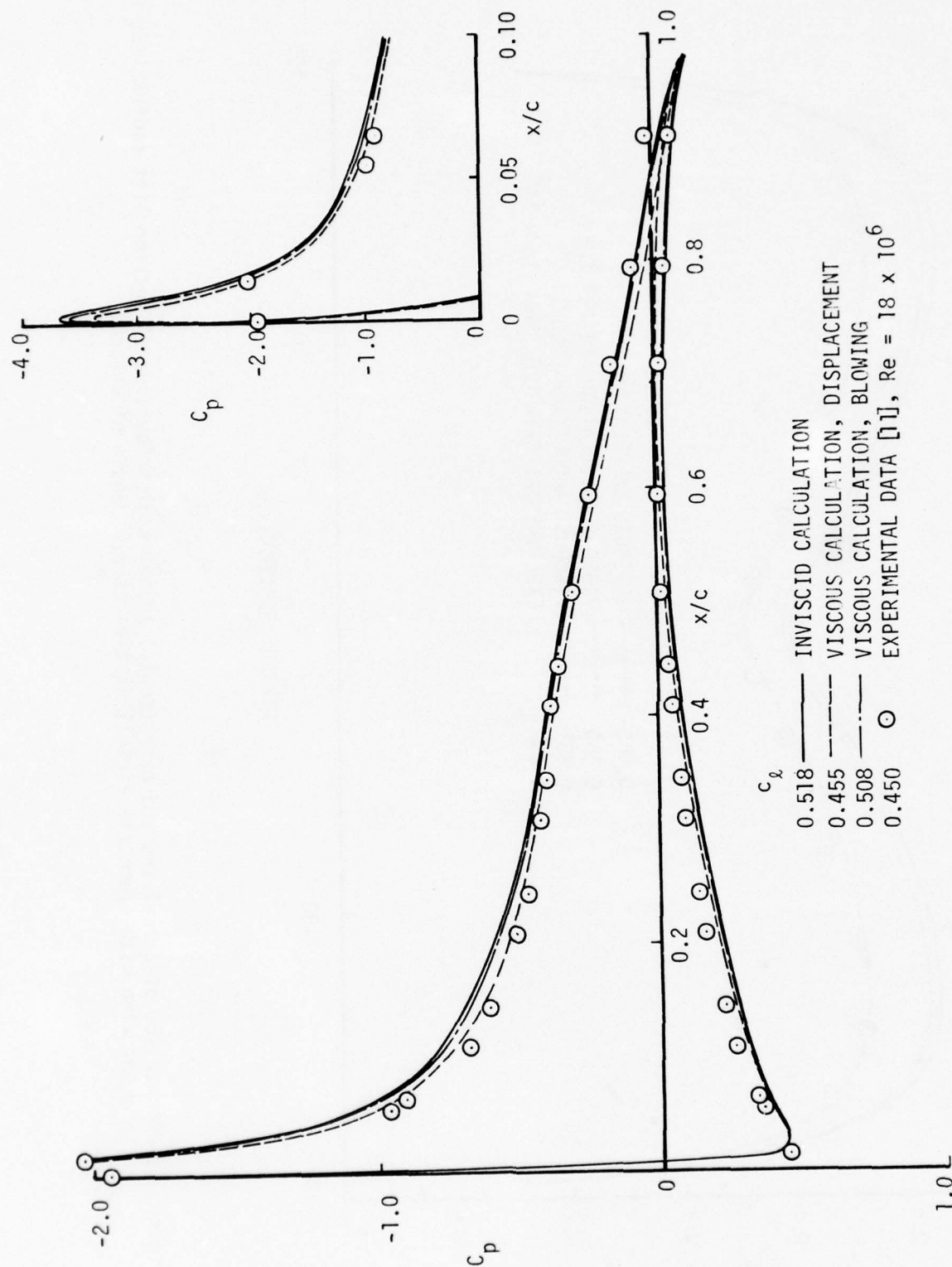


Figure 17. Comparison of calculated and experimental chordwise pressure distributions at 55.5% semi-span for a swept wing with symmetric airfoil section at 8.2° angle of attack.

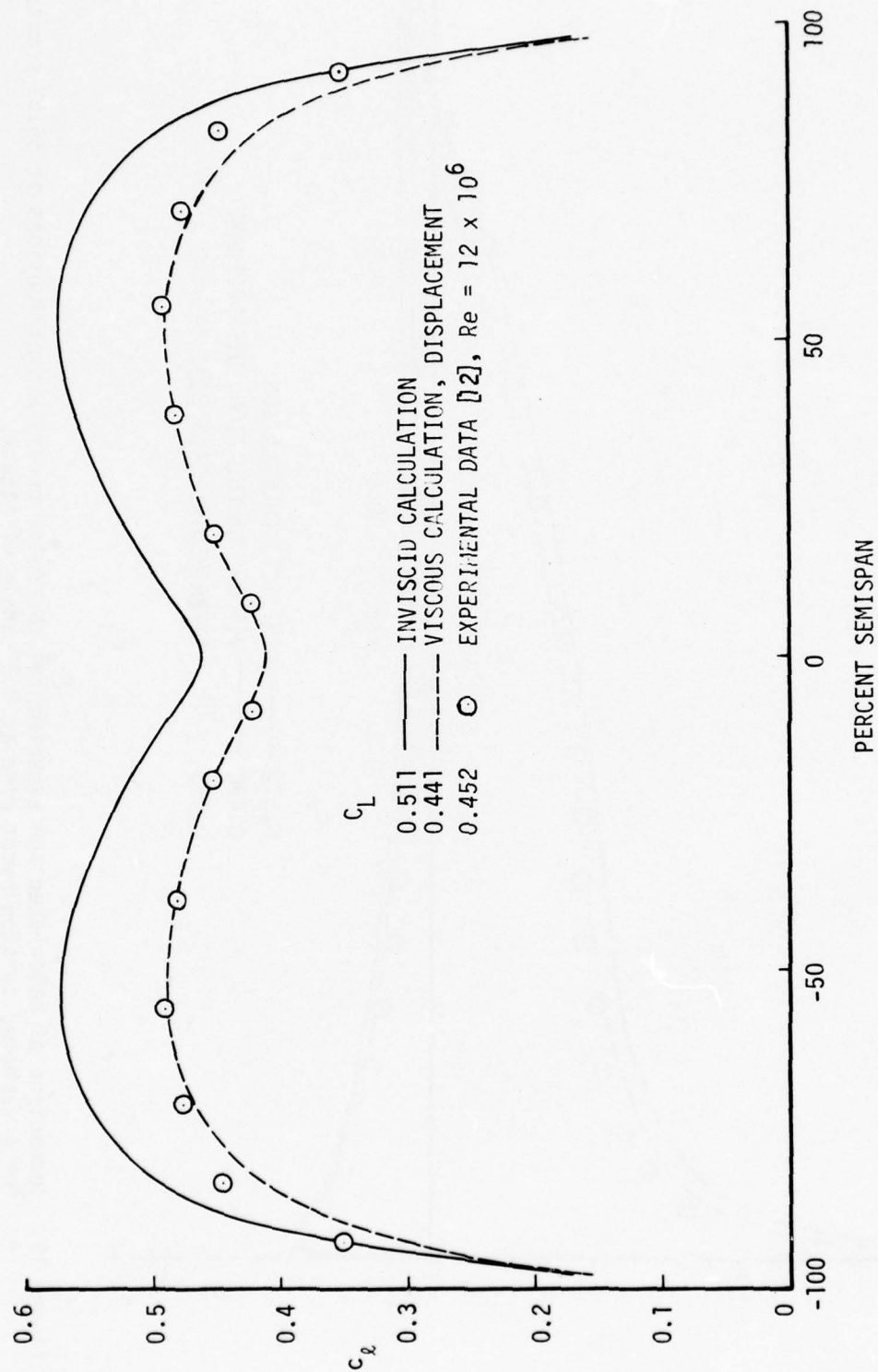


Figure 18. Comparison of calculated and experimental spanwise distributions of section lift coefficient for a cambered twisted swept wing at 8.2° angle of attack.

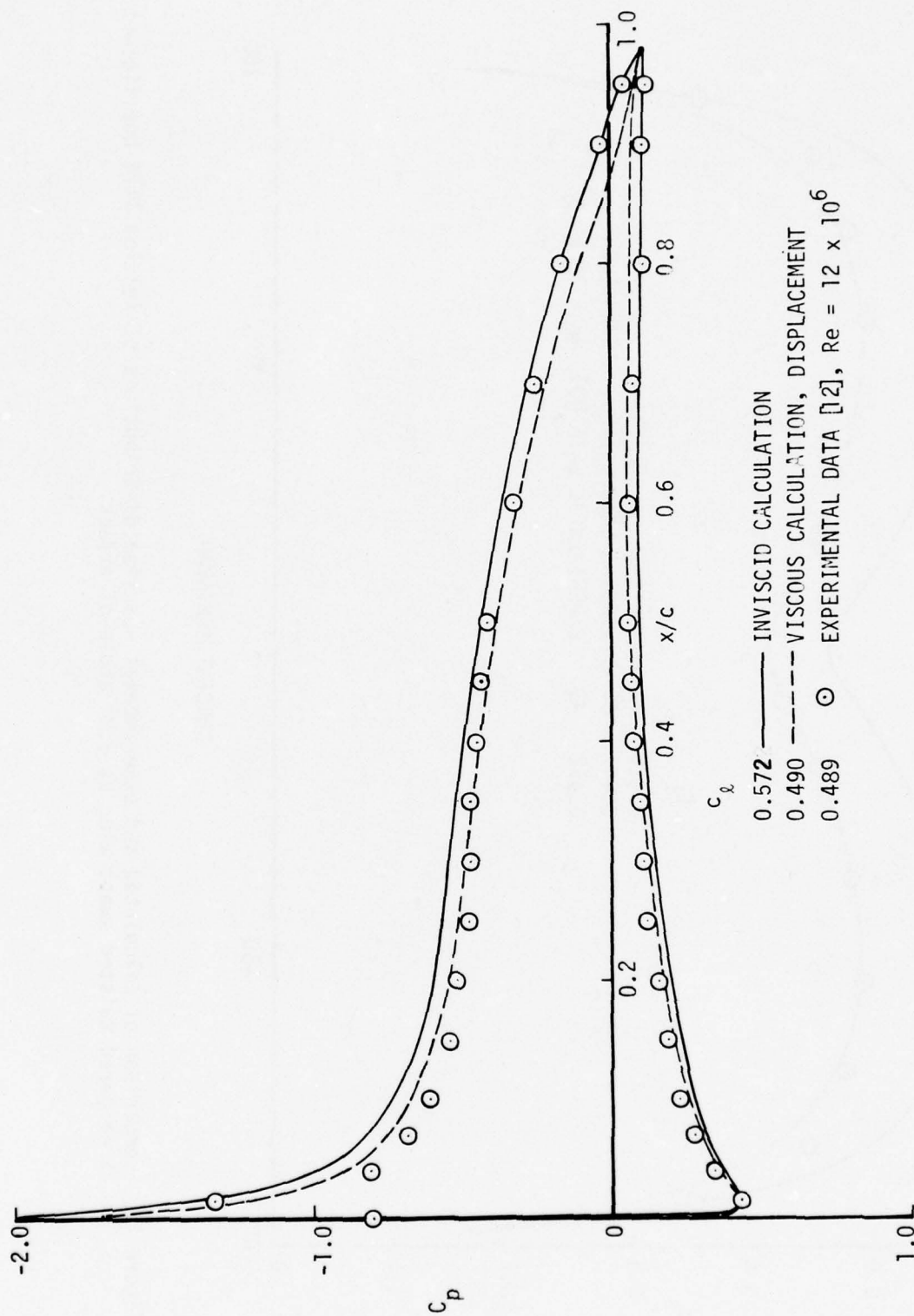
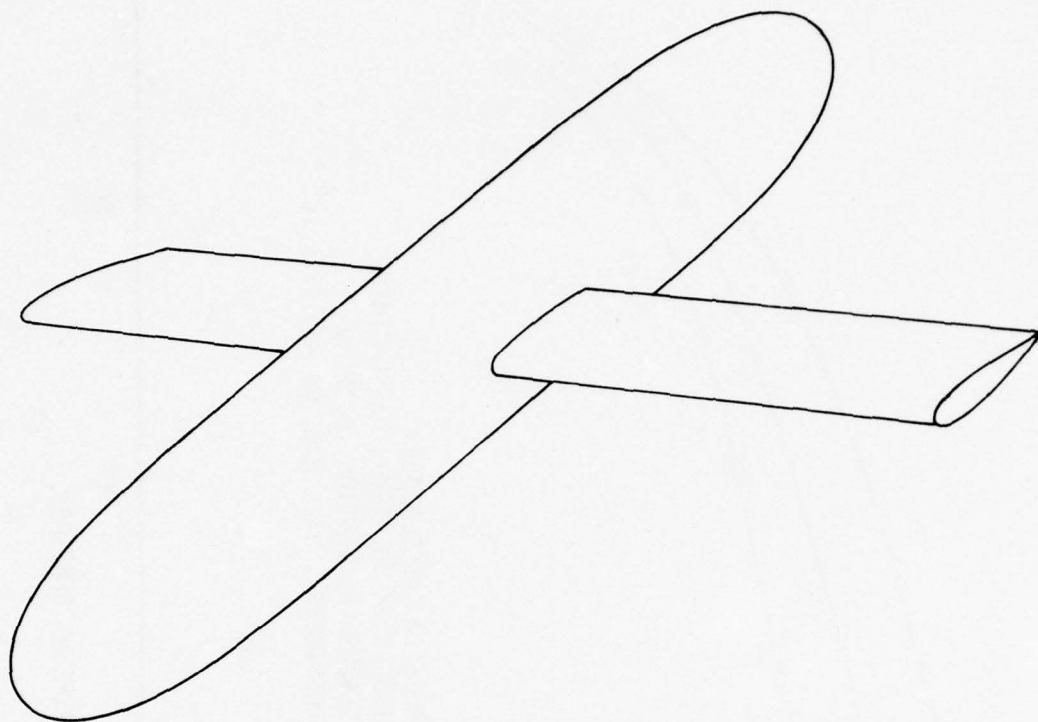
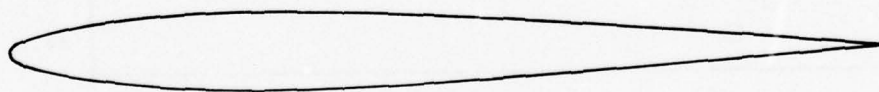


Figure 19. Comparison of calculated and experimental chordwise pressure distributions at 55.5% semispan for a cambered twisted swept wing at 8.2° angle of attack.



a. THE COMPLETE CONFIGURATION



b. AIRFOIL SECTION OF THE WING

Figure 20. A straight wing on a round fuselage.

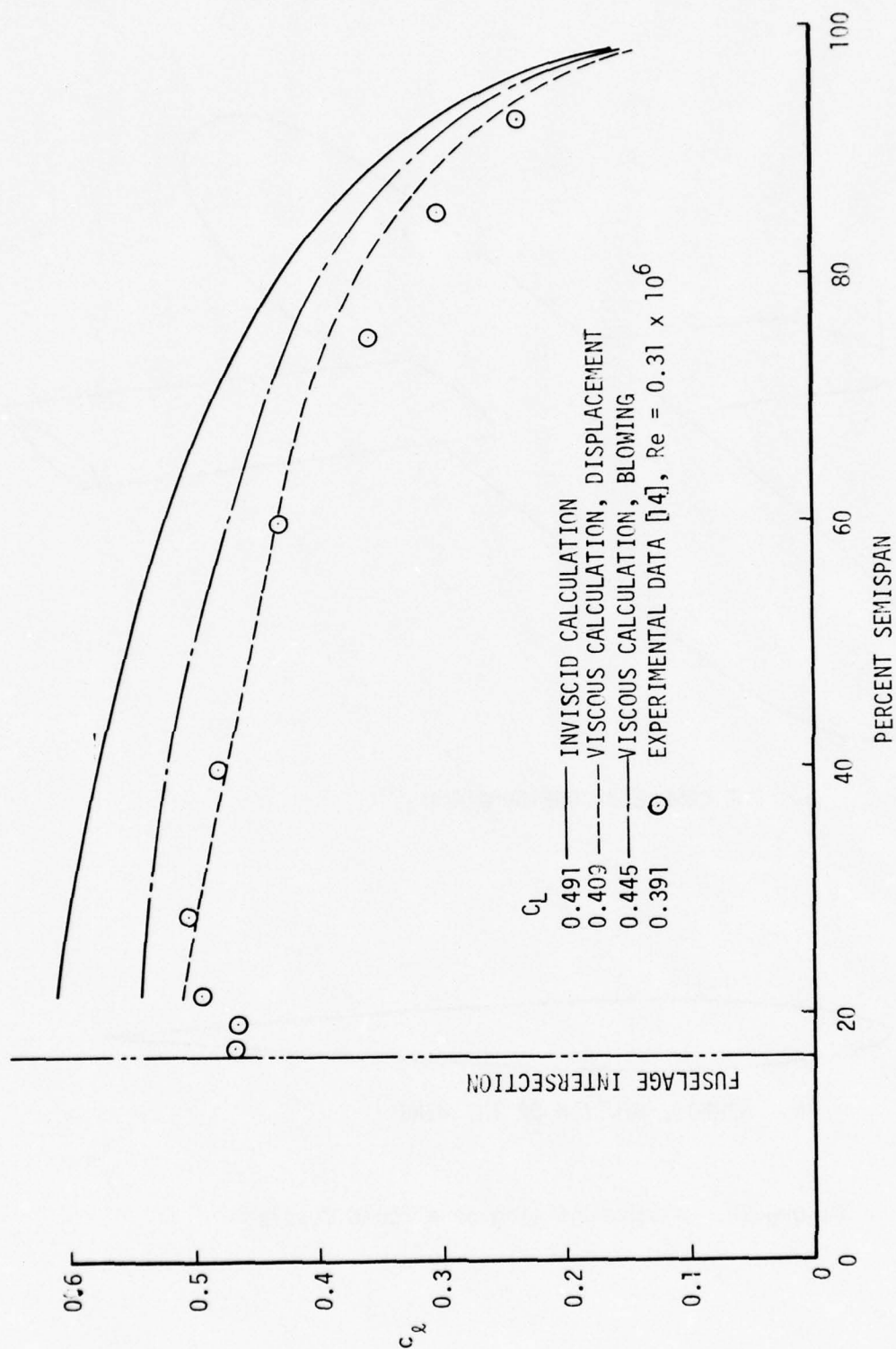


Figure 21. Comparison of calculated and experimental spanwise distributions of section lift coefficient for a straight wing on a round fuselage at 6° angle of attack.

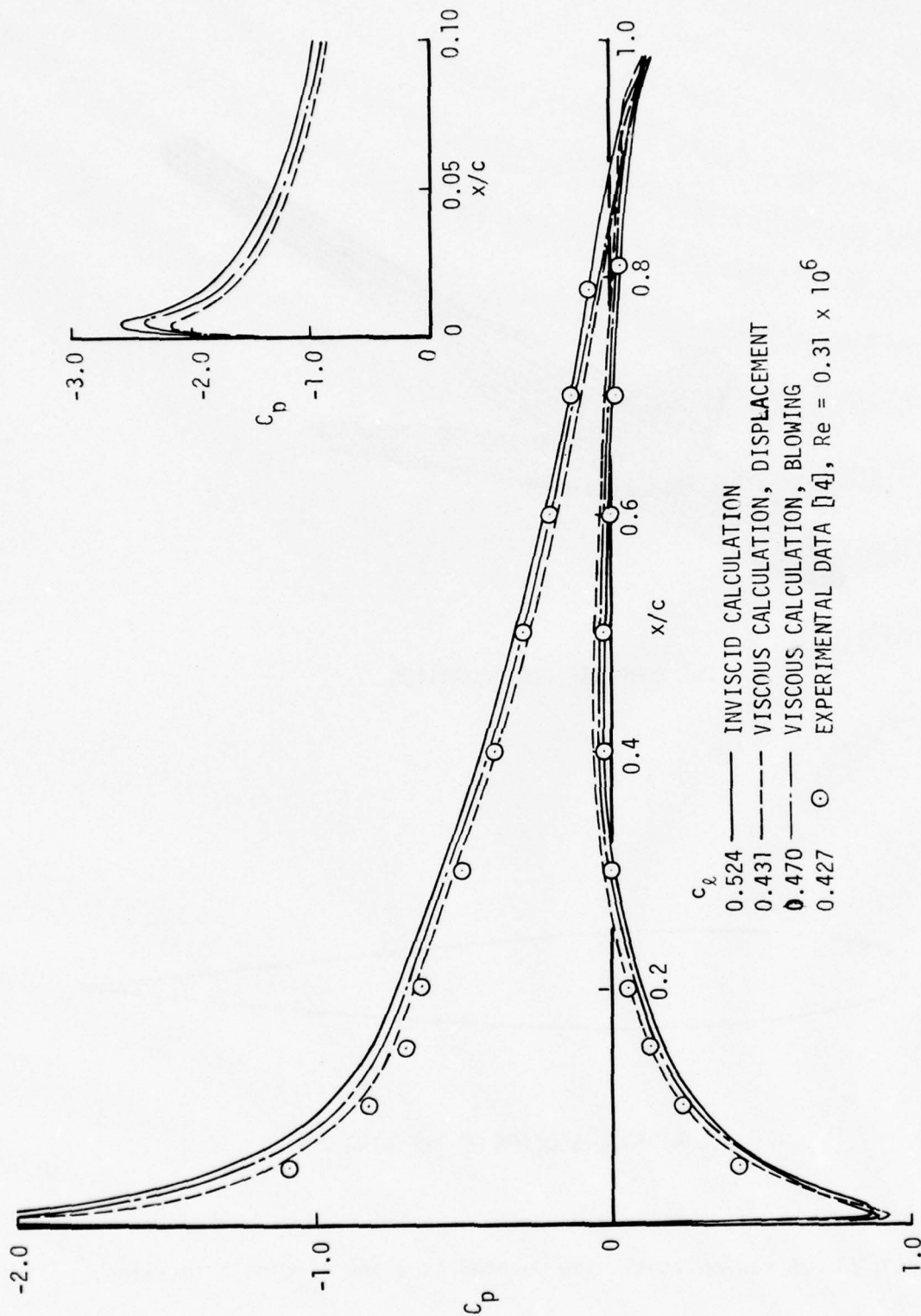
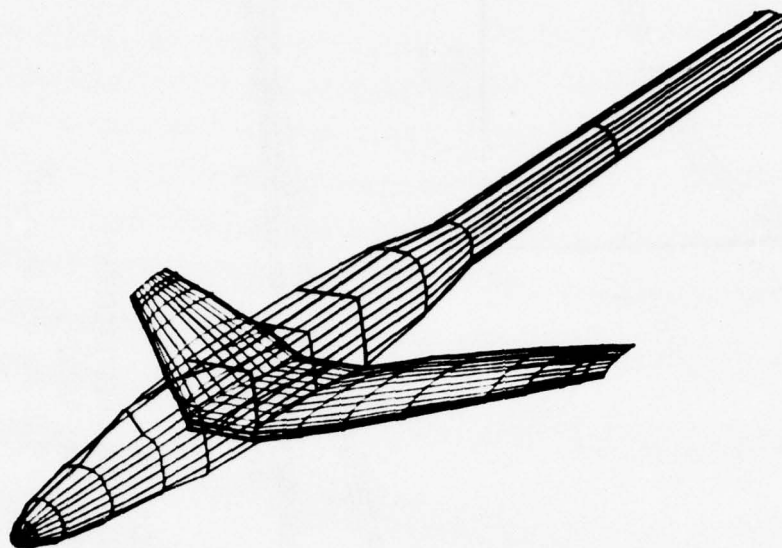


Figure 22. Comparison of calculated and experimental chordwise pressure distributions at 60% semispan on a straight wing mounted on a round fuselage at 6° angle of attack.



a. THE COMPLETE CONFIGURATION



b. AIRFOIL SECTION OF THE WING

Figure 23. A conventional wing mounted as a low wing on a fuselage.

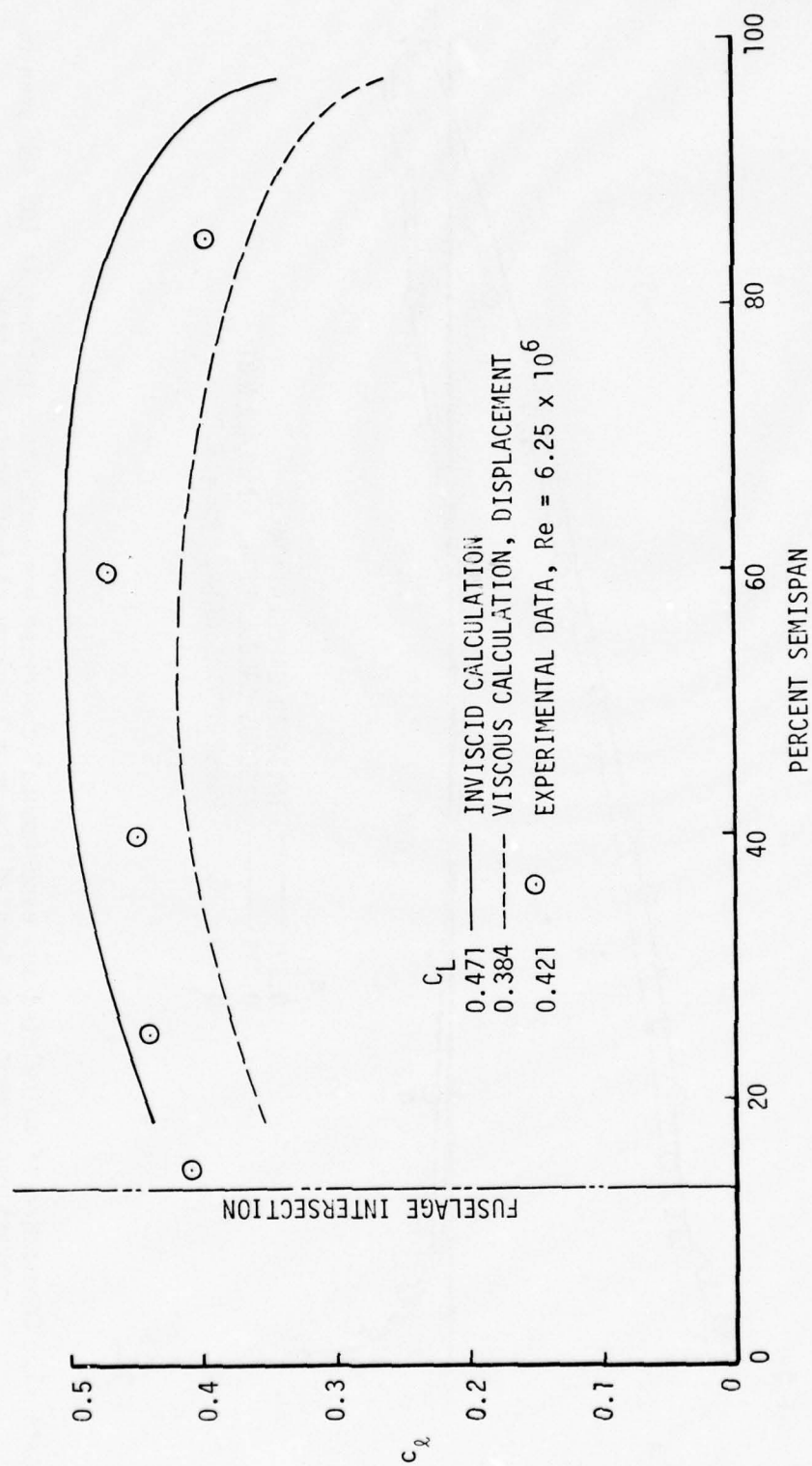


Figure 24. Comparison of calculated and experimental spanwise distribution of section lift coefficient for a conventional swept wing mounted low on a fuselage at 6.9° angle of attack.

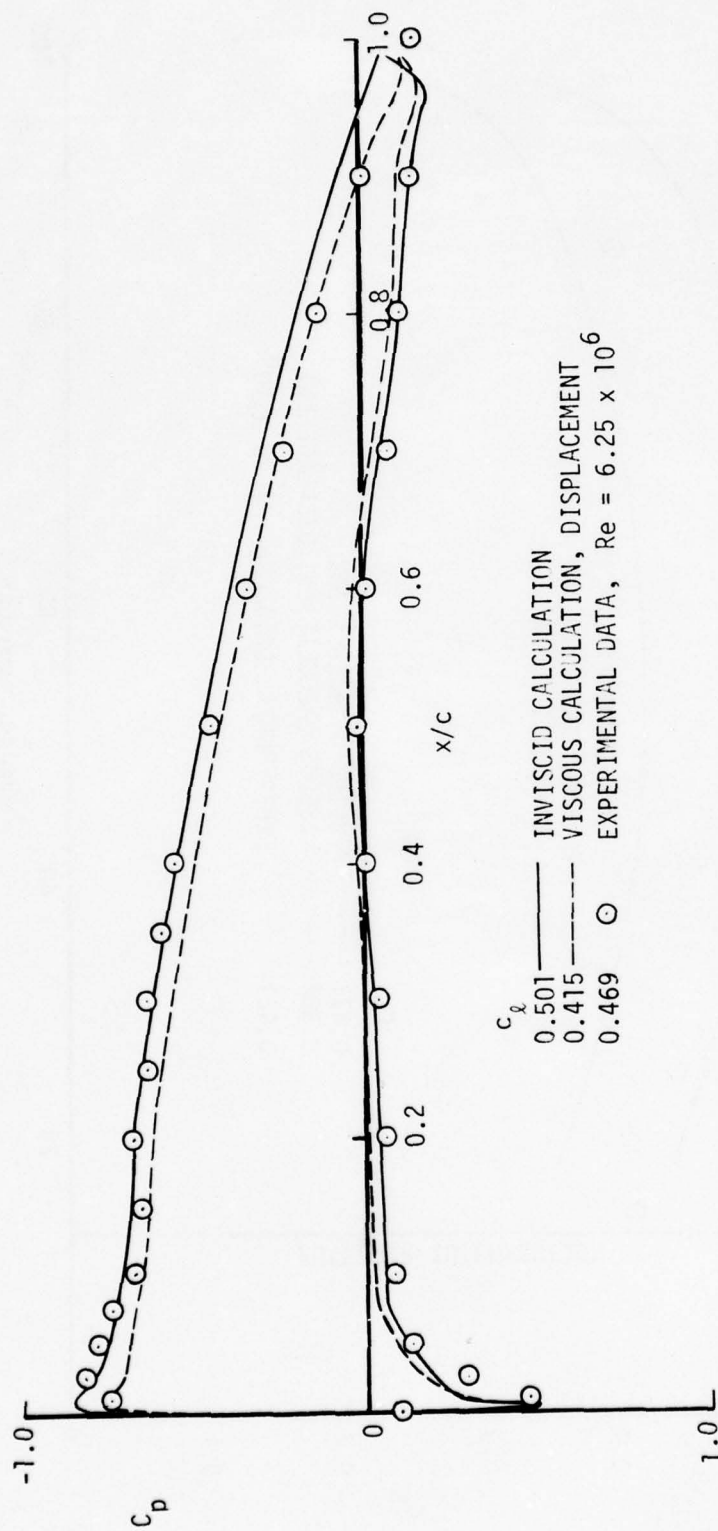
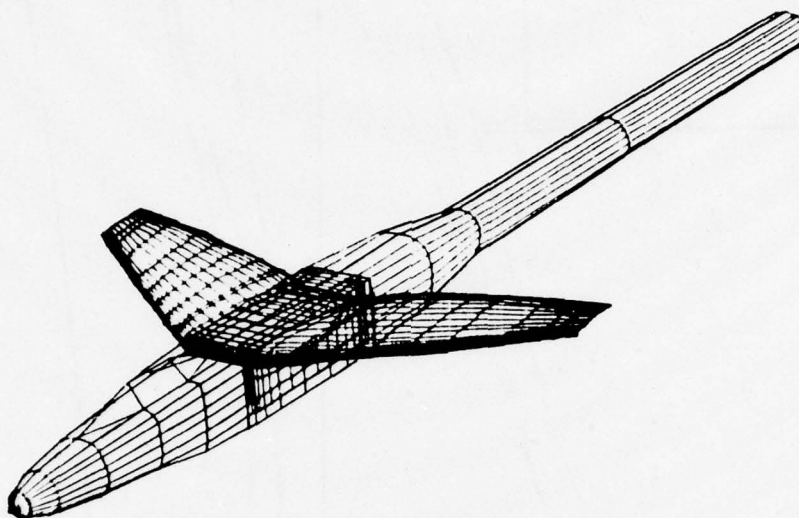
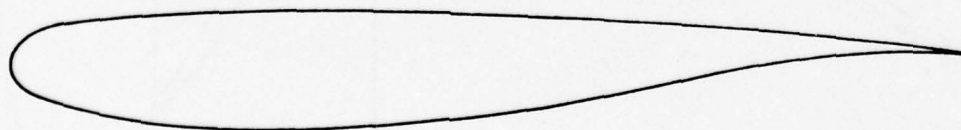


Figure 25. Comparison of calculated and experimental chordwise pressure distributions at 60% semispan on a conventional swept wing mounted low on a fuselage at 6.9° angle of attack.



a. THE COMPLETE CONFIGURATION



b. AIRFOIL SECTION OF THE WING

Figure 26. A supercritical swept wing mounted as a high wing on a fuselage.

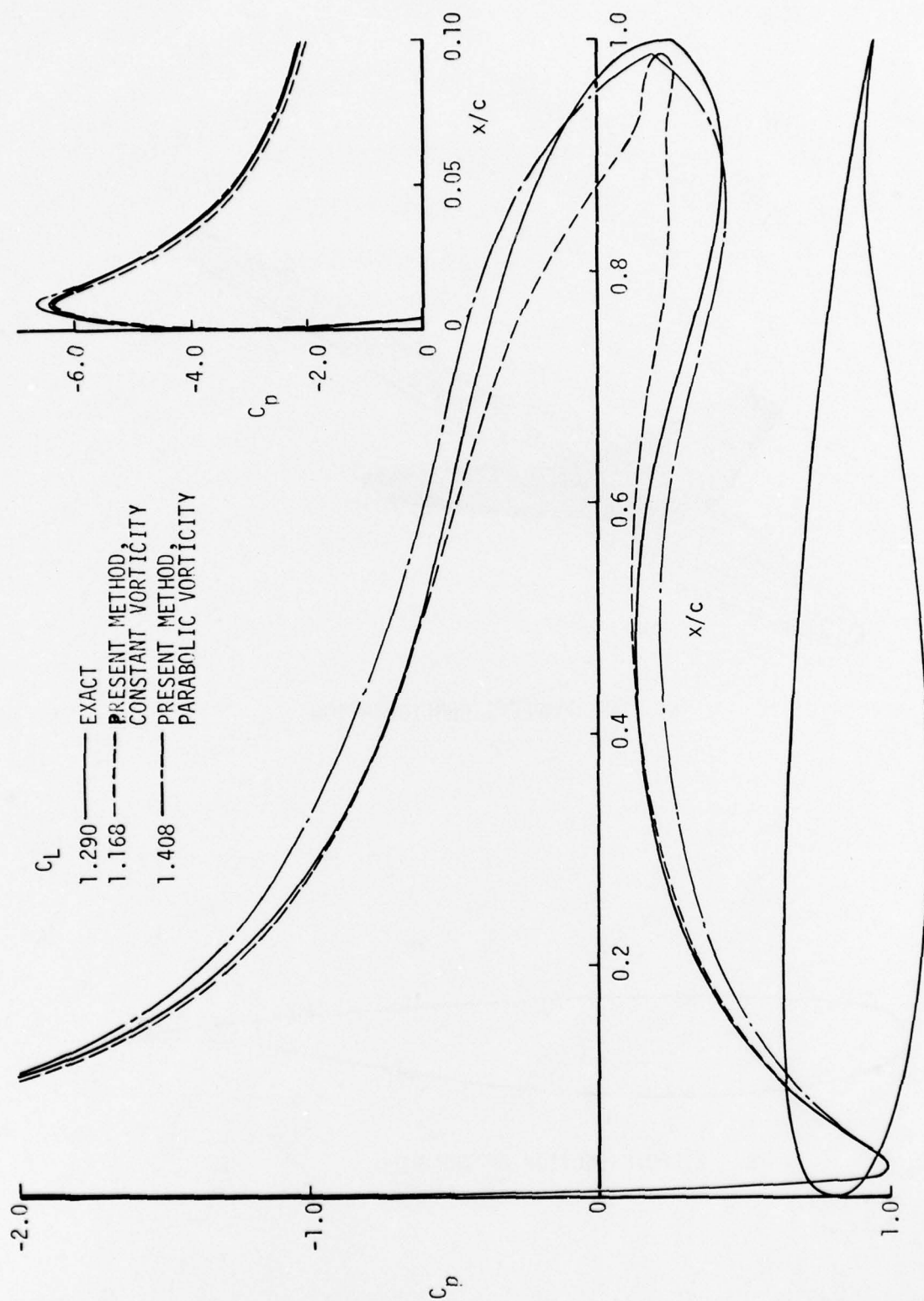


Figure 27. Comparison of calculated inviscid pressure distributions and lifts with exact values for a two-dimensional supercritical airfoil at 7.02° angle of attack.

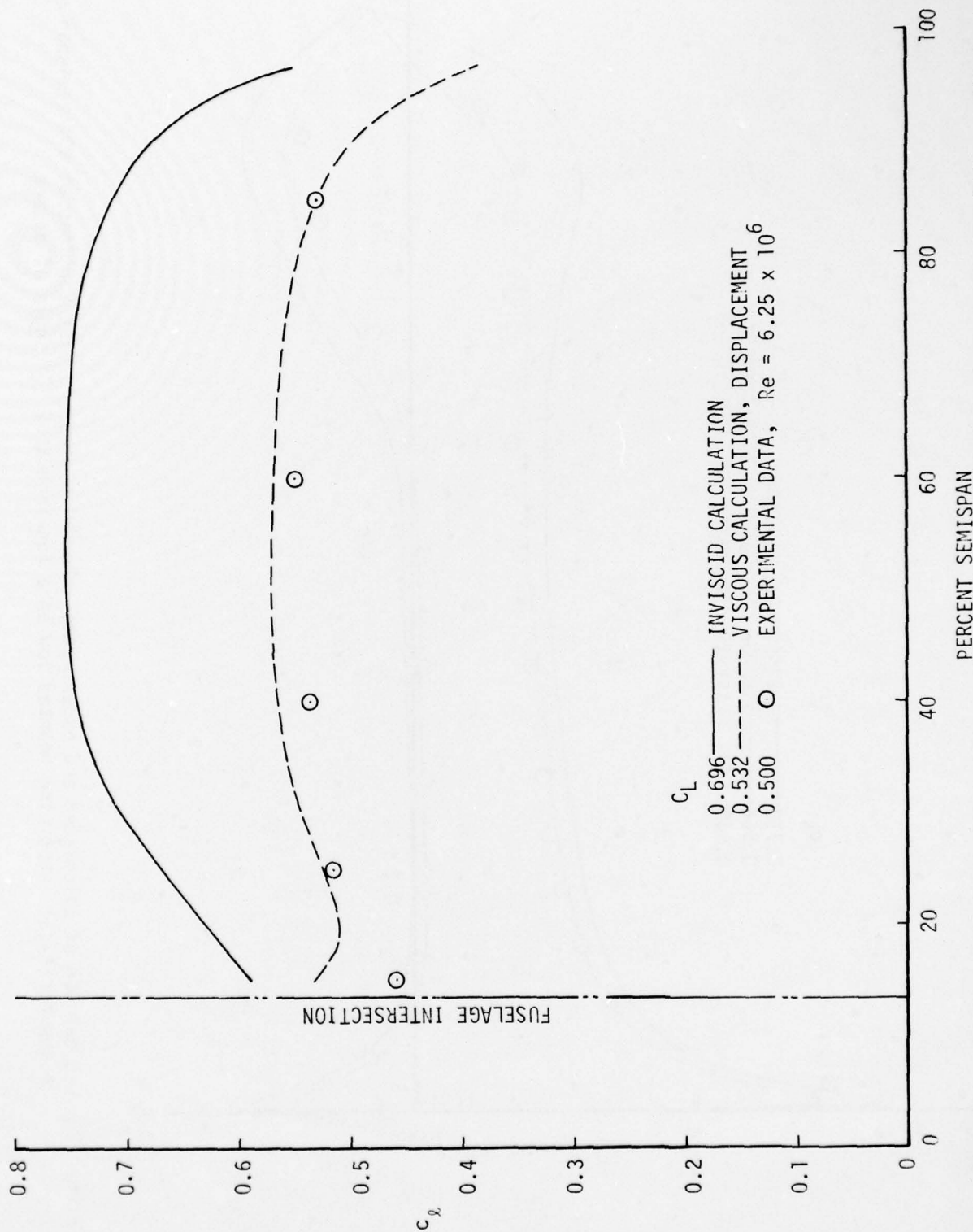


Figure 28. Comparison of calculated and experimental spanwise distributions of section lift coefficient for a supercritical swept wing mounted high on a fuselage at 7.02° angle of attack.

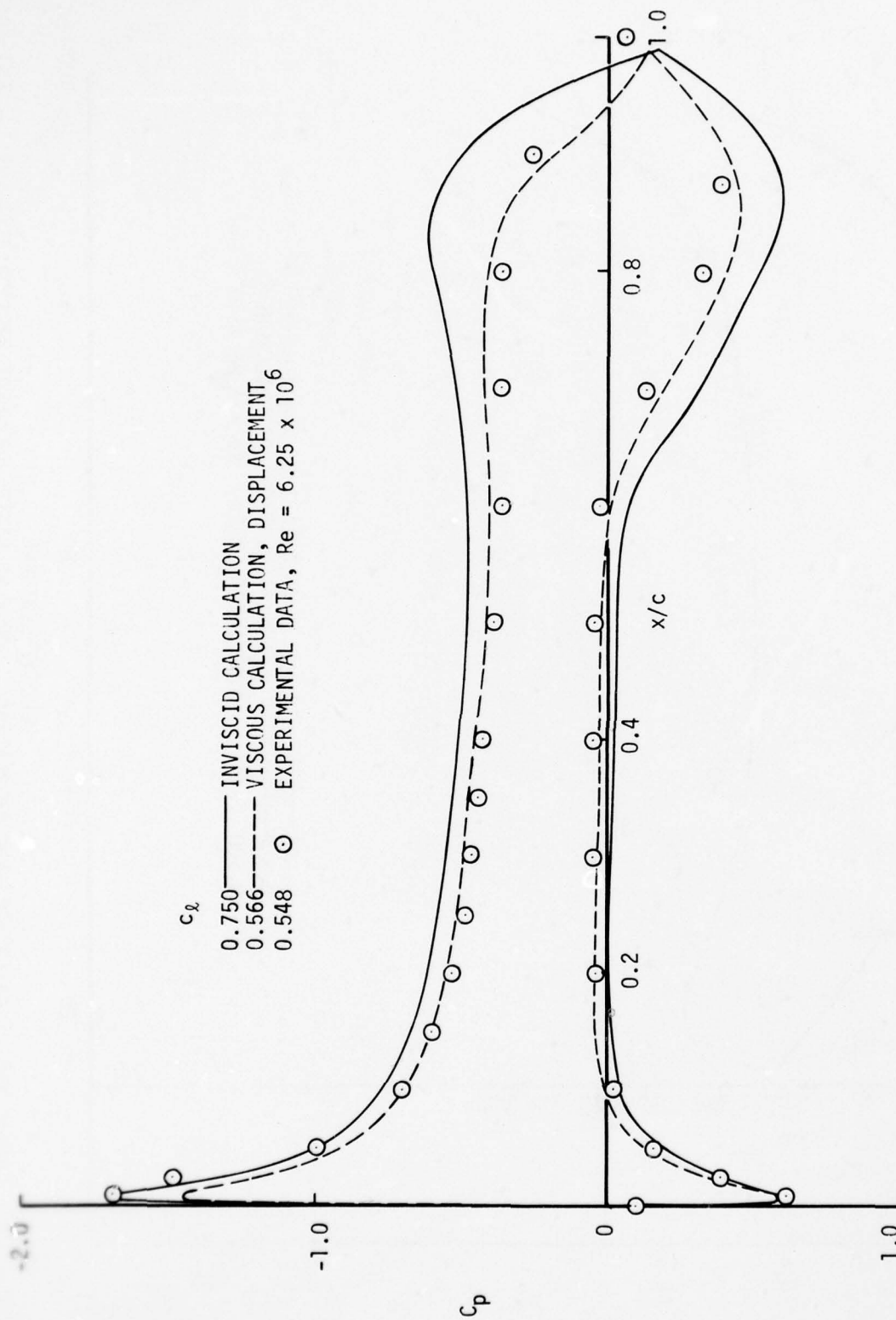
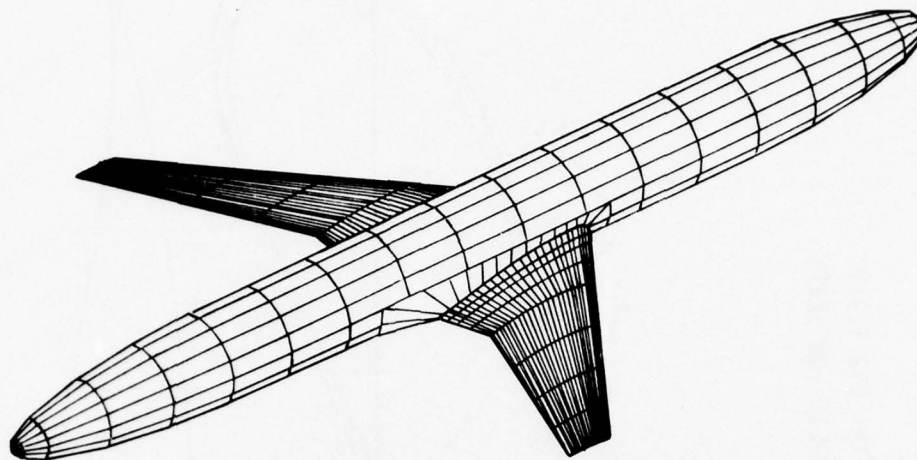


Figure 29. Comparison of calculated and experimental chordwise pressure distributions at 60% semispan on a supercritical swept wing mounted low on a fuselage at 7.02° angle of attack.



a. THE COMPLETE CONFIGURATION



b. AIRFOIL SECTION OF THE WING

Figure 30. A supercritical transport configuration.

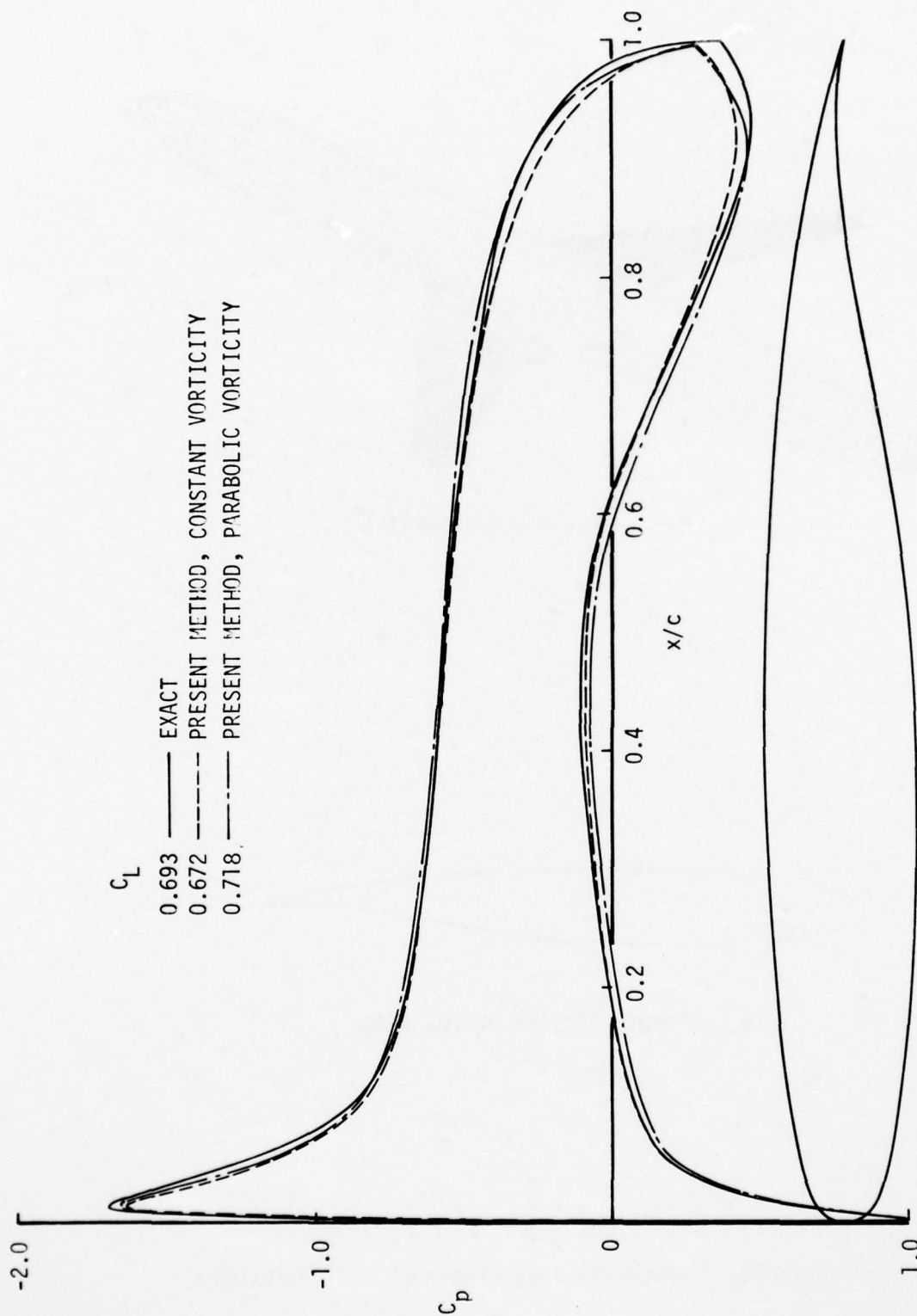


Figure 31. Comparison of calculated inviscid pressure distributions and lifts with exact values for a three-dimensional transport-type supercritical airfoil at 2.06° angle of attack.

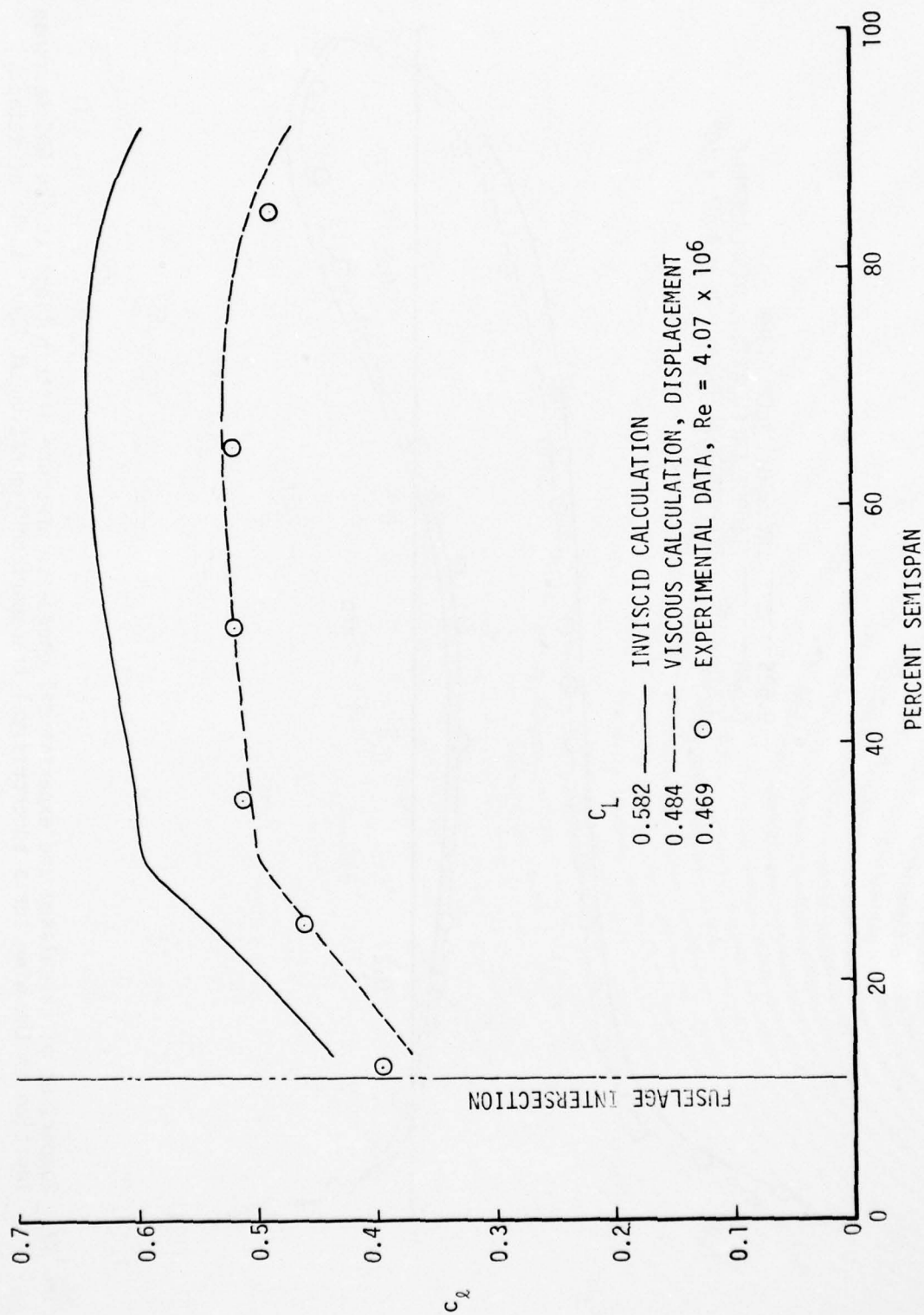


Figure 32. Comparison of calculated and experimental spanwise distribution of section lift coefficient on the wing for a supercritical transport configuration at 2.06° angle of attack.

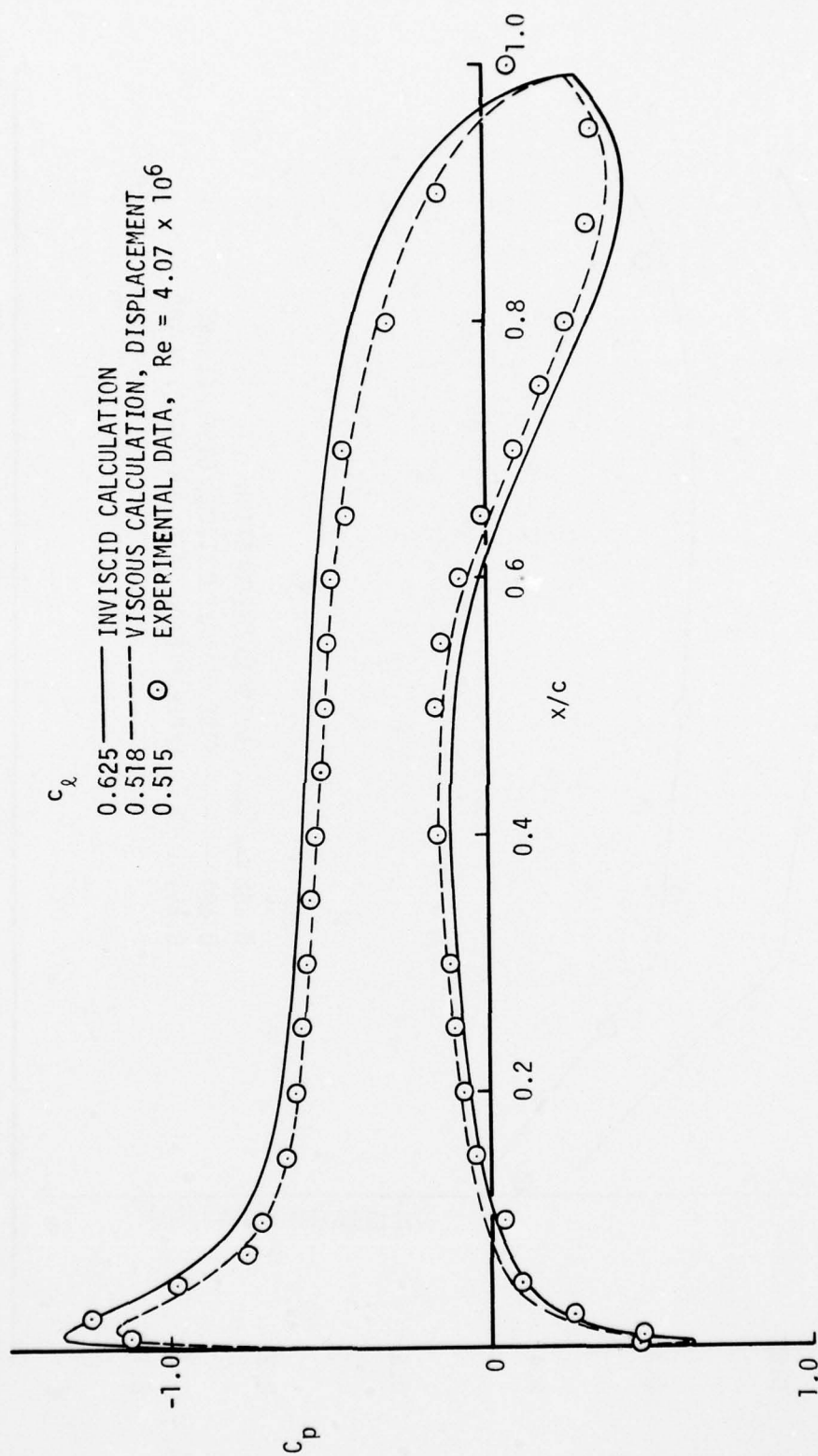


Figure 33. Comparison of calculated and experimental chordwise pressure distributions at the 50% semispan location on the wing for a supercritical transport configuration at 2.06° angle of attack.

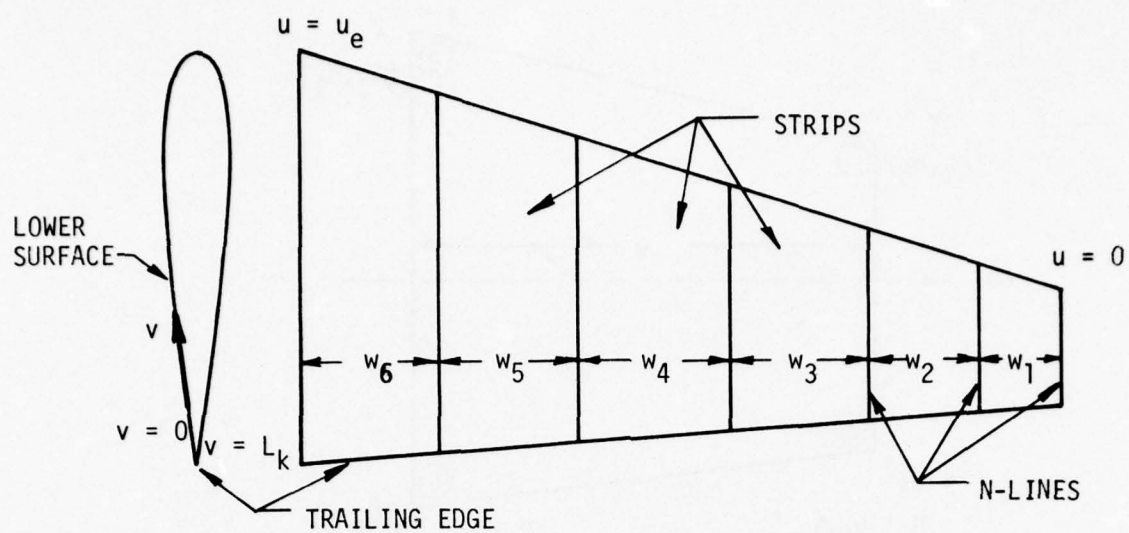


Figure 34. Definition of surface coordinates for a wing.

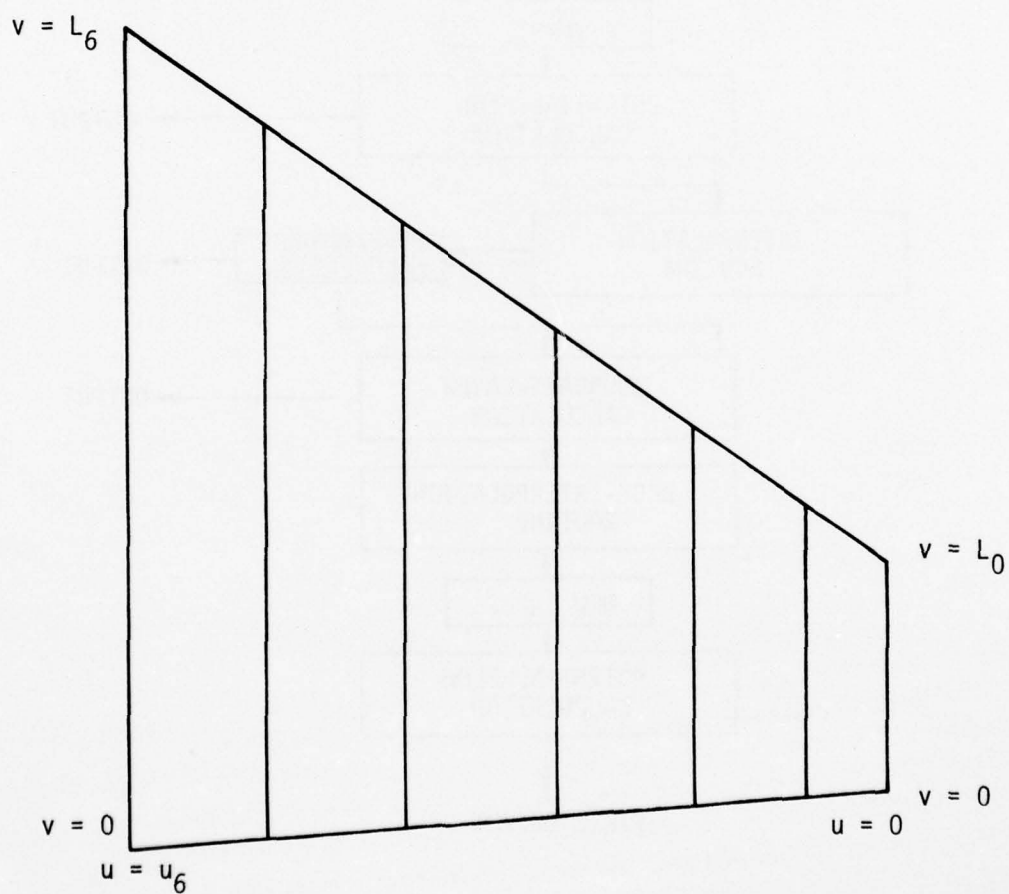


Figure 35. A wing in its coordinate space.

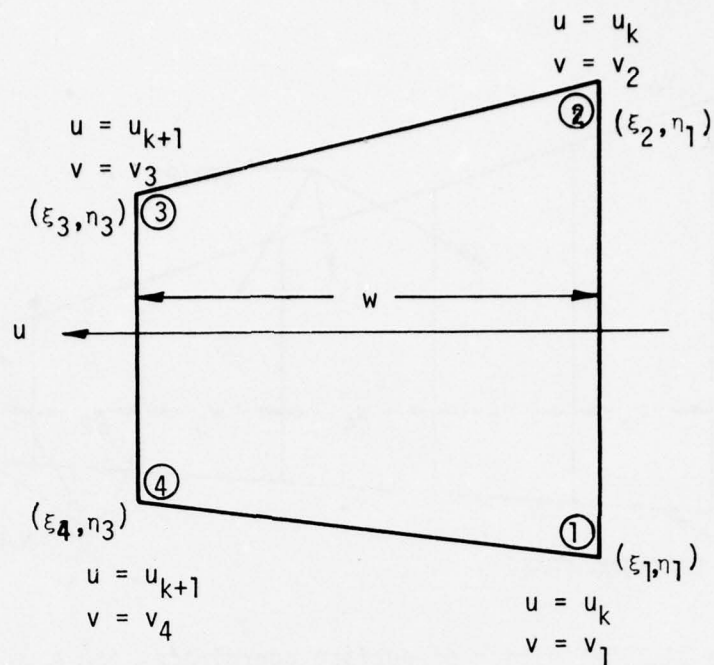


Figure 36. An individual surface panel.

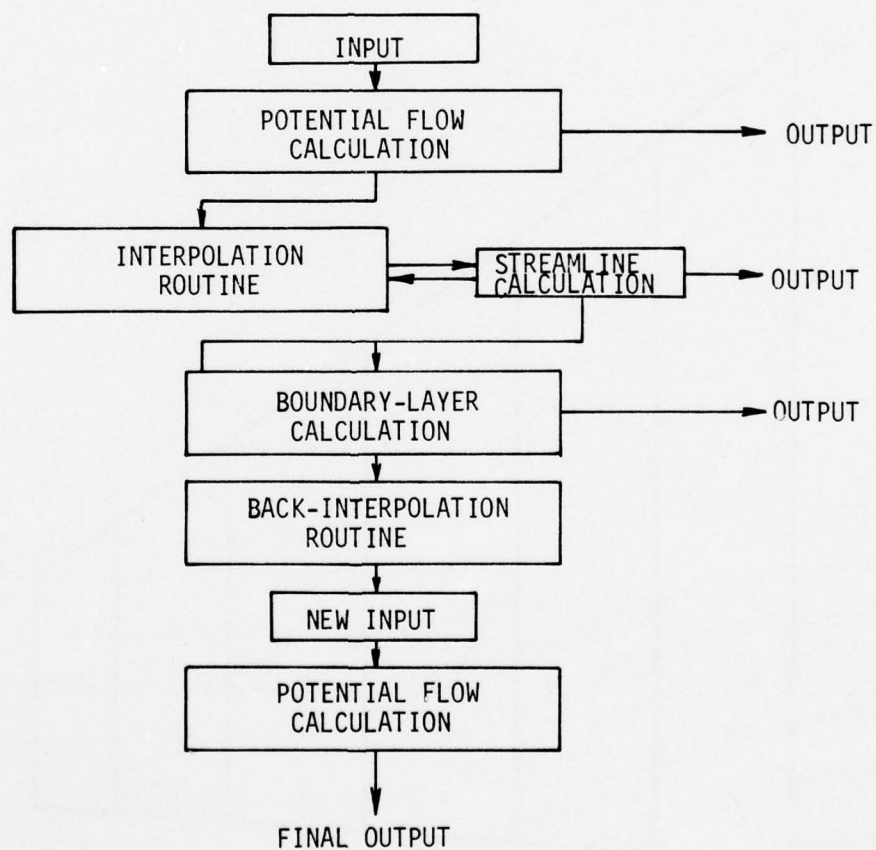


Figure 37. Block diagram of the combined potential-flow small-cross-flow-boundary-layer program.

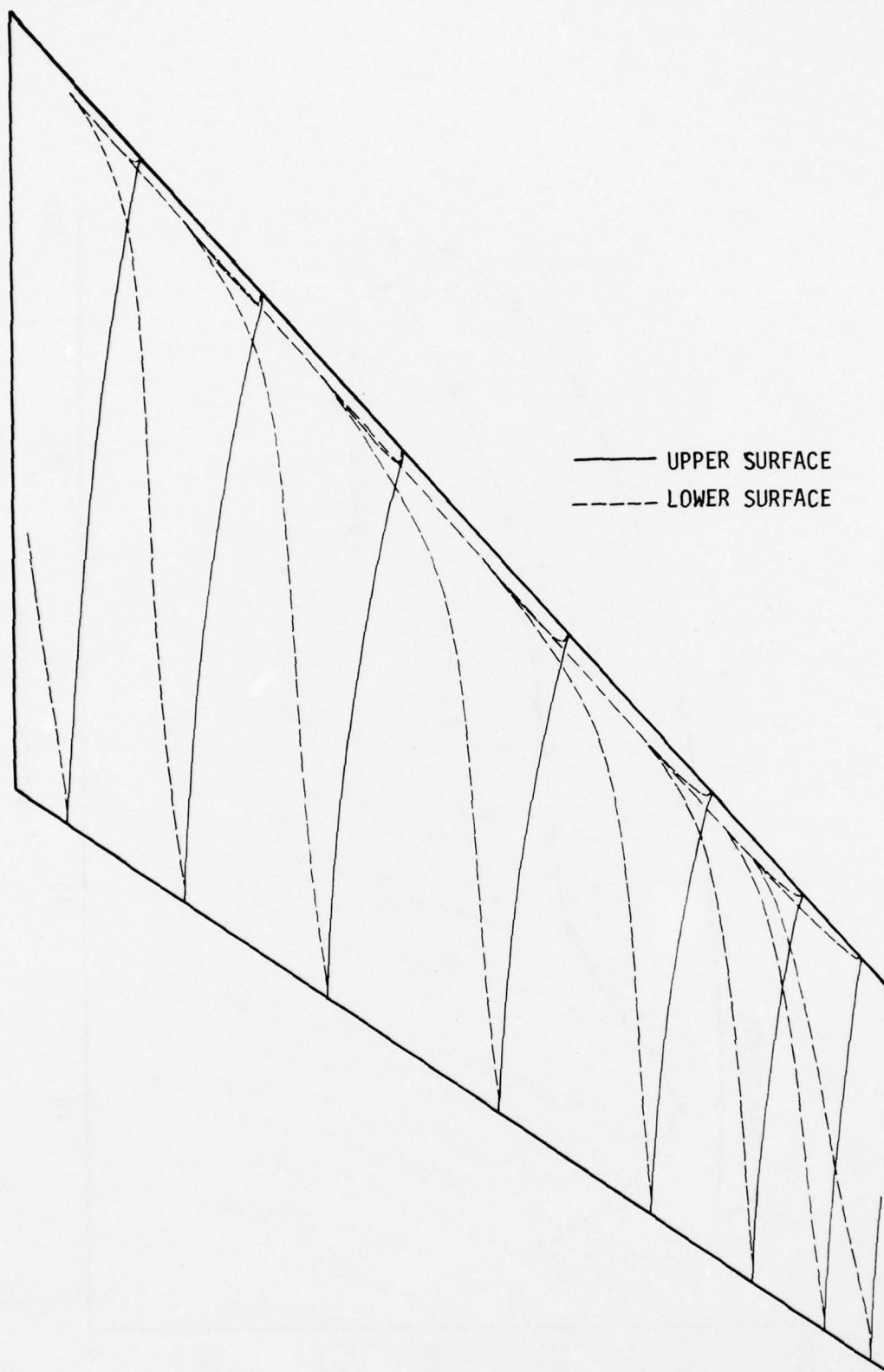


Figure 38. Calculated streamlines on a swept wing with symmetrical airfoil section at 8.2° angle of attack.

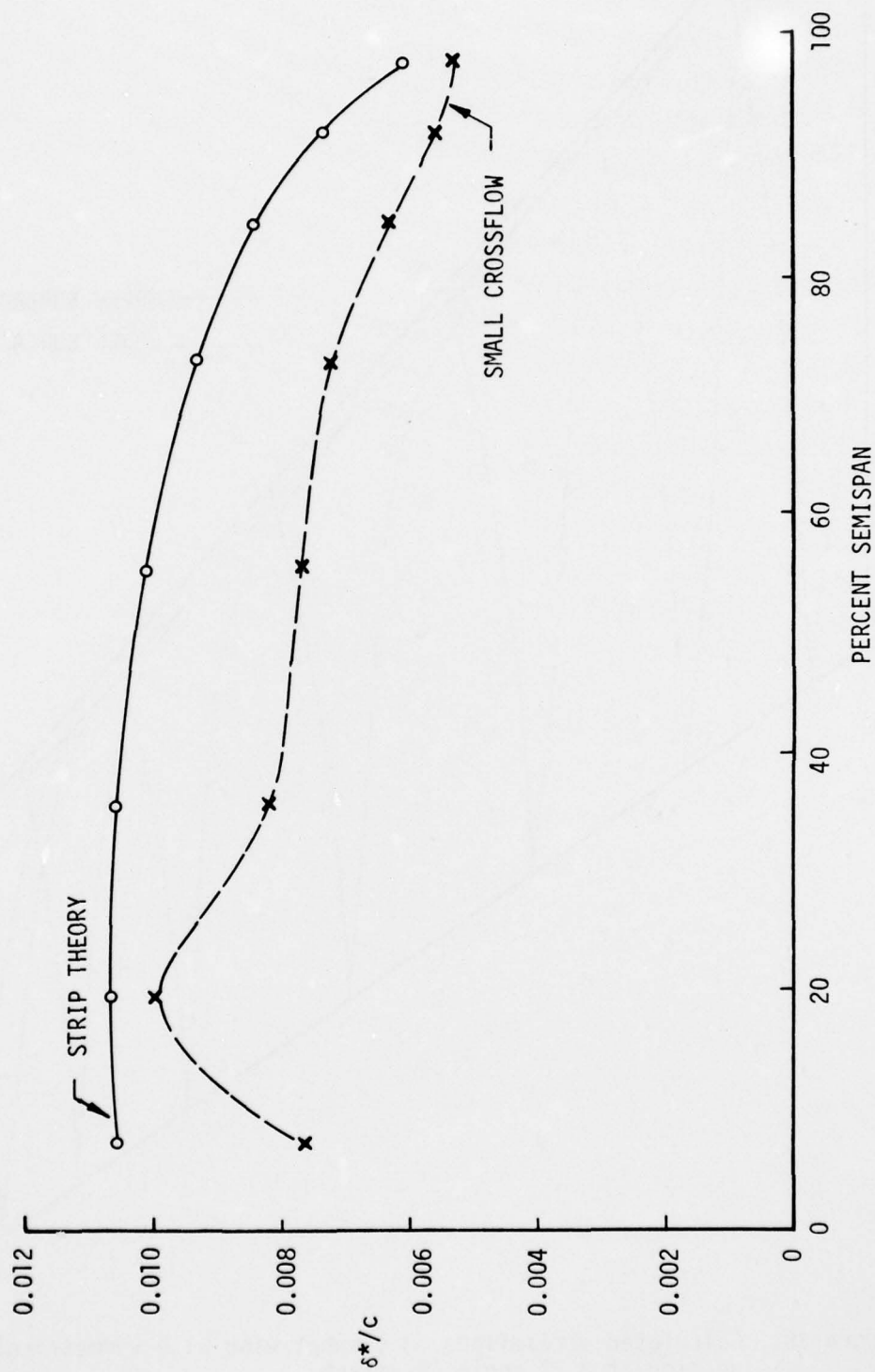


Figure 39. Calculated spanwise distributions of displacement thickness along the upper-surface trailing edge of a swept wing with symmetrical airfoil section at 8.2° angle of attack.

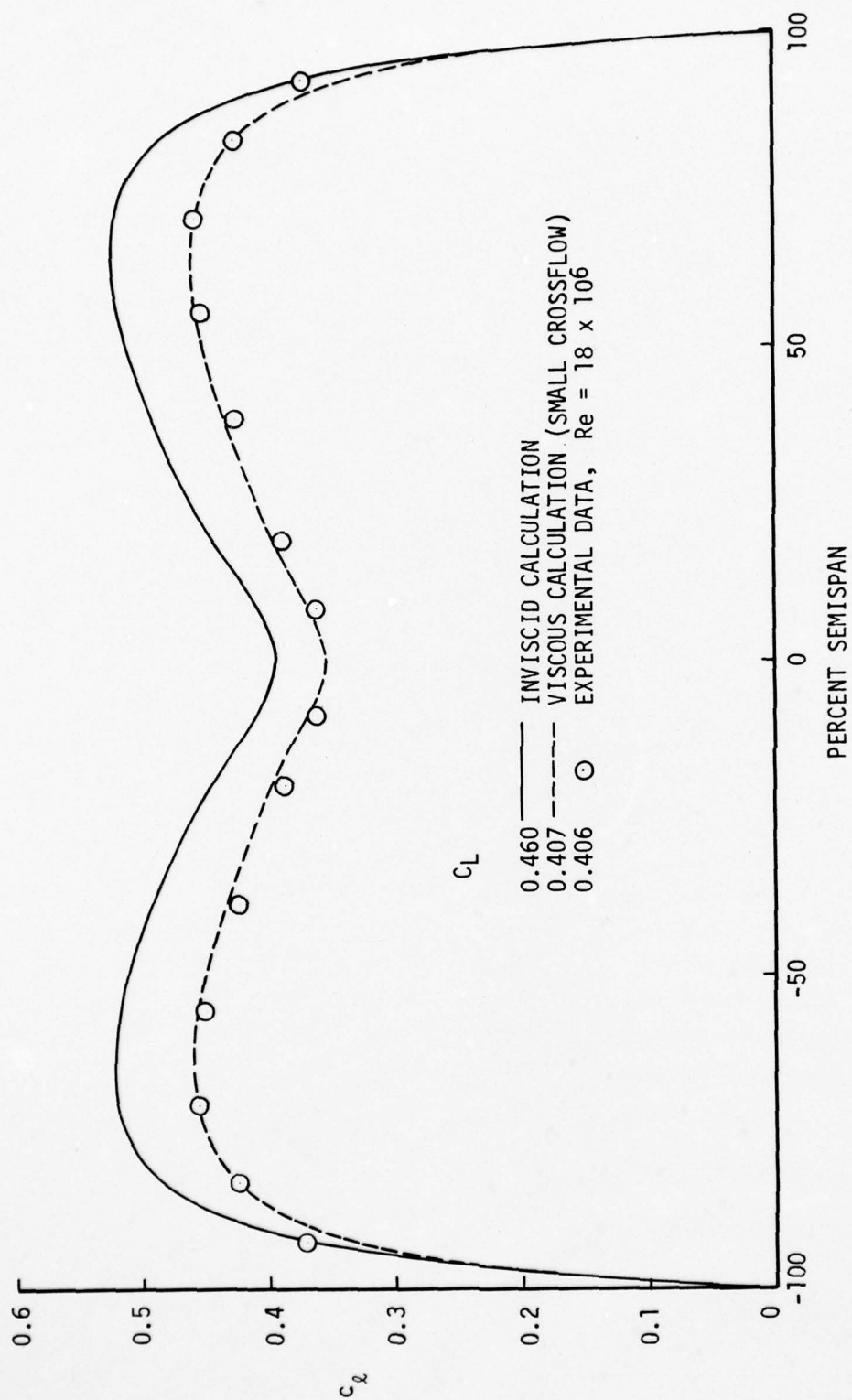


Figure 40. Comparison of calculated and experimental spanwise distributions of section lift coefficient for a swept wing with symmetric airfoil section at 8.2° angle of attack.

Unclassified

SECURITY CLASSIFICATION OF THIS PAGE (When Data Entered)

REPORT DOCUMENTATION PAGE		READ INSTRUCTIONS BEFORE COMPLETING FORM
1. REPORT NUMBER	2. GOVT ACCESSION NO.	3. RECIPIENT'S CATALOG NUMBER
4. TITLE (and Subtitle)		5. TYPE OF REPORT & PERIOD COVERED
A Fully Automatic Combined Potential-Flow Boundary-Layer Procedure for Calculating Viscous Effects on the Lifts and Pressure Distributions of Arbitrary Three-Dimensional Configurations		Final Technical Report October 1973 - March 1977
6. PERFORMING ORG. REPORT NUMBER		7. CONTRACT OR GRANT NUMBER(s)
MDC-J7491		N00014-73-C-0059
8. AUTHOR		9. PERFORMING ORGANIZATION NAME AND ADDRESS
Hess, John L. / Hess		Douglas Aircraft Company 3855 Lakewood Blvd. Long Beach, California 90846
10. PROGRAM ELEMENT, PROJECT, TASK AREA & WORK UNIT NUMBERS		11. CONTROLLING OFFICE NAME AND ADDRESS
11 1 Jun 77		Naval Ship Research and Development Center Bethesda, Maryland 20084
12. REPORT DATE		13. NUMBER OF PAGES
June 1, 1977		89
14. MONITORING AGENCY NAME & ADDRESS (if different from Controlling Office)		15. SECURITY CLASS. (of this report)
12 92p		Unclassified
15a. DECLASSIFICATION/DOWNGRADING SCHEDULE		
16. DISTRIBUTION STATEMENT (of this Report)		
Approved for Public Release; Distribution Unlimited		
16 SR 02301		
17. DISTRIBUTION STATEMENT (of the abstract entered in Block 20, if different from Report)		
17 SR 02301 01		
18. SUPPLEMENTARY NOTES		
19. KEY WORDS (Continue on reverse side if necessary and identify by block number)		
Aerodynamics	Interference Problems	Panel Method
Boundary-Layer	Kutta Condition	Potential Flow
Computer Program	Lift Distribution	Pressure Distribution
Flow Field	Lifting Bodies	Surface Singularity
Fluid Dynamics	Numerical Analysis	Three-Dimensional Flow
20. ABSTRACT (Continue on reverse side if necessary and identify by block number)		
<p>This report describes a method for calculating viscous effects on the lifts and pressure distributions of arbitrary three-dimensional configurations. The approach consists of combining a panel method, which calculates potential flow about arbitrary three-dimensional lifting configurations, with a boundary-layer method. Combined procedures have been constructed using a two-dimensional boundary-layer method in a strip-theory sense and using a three-dimensional small cross-flow boundary-layer method. Various fundamental and procedural aspects of the general calculation scheme are investigated.</p>		

DD FORM 1 JAN 73 1473

EDITION OF 1 NOV 65 IS OBSOLETE
S/N 0102-014-6601

Unclassified

SECURITY CLASSIFICATION OF THIS PAGE (When Data Entered)

116400

116400

Unclassified

SECURITY CLASSIFICATION OF THIS PAGE(When Data Entered)

19. KEY WORDS (Cont.)

Viscous Flow
Vorticity
Wing-Body

20. ABSTRACT (Cont.)

and discussed. Final emphasis is on a completely automatic procedure that performs its calculations in a single computer run without intermediate human intervention. For this purpose the method based on a strip-theory boundary layer has proved very satisfactory. Calculated inviscid and viscous lift and pressure distributions are compared with experimental data for a variety of wings and wing-fuselages having both conventional and supercritical airfoil sections. The agreement of the viscous calculations with experiment appears to be quite good.

SECURITY CLASSIFICATION OF THIS PAGE(When Data Entered)